The Thesis Committee for Mahmoud Hasan Alnazghah
Certifies that this is the approved version of the following thesis:

The Sedimentology and Stratigraphy of the Arab D Reservoir, Qatif Field

APPROVED BY
SUPERVISING COMMITTEE:

Supervisor:

Charles Kerans

Ronald Steel

Langhorne Smith

The Sedimentology and Stratigraphy of the Arab D Reservoir, Qatif Field

by

Mahmoud Hasan Alnazghah, BSc.

Thesis

Presented to the Faculty of the Graduate School of

The University of Texas at Austin

in Partial Fulfillment

of the Requirements

for the Degree of

Master of Science in Geological Sciences

The University of Texas at Austin

August 2011

Dedication

To my mother who has always been the greatest influence in my life.

To my wife whose encouragement and sacrifice have meant to me so much.

To my brother and friend, Aus Al-Tawil, who inspired the carbonator in me.

To my best friend and teacher, Luis Pomar, who took my hand when I first walked on carbonates.

Acknowledgements

I would like to express my uttermost gratitude to my supervisor, Professor Charles Kerans, for his devoted guidance, encouragement, patience, and directions throughout this research. Professor Kerans provided hours of reviews, insights and expertise. I am indebted to Dr. Aus Al-Tawil who not only inspired me by his actions as a teacher and a brother, but also through his care, guidance and advice during the course of my journey. I am grateful to Dr. Langhorne (Taury) Smith who taught me the skills I needed to hold a pencil and describe a core. Luis Pomar inspired me to be a better scientist and not to be afraid from being heterodox and opinionated. I would like to acknowledge Professor Ronald Steel for reviewing my thesis, providing me critical comments and suggestions. I am, also, grateful to Steve Bachtel for his enthusiasm in teaching modern carbonate environments. I would like to thank Fred Read for his teaching and invaluable discussions at the core lab. Wyn Hughes helped me identify micro-fossils in thin section and helped with questions throughout the project. Numerous discussions and conversations with Charles Harman aided me to complete this thesis. I would like to thank all my fellow carbonate graduate students, Nabiel Eldam and Travis Kloss, with whom I shared with long days and nights at the Cave carbonate lab at the Jackson School of Geosciences.

I would like to thank geologists in Saudi Aramco who helped me during the project: Yousef Mousa, Troy Thompson, Nasser Alnaji, Bob Lindsay, Ghazi Al-Eid, Emad Busbait, Khalaf Al-Temimi, and Raed Al-Zawwad. I would like also to thank all Core Facility Personnel who helped me through my project.

I would like to express my gratitude to Saudi Aramco Management for giving me the opportunity to pursue my MSc. and providing me with the data used in this study. Special thanks to my family for their total and unending support through the last two years.

Abstract

The Sedimentology and Stratigraphy of the Arab D Reservoir, Qatif Field

Mahmoud Hasan Alnazghah, MSGeoSci

The University of Texas at Austin, 2011

Supervisor: Charles Kerans

Co-supervisor: Ronald Steel

Co-supervisor: Langhorne Smith

The Late Jurassic Arab D Formation in Saudi Arabia hosts the some of the world's largest hydrocarbon reservoirs including Ghawar, the world's largest oil field, and Khurais, the world's largest supergiant to come into production in the last 5 years. Despite the vast oil reserves within the Arab D, and the central role of this reservoir at Ghawar in making up short-falls in global production, our understanding of the much fundamental characterization work both in terms of modern sequence stratigraphic reservoir frameworks and linked structural/fracture characterization. This study of Arab D reservoir at Qatif, immediately to the north of Ghawar, provides one of the first looks at a modern sequence analysis of this producing interval and illustrates that porosity zonations, and ultimately flow unit architecture may be substantially different than currently in use. The Arab D of the Arabian Plate is a carbonate ramp system of exceedingly low angle ($<1^{o}$) developed during a low-eustatic-amplitude greenhouse Milankovitch setting.

Combined macroscopic and petrographic data analysis allowed recognition of nine depositional facies: 1) spiculitic wackestone, 2) *Planolites*-burrowed wackestone, 3) bioturbated skeletal-peloidal packstone, 4) pelletal packstone, 5) peloidal-skeletal grain dominated packstone, 6) peloidal-skeletal grainstone, 7) skeletal-ooids grainstone, 8) cryptalgal laminites and 9) anhydrite. The depositional facies defined are used to interpret three facies tracts from deep to shallow across the ramp profile: 1) low energy sub-storm wave base (SWB) dominated facies that may illustrate disaerobic tendencies, 2) high energy within-fair-weather-wave-base ramp-crest or mid-ramp facies including foreshore and upper shoreface oolitic and skeletal grainstones that define one of the key reservoir pay zones and 3) back-barrier tidal flats consisting of cryptalgal laminites, sabkha-type anhydrites, and salina-type anhydrites.

Three high frequency sequences are defined: QSEQ 1 is asymmetrical, dominated by subtidal lithofacies; and QSEQ 2 and QSEQ 3 are symmetrical and record a complex history of the fill on an intrashelf basin. Detailed cycle-scale correlations using core-based cycles and wireline log patterns allowed a cycle-scale correlation framework to be established that illustrates a north to south progradation of the Arab D reservoir strata, building landward from the Rimthan Arch.

Diagenetic features observed in the Arab D reservoir include fitted fabric (chemical compaction), dolomitization, and cementation. These features play a major role altering reservoir quality properties as they essentially control fluid flow pathways which ultimately alter primary porosity and permeability.

Table of Contents

List of Tables

List of Figures

List of Plates

Chapter 1: Introduction

Qatif field is one of the most prolific oil-producing fields in eastern Saudi Arabia (figure 1.1). It is a northeast-southwest trending anticline that is approximately 45 km long and less than 7 km wide, covering an area of 220 km^2. The Qatif field was discovered in 1945 (Wilson, 1985) and original oil in place is estimated to be 8.6 billion barrels (Hydrocarbons Technology). The Upper Jurassic Arab D reservoir is one of the main producing reservoirs in the field, along with the Arab C and Lower Fadhili (Al-Dossary et al., 2008). The Arab D reservoir averages 55 m in thickness and is composed of stacked high frequency carbonate cycles deposited on a low-angle ramp in a Milankovitch greenhouse setting. Greenhouse conditions are characterized by small, precessionally-driven, low-amplitude eustatic fluctuations, or, if small ice sheets at the poles exist, obliquity- or eccentricity-related eustatic events of moderate amplitude, fourth order sea level oscillations (Read, 1990; Read, 1995; Matthews and Frohlich, 2002).

The main objective of the study was to develop a geologically sound, high-resolution sequence stratigraphic framework of the Arab D reservoir in Qatif. This was done using detailed core descriptions, petrographic analysis and a limited wireline log suite. This framework, when integrated with petrophysical and engineering data, should help with geosteering of horizontal well drilling, and with additional data, should lead to better reservoir simulation models.

The model is based on the identification of stratal surfaces, unconformities and their correlative conformities and relationships between observed synchronous lithofacies and depositional environments within a chronostratigraphic framework. Models based on sequence stratigraphy concepts differ fundamentally from standard lithofacies frameworks. For instance, Ainsworth et al. (1999) illustrated the difference between

lithostratigraphic and sequence stratigraphic (chronostratigraphic) correlations from the Sirikit oilfield, Thailand (figure 1.2). The sequence stratigraphic framework showed detailed geometry of clinoforms deposited in lacustrine setting and resulted in better prediction of fluid-flow behavior in the reservoir (Ainsworth et. al, 1999). Another example is published by Wehr and Brasher (1996) who illustrated the difference between sequence stratigraphic and lithostratigraphic correlations using a dataset from Cormorant field, North Sea. They showed that lithostratigraphic packages are highly diachronous with limited details about the depositional environments (figure 1.3).

This study examines shallow water deposits on a carbonate ramp formed atop a local paleo-high (Rimthan Arch) and their coeval deeper facies deposited in an intrashelf basin (figure 1.4). The unique location of the Rimthan Arch results in localized depositional patterns within the broader west-to-east dipping Arab carbonate ramp. Under this unique setting, the two general questions are addressed:

1) "Can the high-resolution sequence stratigraphic framework of the Qatif Field be improved through the application of modern sequence stratigraphic analysis of available core and log data?"

2) "What new insights can be generated regarding the paleogeography of the Rimthan-Arabian Basin system and how does this relate to reservoir facies development at Qatif Field?"

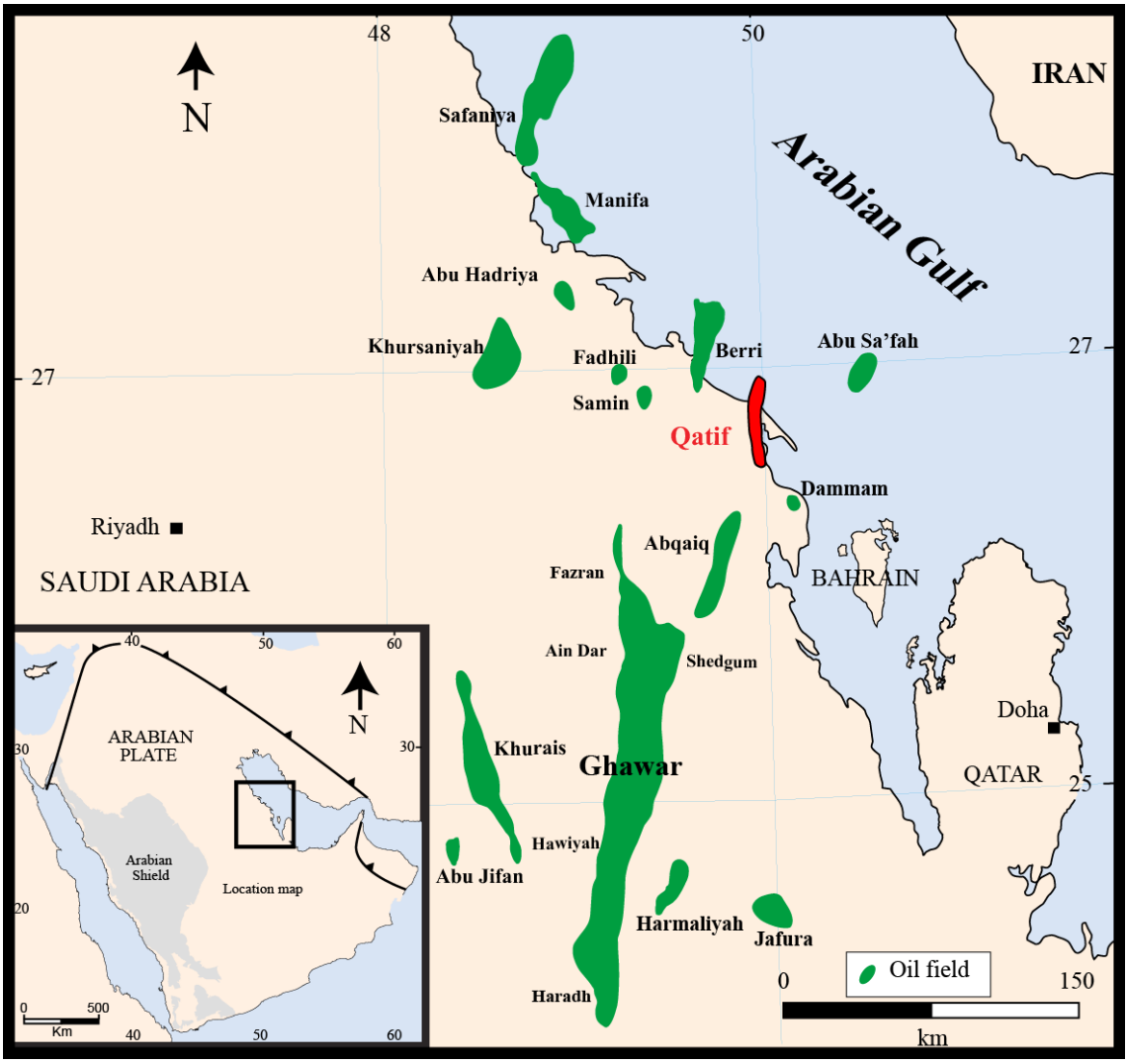

Figure 1. 1: Location map of Qatif field (modified from GeoArabia)

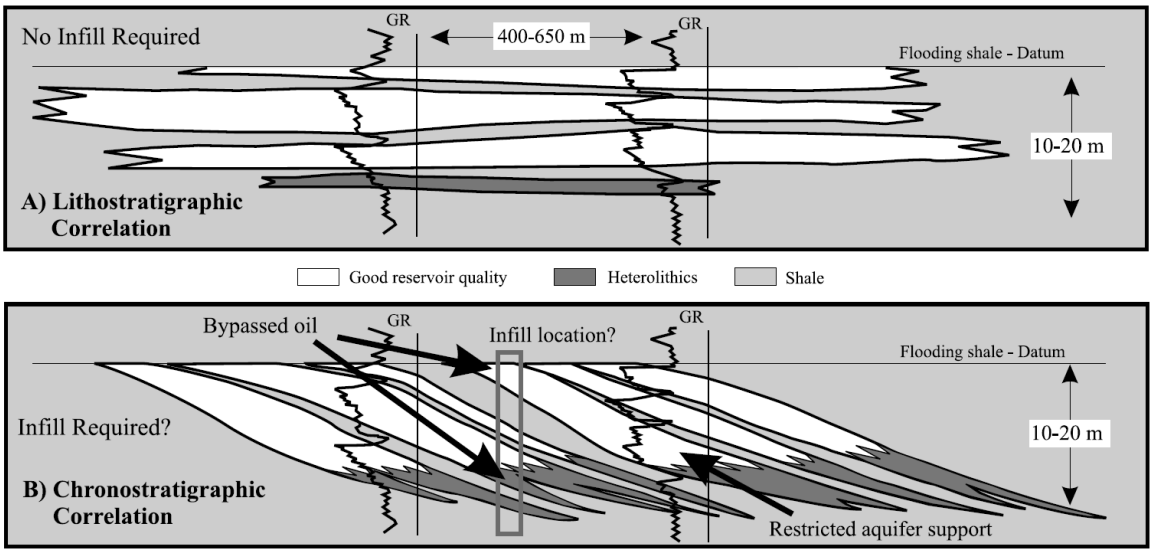

Figure 1. 2: Schematic two-dimensional illustration of lithostratigraphic vs. chronostratigraphic correlation (from Ainsworth et al., 1999)

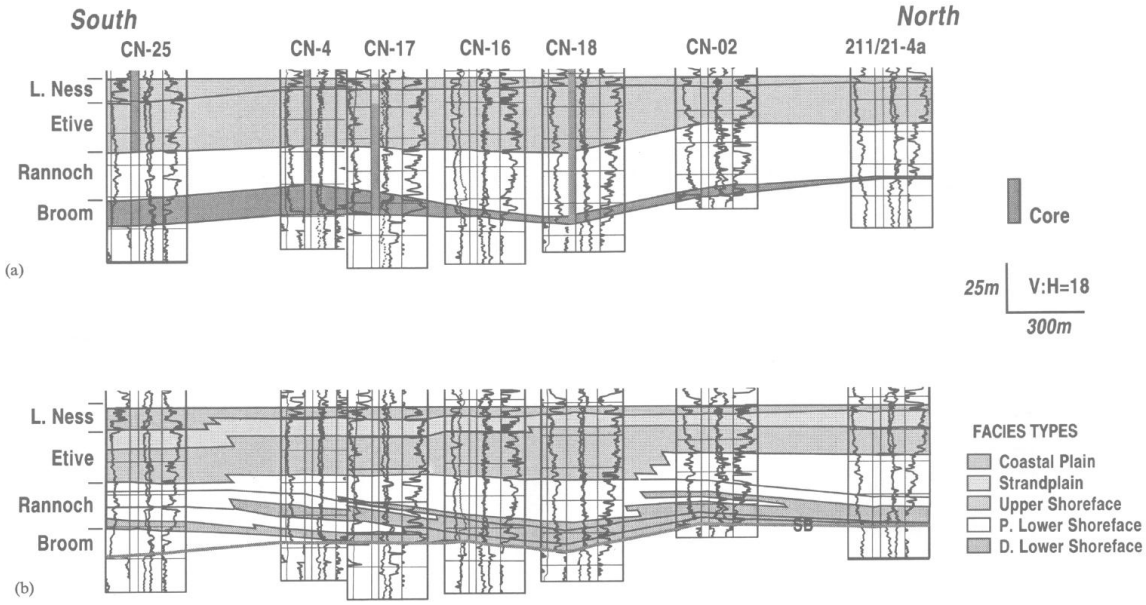

Figure 1. 3: Schematic two-dimensional illustration of lithostratigraphic vs. chronostratigraphic correlation (from Wehr and Brasher, 1996)

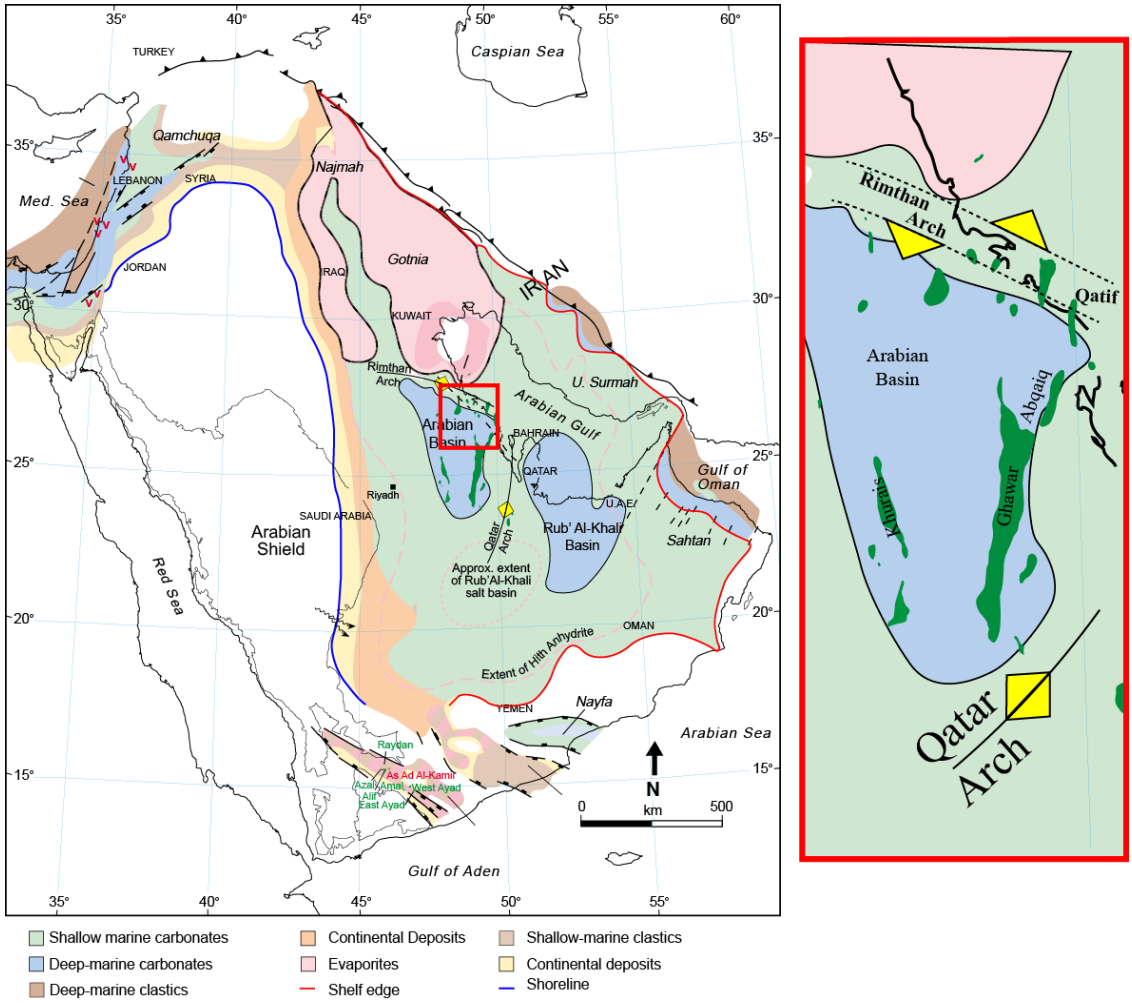

Figure 1. 4: Regional distribution of paleo-facies during Late Jurassic. The distribution reflects a snapshot in time probably in Jubaila time, prior to the filling of the intrashelf basin during the time of the Arab (modified from Ziegler, 2001)

GEOLOGICAL SETTINGS

The Arabian Plate has undergone significant modification through geologic history. Today, its margins are bounded by several compressional and extensional terrains. The northeastern margin of the Arabian Plate is a convergent margin where the Arabian Plate is being subducted beneath the Eurasian Plate, so forming the Zagros Fold Belt (figure 1.6) (Frisch et al., 2011). The northwestern margin of the Arabian Plate is delineated by the Dead Sea Transform that brings a minor extensional component. The Red Sea and Gulf of Aden form an active rift system, initiated in the Oligocene-Miocene. This rift system marks the southwestern margin of the Arabian Plate today (Sharland et al. 2001).

Sharland et al. (2001) used maximum-flooding-surface-based stratigraphy (Galloway 1989) to define 11 low-frequency tectonostratigraphic megasequences (TMS) in the Arabian Plate (AP) containing hydrocarbon plays. The tectonostratigraphic megasequence AP7 that contains the Arab D section of interest lasted about 33 Ma during the Late Jurassic and can be further divided through recognition of 9 higher-frequency maximum flooding surfaces (MFS). In terms of lithostratigraphy, the Upper Jurassic is subdivided into the Tuwaiq Mountain, Hanifa, Jubaila, Arab and the Hith formations (Figure 1.5) (Steineke et al. 1952; Powers et al. 1966; Powers 1968; Murris 1980; Ayres et al. 1982; Le Nindre 1987, 1990, Husseini 1997).

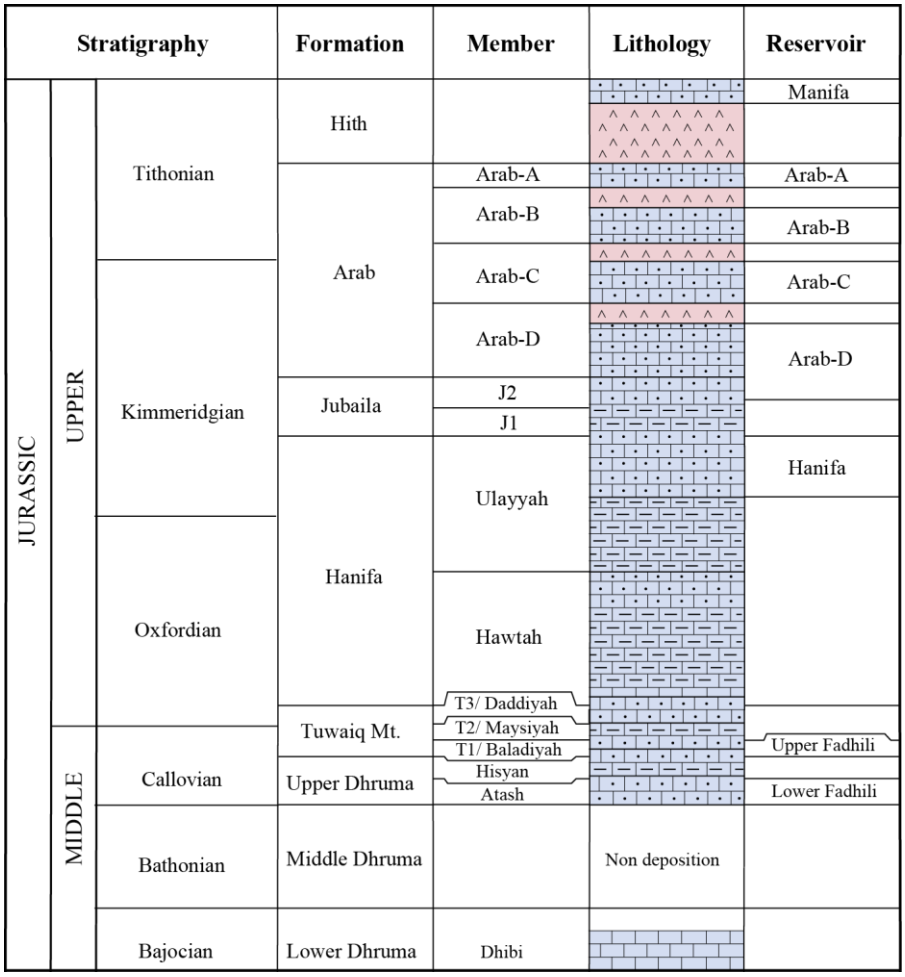

Figure 1. 5: Lithostratigraphy of the AP7 megasequence (Sharland et al. 2001) of the Middle to Upper Jurassic showing the Upper Dhruma to Hith formations. The Arab Formation is subdivided into four members (D-A). Modified from Hughes (1995) and Al-Husseini (1997)

The onset of the Bajocian transgression, following the Aalenian hiatus, resulted in the deposition of the Dhruma and Tuwaiq Mountain formations marking a significant increase in sedimentation rate and increased tectonic subsidence(Le Nindre et. al 2003). The Callovian Tuwaiq Mountain Formation overlies the Dhruma Formation disconformably marking the Bathonian–Callovian boundary (figure 1.5) (Le Nindre 1990, Alsharhan and Nairn 1997).

The Tuwaiq Mountain Formation is about 300 ft thick and comprises three members: the lower Baladiyah, the middle Maysiyah and the upper Daddiyah (figure 1.5) (Enay et al. 1987 cited in Hughes 1995, Powers et al 1966). During the late Callovian transgression, restricted water circulation of the developed Arabian intra-shelf basin led to euxinic conditions which, coupled with high productivity, resulted in the deposition of organic-rich clay and mud-rich carbonates. The average TOC values for these units is about 3 wt.% but can be as high as 13 wt.% (Murris 1980; Carrigan et al. 1995). The marls pass transitionally upward into higher energy, open marine coral- and calcareous-algae-bearing facies corresponding to Upper Fadhili and Hadriya reservoirs (Powers 1968; Alsharhan and and Kendall 1986; Le Nindre 1990; 2003, Alsharhan and Nairn 1997).

The Oxfordian Hanifa Formation is underlain by the Tuwaiq Mountain Formation and is overlain by the Jubaila Formation. Vaslet et al. (1983) subdivided the Hanifa Formation into two members: the Hawtah and Ulayyah (figure 1.5) (cited in Husseini et al 1996). Each member represents a shallowing upward high frequency sequence composed of several high frequency cycles and cycle sets (Mattner and Husseini 2000). The Ulayyah member contains the Hanifa reservoir which is composed of aggrading and prograding grainstones (McGuire et al 1993).

The Early Kimmeridgian Jubaila Formation rests unconformably on the underlying Hanifa Formation separated from it by a clear textural and color shift (Steineke et al. 1958; Powers et al. 1966; Powers 1968). The Jubaila records initial phases of transgression of the Jubaila-Arab-Hith 2nd-order supersequence. The Jubaila Formation is composed of organic-rich (0.5-3.5% TOC), subtidal, laminated wackestones and packstones that become increasingly bioturbated up-section with concommitent loss of organics (Wilson 1981, Meyer et al. 1996, Alsharhan and Nairn 1997).

The Arab carbonate-evaporite cycles represent transgressive-regressive depositional sequences of approximate 5 Ma duration (Sharland et al., 2001; Hughes 2010). These sequences were deposited upon a restricted platform. The more open-marine transgressive hemicycles are characterized by shallow-subtidal carbonates whereas the regressive late highstands are characterized by evaporites.

PALEOGEOGRAPHIC RECONSTRUCTION

During the late Paleozoic, the Arabian Plate was situated approximately 25˚ south of the equator (Al-Fares et al., 1998). During the Late Permian to Middle Triassic, the Arabian Plate started drifting northward to lower latitudes. The opening of Neo-Tethys transformed the eastern side of the Arabian Plate into a passive margin setting. In the Late Triassic, a new passive margin developed in the eastern part of the Arabian Plate as a result of rifting along the northern margin of the plate and was associated with local volcanism and reactivation and enhancement of earlier structural elements (figure 1.6) (Sharland et al. 2001; Ziegler 2001).

The Arabian Plate regional paleogeographic reconstruction for the Jurassic indicates that it was a stable, broad carbonate shelf, modified by the presence of the Arabian, Gotnia, and Rub' Al-Khali intrashelf basins (figure 1.7). These basins and

associated shallow ramp areas were controlled by structural lineaments set up by three tectonic phases (Al-Husseini, 2000). The Arabian Basin is the site where giant oil fields developed such as Ghawar, Khurais, Abqaiq and Qatif developed (Murris 1980; Ayres et al. 1982; Alsharhan and Kendall, 1986; Al-Husseini, 1997; Sharland et al., 2001). During the Jurassic the Arabian Plate was located 5-10º south of the equator (Alsharhan and Magara, 1994; Handford et al., 2002; Markello et al., 2008) with its northeastern and southeastern continental margins bounded by the Tethys Ocean (figure 1.7) (Sharland et al., 2001; Handford et al., 2002).

During the Toarcian, the post- rift thermal subsidence in the northern parts of the plate resulted in the creation of a deep water, intra-shelf Sargelu Basin. The Sargelu Basin differentiated, due to variable subsidence, into two intra-shelf basin. These are the Gotnia Basin and the Arabian Basin that were separated by the Bajocian Rimthan Arch (Figure 1.7) (Murris 1980; Ayres et al. 1982; McGuire et al. 1993; Carrigan et al. 1994; Al-Husseini 1997; Al-Husseini 2000; Sharland et al 2001).

The Qatif Field is set up by a northeast-oriented anticlinal trap that probably formed as part of the Ghawar-En Nala trend that has persisted since Precambrian compressional events. During the Middle Jurassic, the Qatif Field was located on a broad stable, platform where carbonate sedimentation predominated (Murris 1980, Ayres et al. 1982, McGuire et al. 1993, Al-Husseini 2000; Sharland et al. 2001). However, during the Late Jurassic, the development of intra-shelf basins and arches placed the Qatif Field as part of the Arabian Basin developing on the south-facing limb of the NNW trending Rimthan Arch. During the Oxfordian-lower Kimmeridgian, the Hanifa Formation was dominated by low energy, organic rich, euxinic carbonate sediments (Powers et al. 1966, Powers 1968, Alsharhan and Kendall 1986, Alsharhan and Magara 1994, Alsharhan and Nairn 1997). The Hanifa represents the major source-rock bed for most of the Jurassic

reservoirs in Saudi Arabia. Hanifa strata were overlain unconformably by dolomites and mudstones of the Jubaila Formation (Powers et al. 1966; Powers 1968; Murris 1980; Alsharhan and Kendall 1986; Al-Husseini 1997). The Jubaila Formation passes conformably into four grainstone-dominated third-order sequences with basal carbonates and capping evaporites, known as the Arab D (oldest), Arab C, Arab B, and Arab A (youngest) (Alsharhan and Nairn, 1997). The Kimmeridgian Arab Formation carbonate members of the A, B, C and D sequences represent reservoir facies, whereas the capping evaporites are excellent seals (Steineke et al. 1952; Powers et al. 1966; Powers 1968; Murris 1980; Alsharhan and Kendall 1986; Alsharhan and Magara 1994; Alsharhan and Nairn 1997; Al-Husseini 1997).

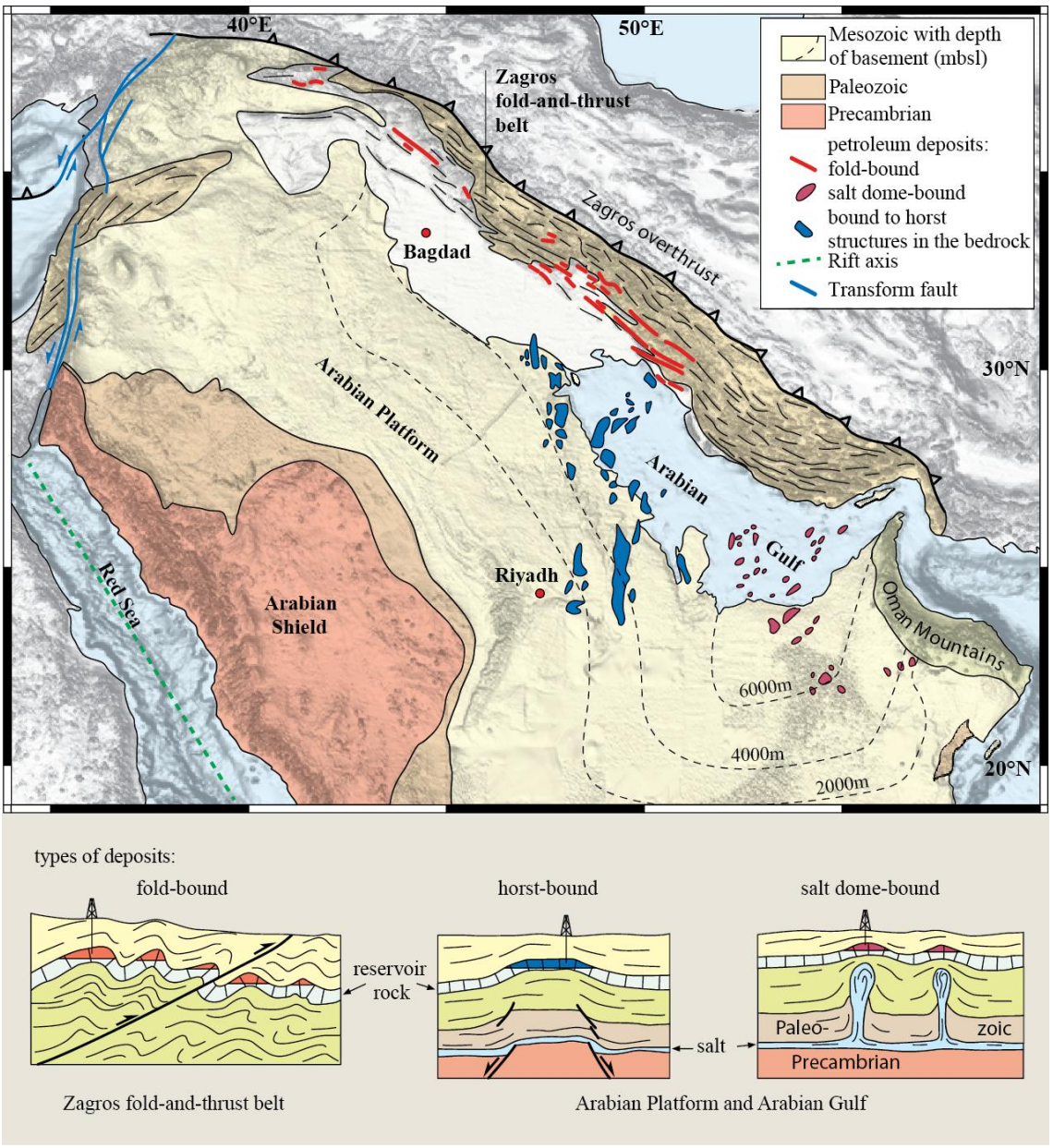

Figure 1. 6: Map showing the Arabian Plate boundaries. The location of Zagros thrust belt is believed to represent the zone where the true margin of the Kimmeridgian ramp. The generalized cross sections represent the different trapping styles of the Jurassic petroleum traps between the Arabian platform and the Zagros thrust belt (modified from Frisch et al. 2011)

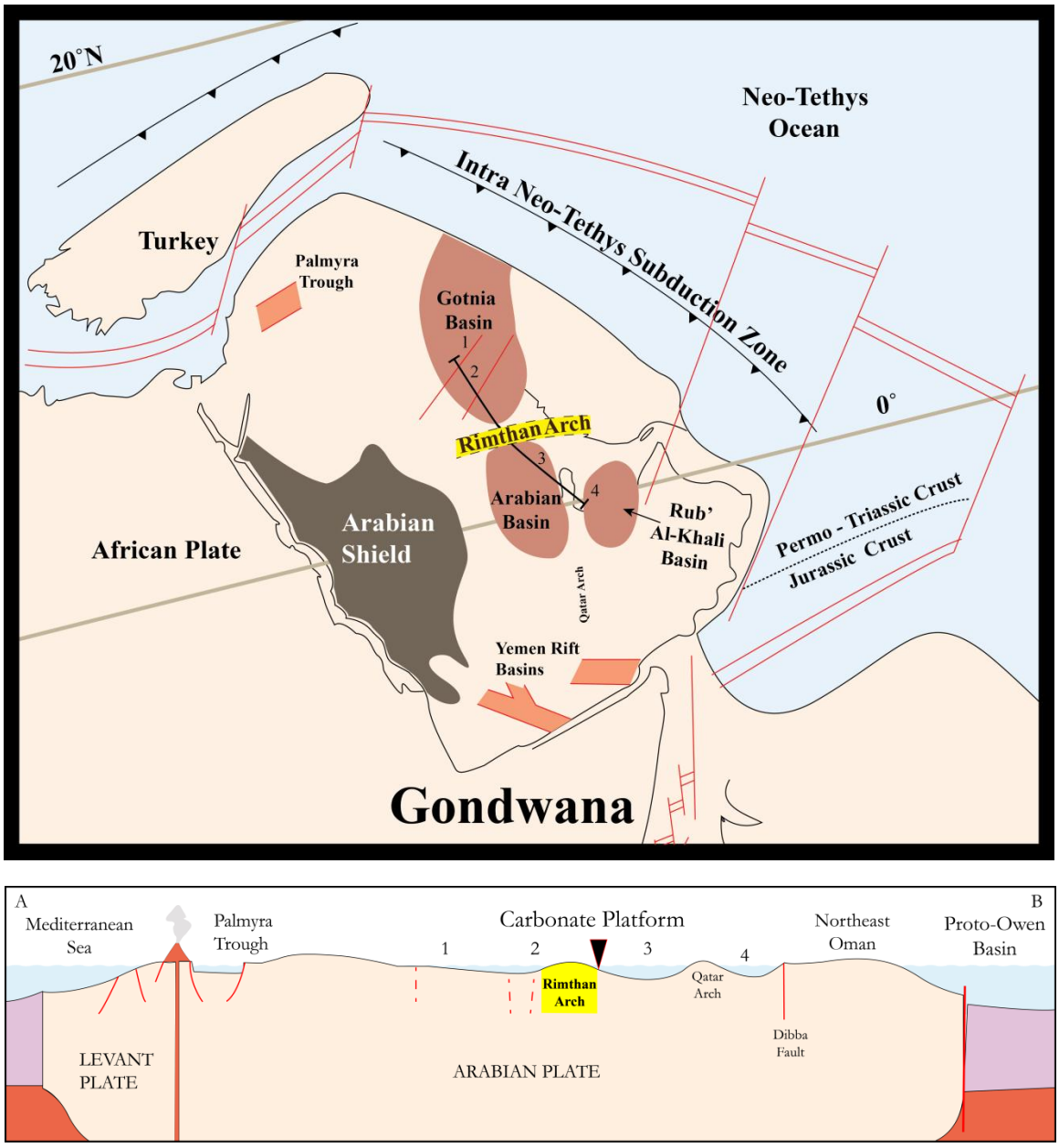

Figure 1. 7: The paleogeographic location of the Arabian Plate during AP7 megasequence. Intrashelf basins were present in the Iraq-Kuwait (Gotnia), central Saudi Arabia (Arabian) and southern Gulf (Rub Al-Khali) areas and due to their nature of depth and restriction they were sites of source rock deposition. The location of the intrashelf basins was controlled by old structural lineaments such as Rimthan and Qatar Arches. The lower diagram displays a cross sectional view of the developed intrashelf basins including the Gotnia, Arabian and Rub Al-Khali basins. The triangle indicates location of Qatif field (modified from Sharland et al. 2001)

PREVIOUS WORK ON RESERVOIR-SCALE SEQUENCE STRATIGRAPHY

The Arab D reservoir has been the subject of many detailed and more general regional studies, both in Saudi Arabia, as well as in Qatar and the United Arab Emirates where these carbonates are important reservoirs. The vast majority of these studies were conducted as in-house unpublished works, but Mitchell et al. (1988), Meyer and Price (1993), Handford et al. (2002), and Lindsey et al. (2006) stand as the key published works.

Mitchell et al. (1988) defined six depositional facies in the Arab D of Ghawar Field; five of which are carbonate facies, being capped by massive anhydrite (table 1). They noticed an overall thinning of the anhydrite northward and of the carbonate southward with significant volume reduction in the grainstones towards the south. Thus, the unique facies distribution suggested that the depositional profile deepened from south to north as a result of lateral facies change and shallowing from carbonate in the north to coeval anhydrite in the south. Thus, the Arab D reservoir was subdivided into four zones. Mitchell et al. (1988) interpreted these reservoir zones as two shallowing upward cycles (figure 1.8).

Meyer and Price (1993) defined 10 lithofacies (table 1) and proposed that the Arab D reservoir can be divided into a Lower and an Upper zone where distinctive bedding characteristics are observed (figure 1.9). The bedding styles of the depositional strata reflect the hydrologic regime that dominates the site of deposition. While, the cross-bedded, well sorted, medium to fine sands dominating the upper shoreface and the foreshore suggest everyday hydrologic processes such as tides, currents and longshore drift; the graded and hummocky cross bedded turbidites reflect a storm-dominated zone below the fair weather wave base. The in-situ skeletal facies (*Stromatoporoids, Cladocoropsis, Foraminifers)* were located between the lower shoreface and the fair-

weather wave base. The proposed model suggests that the lower Arab D zone consist of classic turbidites overlain by amalgamated carbonate sands. The Lower Zone is composed of muddy and grainy turbidites overlain by amalgamated, graded and/or hummocky cross-stratified carbonate sand and gravel units. The Lower Zone turbidites consist mainly of the Micritic and Bivalve-Coated grain Intraclast (BCI) lithofacies whereas the graded and hummocky cross-stratified beds are mainly composed of skeletal carbonate beds. The Upper Arab D Zone consists of burrowed skeletal grainstones with bulbous stromatoporoids, whole branching *Cladocoropsis*, fragmented *Cladocoropsis*, foraminifera. Mixed skeletal-peloidal sands, cross-bedded oolite and the transitional skeletal peloidal sand lithofacies are present as well and the entire set is capped by anhydrite. Meyer and Price concluded that the observed vertical facies succession of the Arab D at Ghawar represents a single phase of progradational infill of an intrashelf basin over which subsequent deposits prograded.

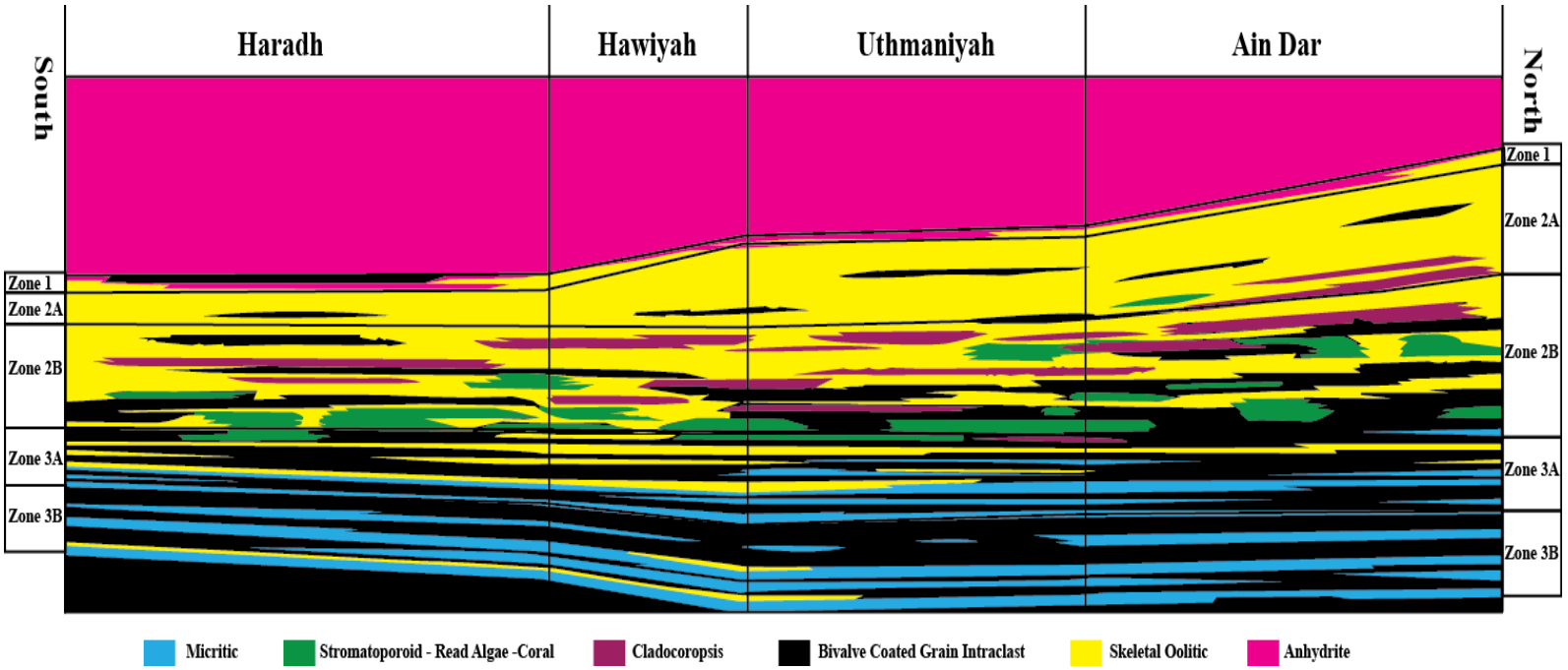

Figure 1. 8: Mitchell et al. Arab-D depositional lithofacies, south-north cross section, Ghawar Field. Anhydrite thins and is replaced by carbonates to the north. Modified from Mitchell et al., 1988

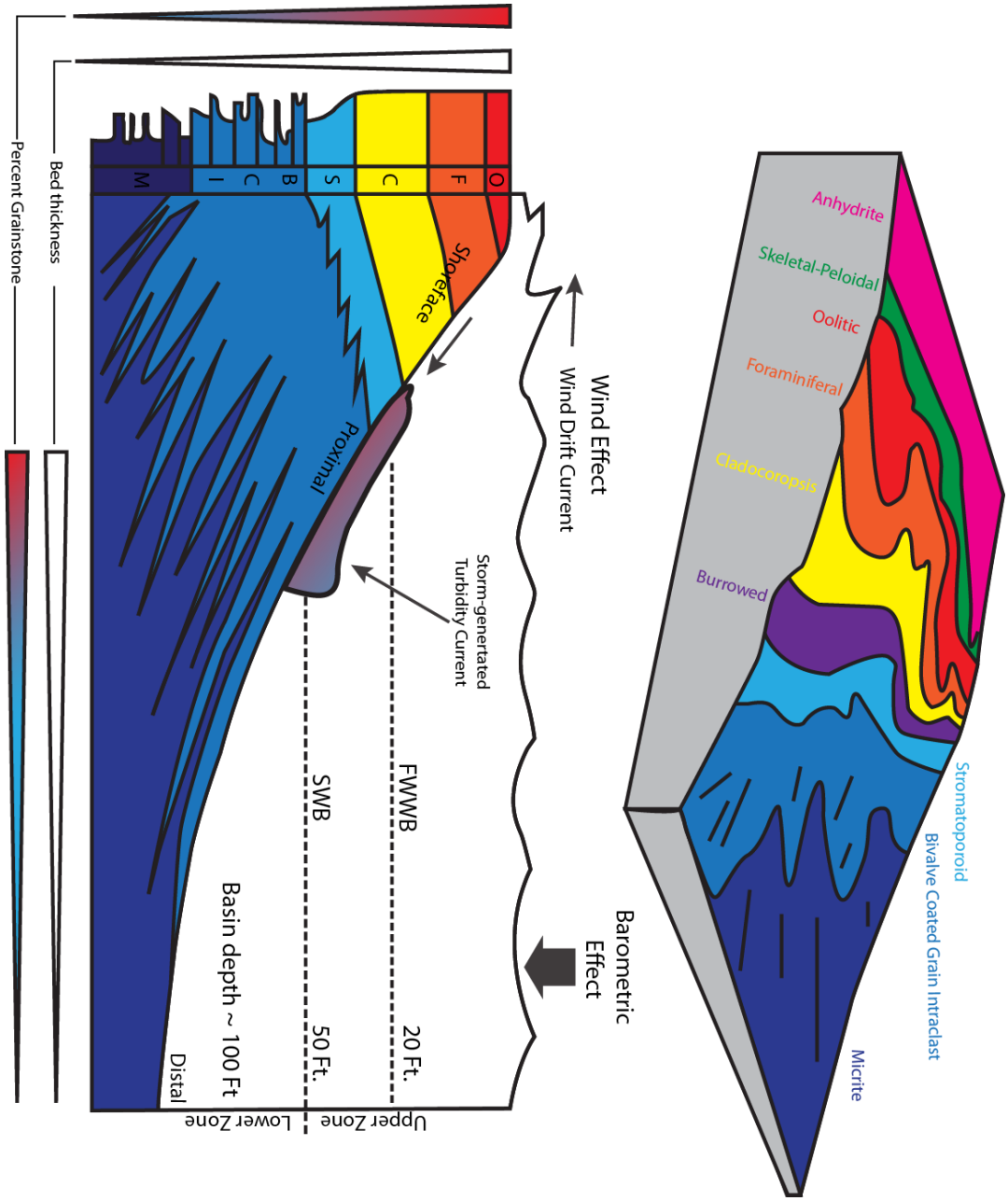

Figure 1. 9: The Arab D is subdivided into a lower and an upper zone based on bedding styles and characteristics. The deposition in the Lower Zone is dominated by the micritic and BCI lithofacies deposited under the influence of storms where hummocky cross stratified and graded beds are common. The Upper Zone represents several higher-energy lithofacies with a much more faunal diversity. The dip of the shingled clinothems is reduced upsection. Modified from Meyer and Price, 1993

Handford et al. (2002), using the most extensive core dataset yet published, subdivided the Arab D section into 9 facies deposited in the Arabian intrashelf basin interpreted to be lying within a broad ramp extending from northern offshore fields to the Arabian shield (figure 1.10). This configuration was attributed to the transition from a paleogeographic high in the northern Ghawar to deeper intrashelf basin to the south. Handford et al. (2002) showed that the depositional profile deepens from north to south except extreme ends of northern Ghawar, Abqiq, Qatif and Berri.

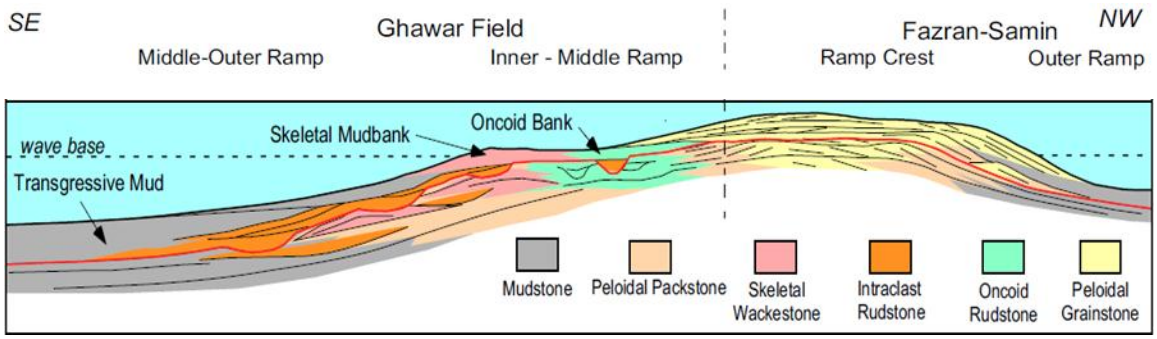

Figure 1. 10: Handford et al. generalized depositional model of the Arab-D in Ghawar Field. The sequence boundary marked in red equivalent to top of cycle one of Mitchell et al. (1988). (Modified from Handford et al., 2002)

Sequence stratigraphic interpretations of the Arab D are limited. Mitchell et al. (1988) have considered two shallowing upward cycles within the Arab D: the first comprises Zone 3 and the second comprises Zone 1 and 2 (figure 1.8). The base of the first cycle (Zone 3B) is composed of low porosity, mud dominated micritic lithofacies deposited in relatively deep subtidal settings. It is overlain by porous skeletal and oolitic grain dominated packstones and grainstones with minor stromatoporoid-coral lithofacies suggesting that it was deposited in shallower subtidal environment with higher energy settings. The second cycle start at the base of Zone 2B where mud dominated packstones decrease in abundance and upwards and becomes more grain dominated, subtidal and

open marine, with the upper third extensively dolomitized. This is overlain by Zone 2A which is composed mainly of skeletal and oolitic grainstones and grain dominated packstones deposited in shallow, high energy, current and tide swept settings. Zone 1 caps the 2nd cycle and represents the transition from high-energy shallow water grainstons of Zone 2A to sabkha evaporites of the lower portion of the Arab D Anhydrite. The sequence boundary is placed under the overlying anhydrite (figure 1.14).

Le Nindre (1990 cited in Al-Husseini 1997) has assigned sequences based on lithological, depositional and biostratigraphic relationships. He correlated them to the Haq et al. (1987) global sea-level curve, based on which, he interpreted the anhydrite as highstand deposits and the carbonates as transgressive deposits. On the contrary, McGuire et al. (1993) have assigned the anhydrite to lowstand and transgressive deposits, whereas the carbonates to highstand. Meyer and Price (1993) interpreted the Arab D as one shallowing upward succession deposited in a storm-dominated shelf where prograding shingled lithofacies of the main reservoir dip less steeply than the lower part of the reservoir (figure 1.14).

Handford et al. (2002) have interpreted the upper Jubaila and the Arab D to comprise two high frequency sequences (figure 1.11). The first sequence consists of the lowstand and transgressive system tracts of upper Jubaila interbedded mudstones and the highstand of the lower Arab D. The shallowing of the Lower Arab D is recognized by the prevalence of oncoids and intraclastic rudstones associated with lowering of storm wave base as a result of relative sea level fall. Thus, the first sequence is represented by low energy, interbedded mudstones overlain by oncolitic and intraclastic rudstones. The second sequence starts at the base of the Middle Arab D where a distinct transgression is recognized in association with faunal change. The Middle Arab D is characterized by wide spread, open marine stromatoporoid and coral facies which are overlain by mud

rich, burrowed packstones with whole and broken cladocoropsis. The Upper Arab D is characterized by the overlying high energy, prograding cladocoropsis grainstones and packstones. The significant change in the nature of facies occurred in comparable depositional environments marks the turnaround from a retrogradational to progradational stacking patterns and separates the Middle from the Upper Arab D and is marked by a regional hot gamma ray signature. The Upper Arab D is characterized by grain-supported facies succeeded by a series of downstepping oolitic grainstones in northern Ghawar Field. The overlying anhydrite was deposited under lowstand and transgressive conditions following the deposition the Upper Arab D carbonates.

Lindsay et al. (2006), using the same depositional facies as Mitchell et al. (1988), have constructed a sequence framework and depositional model (figure 1.12) where they have divided the Arab D reservoir into two composite sequences from one-dimensional analysis (figure 1.13). The first composite sequence comprises the upper part of the Jubaila Formation and its sequence boundary is located at the base of Zone 2B which is marked by a flood back, where deeper facies were deposited on top of 3A, marking the Arab D – Jubaila contact. The second composite sequence starts at the base of Zone 2B and its sequence boundary is marked by collapse breccia at the upper part of the Arab D carbonates.

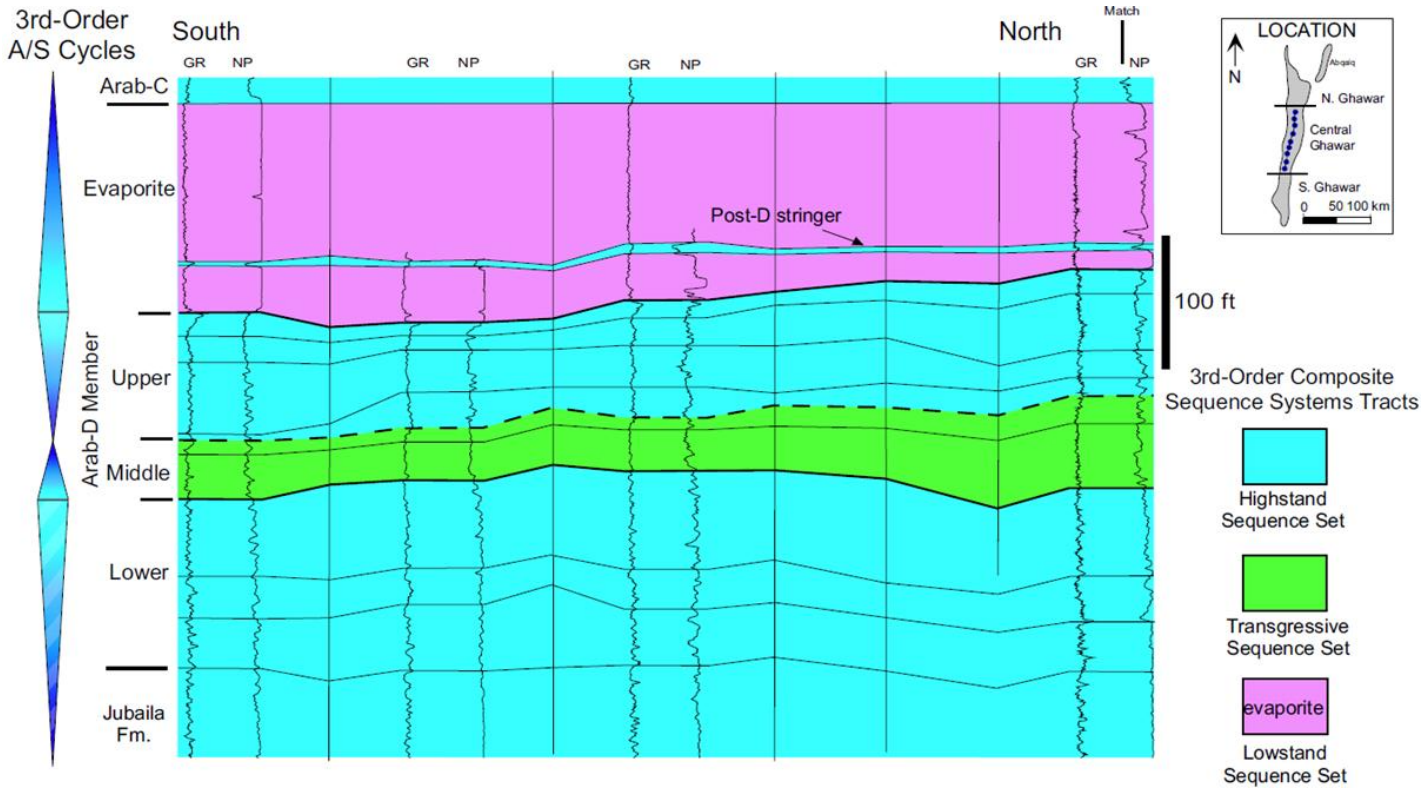

Figure 1. 11: North-south stratigraphic cross section of the Arab-D member in central Ghawar field showing interpreted system tracts and composite sequences (Handford et al. 2002)

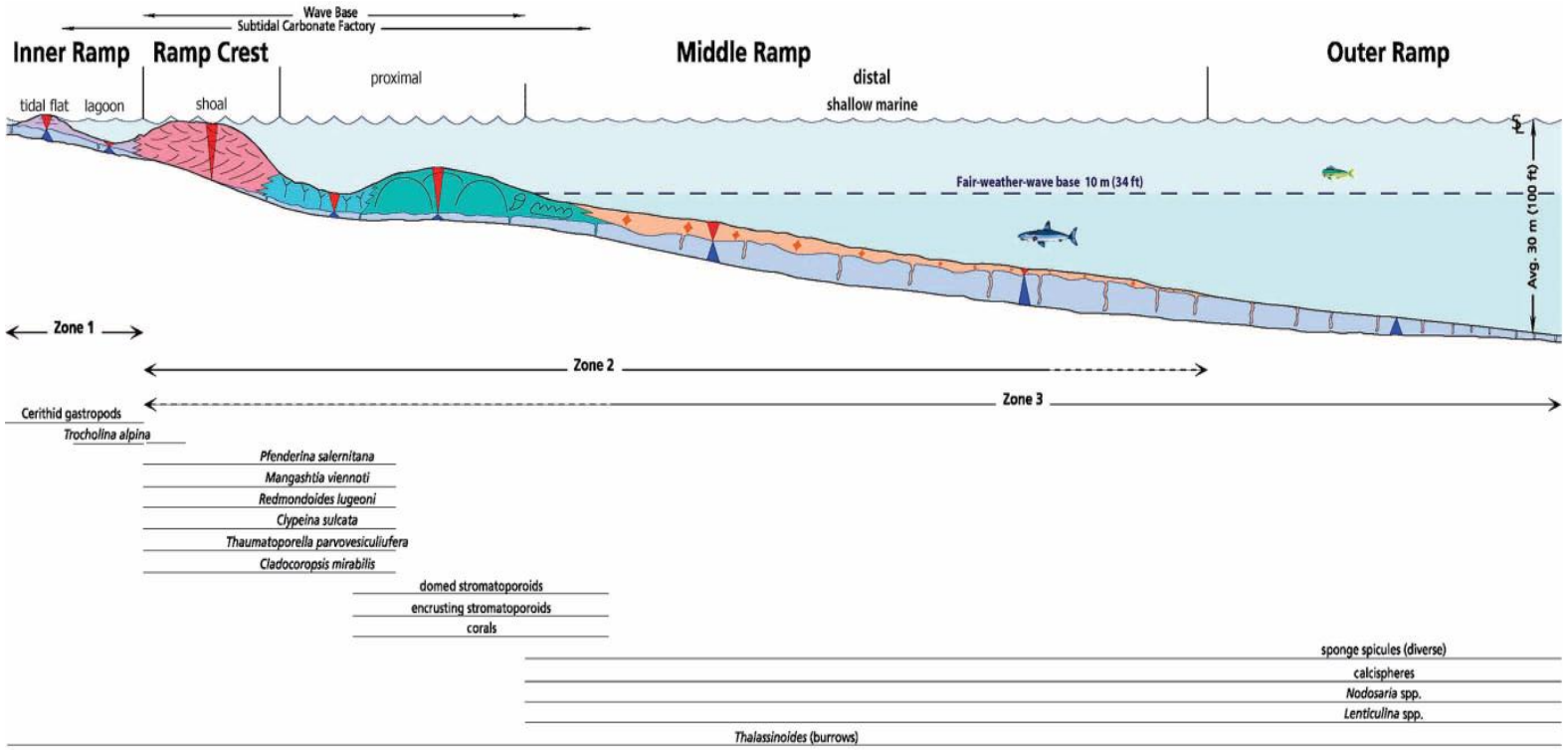

Figure 1. 12: Idealized depositional model of the Arab-D reservoir carbonate ramp in Ghawar field. This model depicts deposition of one carbonate cycle from the inner ramp, ramp-crest shoal, proximal, and distal middle ramp to outer ramp. It is integrated with micropaleontology showing the distribution of microfossils. (Lindsay et. al 2006)

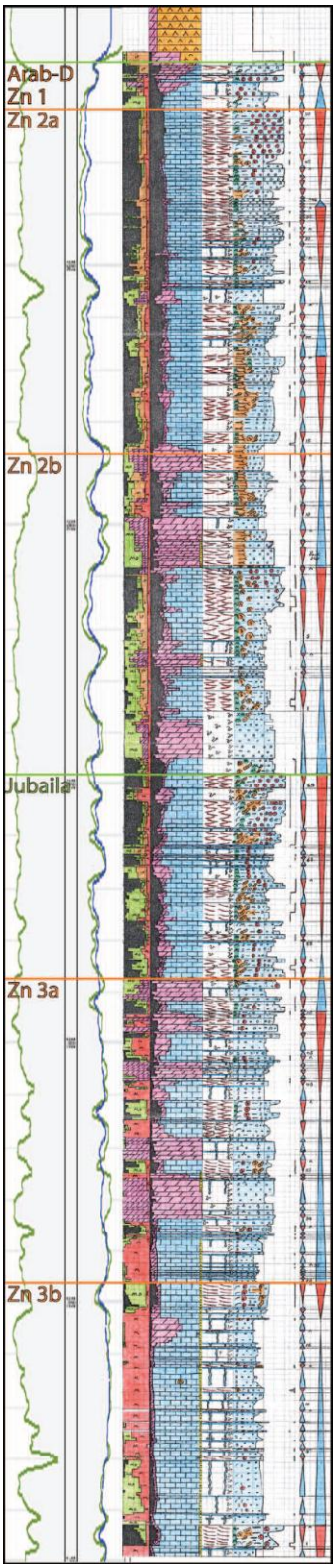

Figure 1. 13: One-dimensional analysis of stratigraphic framework showing different zones (equivalent to Mitchell et al., 1988), high-frequency cycles and cycle sets.

	Author	Wilson (1985)	Mitchell et al. (1988)	Meyer and Price (1993)	Handford et al. (2002)	Lindsay et al. (2006)
	Study Data	Qatif	*Ghawar (Haradh-Hawiyah-Uthmaniyah-Ain Dar)*	*Ghawar (Uthmaniyah-Hawiyah)*	*Ghawar-Khurais-Abqaiq-Qatif-Abu Sa'afah-Berri-Arab Exposure*	*Ghawar (Shedgum)-Wadi Laban-Wadi Nisah-Wadi Hilwah*
		Anhydrite (nodular)	Anhydrite	Anhydrite	Anhydrite (nodular/massive)	Anhydrite (nodular/bedded/massive/palmate)
Proximity	Proximal				Paleosol breccia and rooted wackestone	
		Upper Coarse Grainstone	Skeletal-Oolitic Grainstone - GDP	Oolite	Ooolitic Grainstone-GDP (FPD)	Skeletal-Oolitic Grainstone - GDP
		Fine Grainstone		Skeletal Peloidal Foraminifera	Stratified foraminifera Peloids Grainstone-Packstone	
		Fine Grainstone (dolomitized)				
			Cladocoropsis Grainstone - Packstone	Fragmented Cladocorpsis Cladocoropsis	Burrowed to Stratified Cladocoropsis wackestone-grainstone boundstone	Cladocoropsis Grainstone - Packstone
				Burrowed Skeletal Peloidal		
Facies			Stromatoporoid-Red Alagae-Coral Boundstone	Stromatoporoid	Coral, Stromatoporoid packstone to boundstone	Stromatoporoid-Red Alagae-Coral Boundstone
					Oncoid and Intraclasts rudstone	
			Bivalve-coated grain-intraclast Packstone-Wackestone	bivalve-coated grain-Intraclast		Bivalve-coated grain-intraclast Packstone-Wackestone-GDP
	Distal	Burrowed Wackestone			burrowed skeletal peloidal wackestone-packstone	
			Micritic Wackestone-Mudstone	Micritic	lime mudstone-wackestone	Micritic Wackestone-Mudstone
	?		Dolomite (Indeterminate)		Peloidal dolowackestone-dolomudstone	Dolomite (Indeterminate)
	Stratigraphic Framework	Current swept (high energy) shallow water grainstones filling a restricted shelf basin and was cut by tidal deltas and capped by evaporites	open normal marine and relatively deeper water lithofacies existed to the north of Ghawar as carbonates thickened and facies climbed section to the north	shingled lithofacies arrangement in which prograded lithofacies in the main part of the reservoir dip less steeply than bedded strata in the lower part of the reservoir	Coral/Stromatoporoid Facies developed during transgression and were submerged during maximum flooding. Base level fall lead to the deposition of seaward-stepping clinothems composed mainly of grainstones/packstones and capped by the lowstand deposits of anhydrite.	Coral/Stromatoporoid facies developed deeper settings to the south while equivalent higher energy facies developed to the south controlled by the palimpsest topography
	Setting	Ramp northward progradation	Ramp Northward progradation	Ramp northeast progradation	Ramp northward progradation	Ramp 80% southward progradation 20% northward progradation ; split occurs around Shedgum

Table 1. 1: A summary of previous work conducted on the Arab D

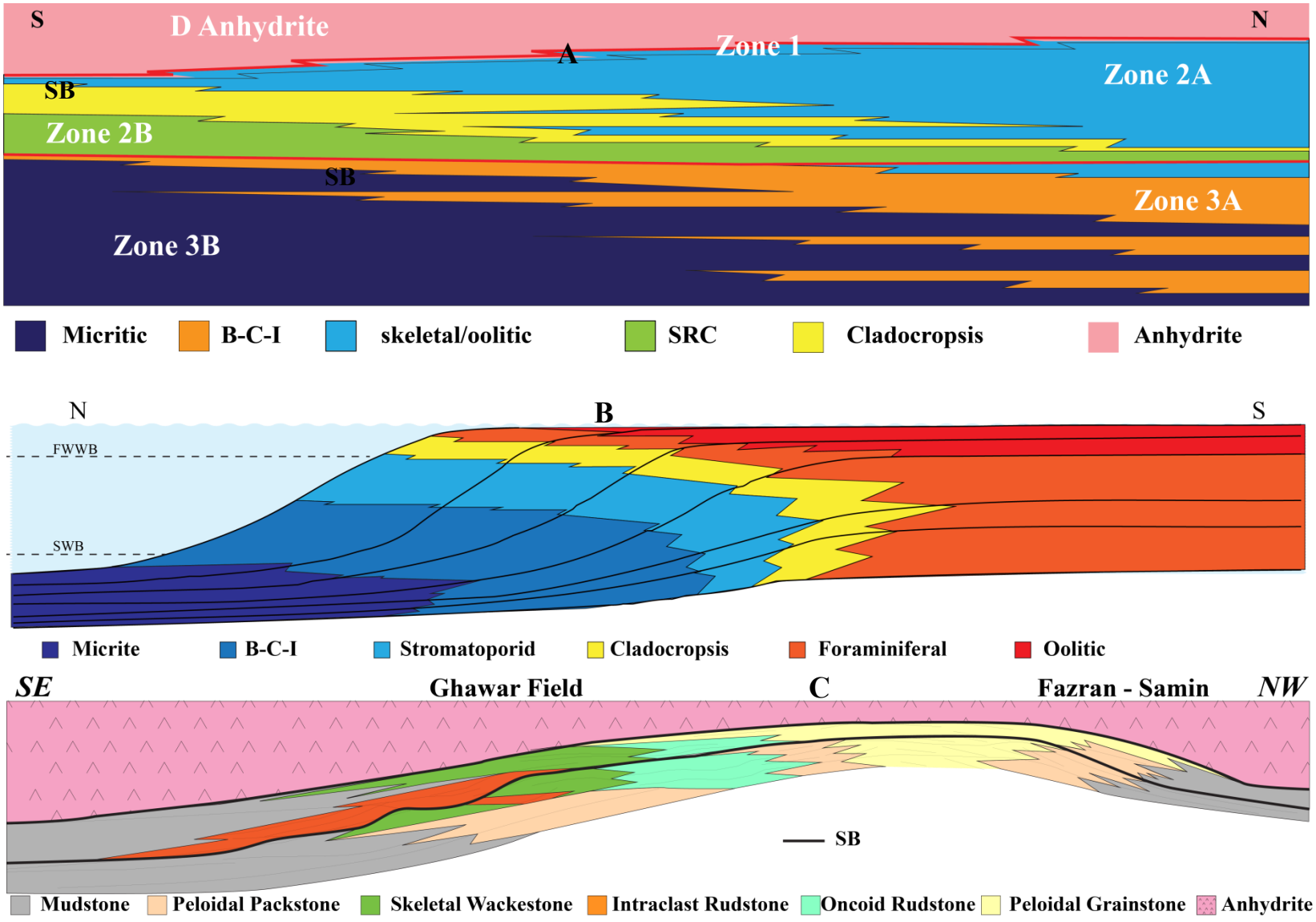
S
D Anhydrite
N
A
Zone 1
Zone 2A
SB
Zone 2B
SB
Zone 3A
Zone 3B
Micritic
B-C-I
skeletal/oolitic
SRC
Cladocropsis
Anhydrite
N
B
S
FWWB
SWB
Micrite
B-C-I
Stromatoporid
Cladocropsis
Foraminiferal
Oolitic
SE
Ghawar Field
C
Fazran - Samin
NW
SB
Mudstone
Peloidal Packstone
Skeletal Wackestone
Intraclast Rudstone
Oncoid Rudstone
Peloidal Grainstone
Anhydrite

Figure 1. 14: Schematic models showing the stratigraphic framework of previous work on the Arab D reservoir, Saudi Arabia (previous page)

Model	# of sequences	Progradation Direction	Comments
Mitchell et al., 1988 (A)	2	N-S	Diachronous evaporite-carbonate transition (time transgressive)
Meyer & Price, 1993 (B)	1	SW-NE	Single sequence from top Jubaila to top Arab D
Handford et al, 2002 (C)	2	N and S	Evaporite-carbonate contact is not time transgressive. Therefore, thicker evaporites in the south implies onlap of topographic highs during transgressive and lowstand of sea level

Table 1. 2: Summary of stratigraphic framework of previous work on the Arab D reservoir

METHODOLOGY

Notable in this previous work is the lack of detailed analysis of reservoirs other than the Ghawar complex. In 1999 Aramco began an effort to extend its effort in sequence stratigraphic analysis of the Arab D in associated large fields including Khurais Abu Jaffan, Harmalia, and this study at Qatif. The previous work of others emphasized the need to learn basic facies and stacking patterns from core material first, before linking this to well logs and seismic data. This study represents the first integrated examination of the Qatif cores in a sequence stratigraphic framework.

A total of 19 cores (~2,500 ft), housed at the Saudi Aramco Core Storage Facility, Dhahran, Saudi Arabia, provide a continuous sedimentary record of the Arab D reservoir in Qatif Field. The 10 best cores were selected, based on their condition and location to construct a north-south transect across the field (figure 1.15). In general, the distribution of the cores across the field occupied a central location across the long axis with limited distribution across the field's flanks. A total of 565 thin sections were made by sampling four of the cores systematically, where permitted, at one-foot interval for petrographic analyses.

A standardized Aramco carbonate logging form (figure 1.16) was used to document a complex suite of lithofacies deposited in diverse depositional environments, ranging from restricted supratidal to distal deeper lithofacies. The form uses a modified Dunham (1962) carbonate classification scheme of carbonate rocks is used, which incorporates Embry and Klovan's (1971) additional terms for depositional facies (figure 1.1). In addition, the form has several tracks to record lithological data including sedimentary structures, texture and grain type and size. Furthermore, stylolites and fractures were recorded where observed. The lithology of the cores was studied by

examination under a binocular microscope in both dry and wet conditions. Thin sections made from cores' samples were used to refine facies description, assess porosity, describe pore types, and record diagenetic modification of grains and matrix. Ultimately, an idealized depositional profile is generated based on the interpretation of lithologies and depositional environments. The data was then integrated into a stratigraphic framework based on high-frequency cycles (HFCs) and high-frequency sequences (HFSs).

The core description sheets were digitally drafted and were plotted, as raster logs, along with gamma ray logs using Petra software. The core descriptions were depth shifted and calibrated to gamma ray (GR) using density-neutron logs. However, only the GR log was used as means of correlation in this study. Several shallowing up, high-frequency cycles have been defined and mapped based on facies stacking patterns. The defined cycles have been correlated across the field to develop a general model of facies architecture and sequence stratigraphic framework of the reservoir.

Thin sections were used for petrographic analysis to ensure consistency of core descriptions. They were analyzed to describe lithology, depositional textures and biocomponents. In addition, the thin sections were a fundamental key for determining different diagenetic features and their timing.

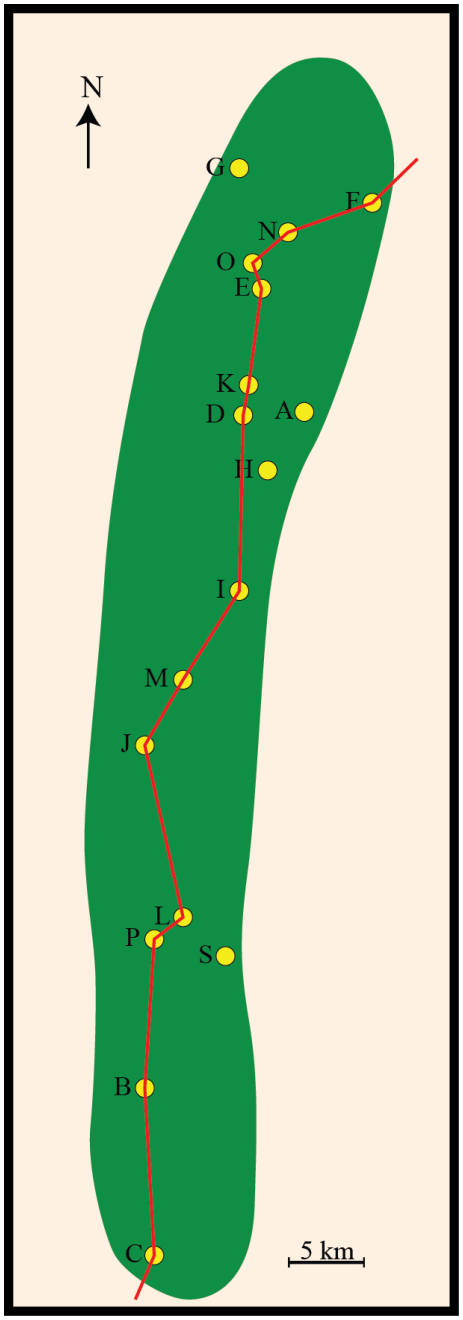

Figure 1. 15: Map showing the location of wells of the study. The line of cross section constructed is drawn in red.

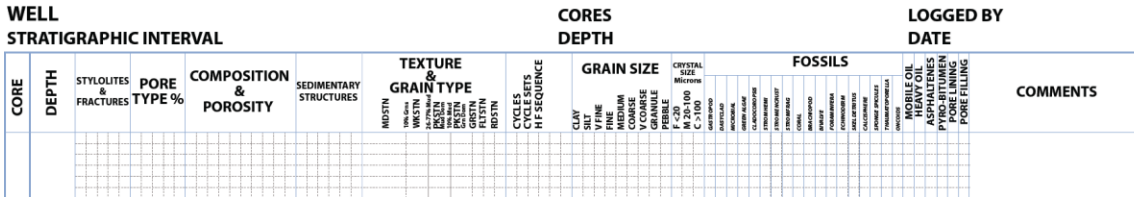

Figure 1. 16: Standardized Saudi Aramco carbonate logging form

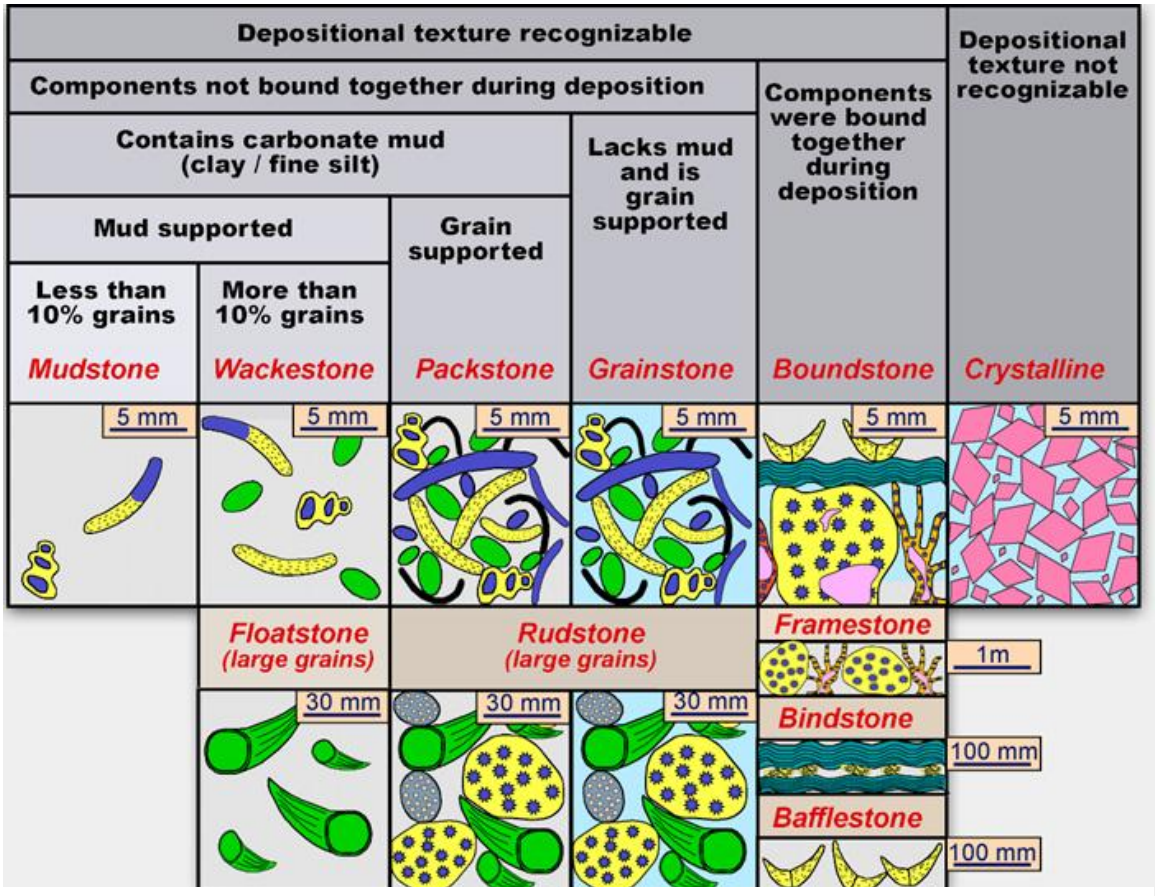

Figure 1. 17: Dunham classification (1962) modified by Klovan and Embry (1971) (from Bureau of Economic Geology – Online Learning Modules)

Chapter 2: Depositional Lithofacies

LITHOSTRATIGRAPHIC TERMINOLOGY

The lithostratigraphic units represent the sedimentary strata that conform to Steno's the Law of Superposition which states "sedimentary layers are deposited in a time sequence, with the oldest on the bottom and the youngest on the top". The lithostratigraphic units include lithofacies, vertical facies succession and lithofacies tracts that make up the basis of the chronostratigraphic units (Kerans and Tinker, 1997).

Lithofacies

Lithofacies represent three-dimensional rock units recognized for a distinctive set of characteristics such as mineral composition, sedimentary structures, bedding characteristics, allochem types and indicator fossils (Kerans and Fitchen, 1995; Kerans, 1995; Kerans and Tinker, 1997). Each lithofacies includes all the features that reflect specific environmental conditions including, but not limited to, types of carbonate-producing organisms, water depth, water chemistry, latitude, temperature, sunlight intensity, turbidity, water circulation, ρCO_2, salinity and nutrient supply (Wilson, 1975; Hallock and Schlager, 1986; Kerans and Fitchen, 1995; Schlager, 2000, 2003; Pomar and Hallock, 2008). For instance, *Planolites*-burrowed wackestone suggests relatively low oxygenation levels that could be attributed to restricted water circulation or an increase in water depth, whereas, a skeletal-peloidal, cross-bedded grainstone would indicate more open marine and higher-energy conditions. Indicator facies are lithofacies deposited at specific water depths and can serve as paleobathemtric markers (Kerans, 1995). Examples of these include chicken-wire anhydrite (supratidal), cryptalgal laminites

(upper intertidal – supratidal), ooid grainstone (intertidal – shallow subtidal). Recognition of these indicator facies helps constrain the lateral facies distribution and how different lithofacies that are time equivalent can be correctly correlated. For instance, ideally cryptalgal laminites will not be correlated basinward to chicken-wire anhydrite as it always occupies the region in front of it and rather will be correlated to the oolites.

Vertical Facies Successions

Vertical facies successions represent the typical repetitive, upward-shallowing succession reflecting the filling of the accommodation space created during cycle-scale sea-level rise (Kerans and Tinker, 1997). The described cores of the upper high-frequency sequence in the Arab D of Qatif field illustrate the repetition of upward-shallowing cycles where subtidal deposits are capped by shallower subtidal, intertidal and/or supratidal deposits. Thus, each cycle records the filling of accommodation created during a low-eustatic-amplitude greenhouse Milankovitch setting. Despite the limited evidence, the cycles are capped by exposure surfaces that become conformable when correlated to relatively deeper parts of the succession. Thus, it is crucial to understand the lateral relationships between indicator and depositional facies when correlating up- or down-dip.

Lithofacies Tract

A lithofacies tract is defined as a genetically linked association of lithofacies and vertical lithofacies successions that records a discrete energy, water depth, sediment supply setting (Kerans and Fitchen, 1995; Kerans and Tinker, 1997), i.e. defined based on the interpretation of the depositional processes. For example, ramp crest, representing the

zone between sea-level and the base of fair-weather wave, can be characterized by skeletal-peloidal shoals, oolitic shoals and/or cryptalgal laminites. Thus, the suite of these facies can be termed as ramp-crest lithofacies tract.

LITHOFACIES DESCRIPTION

The fundamental first step in the modern carbonate reservoir characterization workflow is to describe depositional lithofacies and to develop a depositional model for the given stratigraphic/structural setting. To that end, 762 m of core from 19 wells were described in detail and these descriptions were plotted against wireline log patterns and used as the basis of both depositional and diagenetic frameworks.

Nine major depositional facies have been defined in the Arab D Reservoir of the Qatif Field, forming the basis for interpretation of the environments of deposition (EOD's). However, several diagenetic processes such as cementation, chemical compaction, dissolution and dolomitization have obscured the fine textural details of the original depositional facies in portions of many of the cores. Dolomitization of the Arab D at Qatif is fabric-destructive, obscuring large sections of the depositional fabric of individual cores. In addition, meteoric leaching causes some grainstones to appear as muddy facies as a result of aggrading neomorphism. As a result, the interpretation of the depositional paleoenvironments has been complicated locally. However, the presence of specific faunal assemblages and preserved sedimentary structures from detailed core descriptions of the 19 wells are sufficient to allow for construction of a detailed depositional model. Below I will detail the key attributes of the 9 depositional lithofacies and their diagenetic characteristics, with brief interpretations of depositional environments for each.

Spiculitic Wackestone

The spiculitic wackestone forms thin (5-60 cm) beds of homogeneous grey-tan color. The spiculitic wackestones typically form the base of the Qatif upward-shallowing succession and are then succeeded by *Planolites* lithofacies (see below). The main allochems within the spiculitic wackestone are 45-125 µm monaxon and tetraxon sponge spicules (plate 2.1) of siliceous Demospongia (Clarkson, 1998; Flugel, 2004; Hughes, 2004). The silica is commonly dissolved leaving moldic porosity (2-10%) which later may be cemented by blocky calcite. In cores, the spicule molds may be filled with tar making their identification easy (plate 2.2). In addition, rare foraminifera (Kurnubia), disarticulated ostracods and less common disarticulated brachiopods coexist with the sponge spicules in assemblages that may represent transported small-scale gravity flows. In some wells variable amounts of dolomite crystals (up to 20%) can be found as part of the matrix of the wackestones with crystal size ranging between 20 to 45 microns.

The predominance of mud and a monospecific faunal assemblage is indicative of a stressed, low energy setting interpreted here to be a restricted intrashelf basin. A distinct subfacies of the spiculitic wackestones is represented by thin (5-20cm) beds of darker, organic or clay-rich skeletal wackestone that is most obvious on the wireline logs as distinctive 5-40 cm thick high API gamma count intervals (figure 2.1). These beds are highly traceable and appear to represent short-lived anoxic events within the overall disaerobic deeper water section. These beds combined with the more abundant spiculitic wackestones may represent productivity cycles in the deeper intrashelf basin, analogous to those described by Bottjer et. al (1986) from the Cretaceous of southern England.

Planolites-burrowed Wackestone

The *Planolites*-burrowed lithofacies is characteristically homogenous, light brown to dark grey, bioturbated mudstone to wackestone. These mud-dominated carbonates are characterized by extensive, horizontal, non-branching burrows of *Planolites* (plate 2.1 (D), 2.3) that occur in monospecific assemblages (Alpert, 1975; Pemberton and Frey, 1982; Savrda and Bottjer, 1991). The upper and lower contacts of this lithofacies are conformable and gradual, passing upward into *Thalassinoides*-burrowed MDP and downward to spiculitic wackestone. However, as the ramp progrades and fills available accommodation, the setting at Qatif becomes more restricted and the *Planolites* lithofacies is overlain by pelleted packstones (see below). The main allochems are disarticulated ostracods, echinoderm and brachiopod fragments and up to 2% peloids and some sponge spicules at the base. The main diagenetic feature is partial dolomitization where dolomite rhombs range in size between 25 and 60 microns. The *Planolites* lithofacies in association with the absence of other open marine faunal assemblages suggests that these lithofacies were deposited in a stressed environment in an intrashelf basin where circulation was diminished, likely resulting in elevated salinities and reduced oxygenation. *Planolites* wackestones contain common stylolites coinciding that are interpreted as cycle-scale flooding events and result in a significant increase in gamma ray response (Raspini, 2001) (figure 2.1).

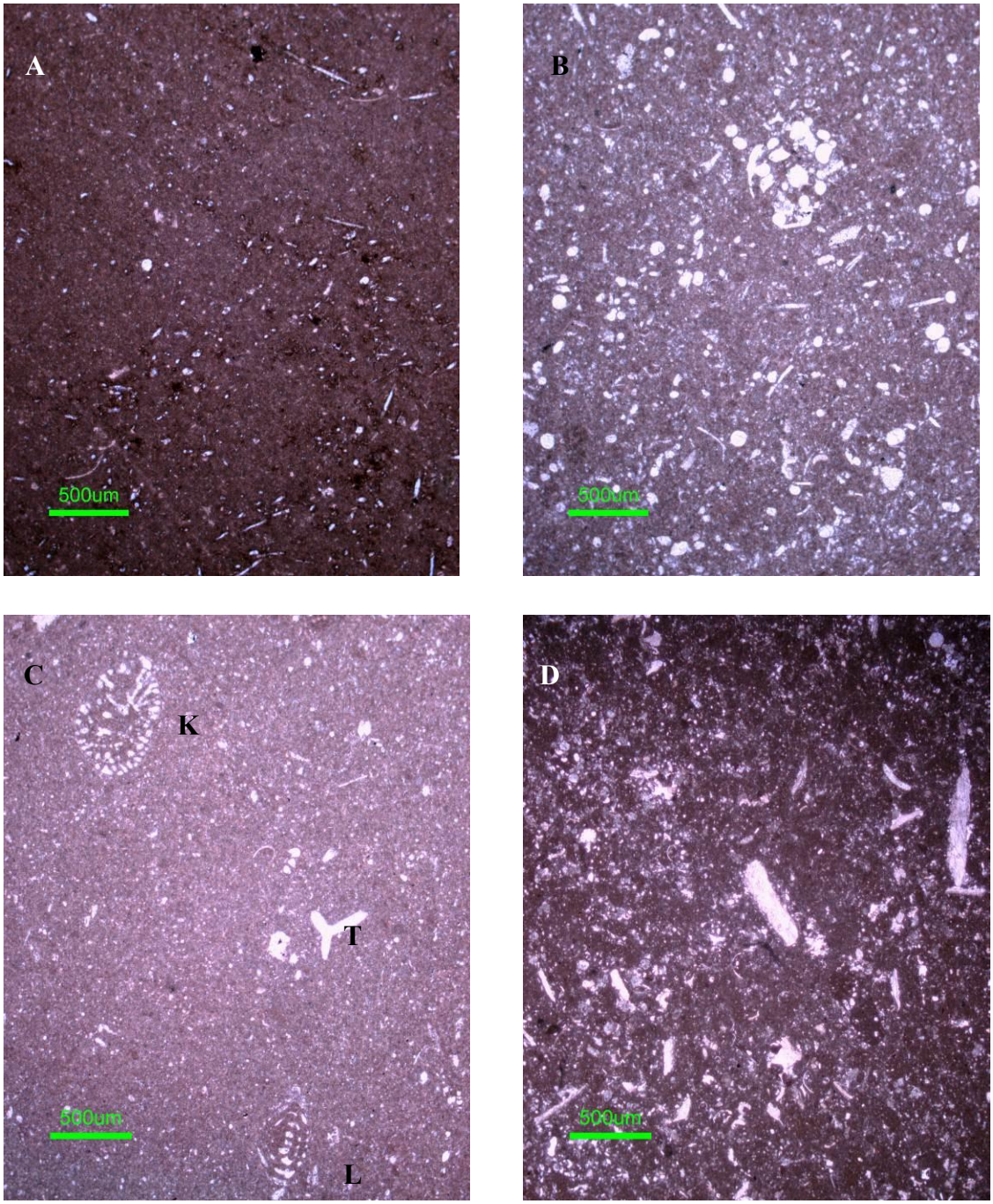

Plate 2. 1: A, B, C show spiculitic wackestone facies photomicrographs. Dissolved spicules (*Tetraxon* (T) and *Monaxon* (M)) create moldic pores (A) that may be filled with calcite (B). *Kurnubia* (K) and *Lenticulina* (L) indicative of deep water conditions. D shows Planolites-burrowed facies photomicrograph.

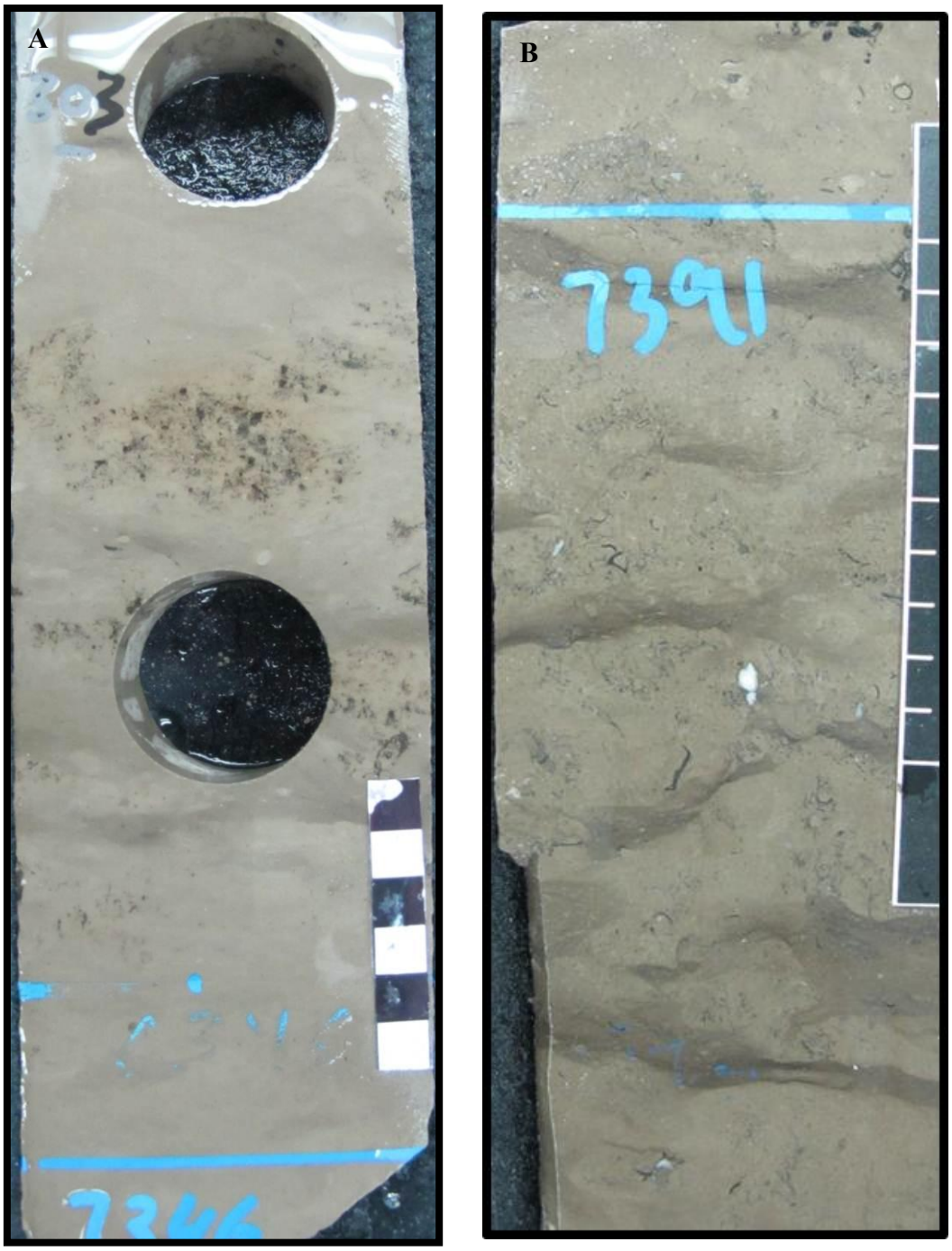

Plate 2. 2: Spiculitic wackestone lithofacies core slabs from well P. Black patches in core slab A are moldic pores filled with tar. Core B shows brachiopods and echinoderms that may have been brought by small-scale gravity flows. Scale bar is in cm.

Plate 2. 3: *Planolites* burrowed wackestone core slabs. A) Burrows churn up sediment creating porosity that is occluded with tar during hydrocarbon migration. B) Planolites lithofacies overlain by rip-up clasts interpreted as small-scale ravinement surface. This horizon is marked by increased GR response (well P). Large stylolite at the base is associated with a significant GR response. Scale bar is in cm.

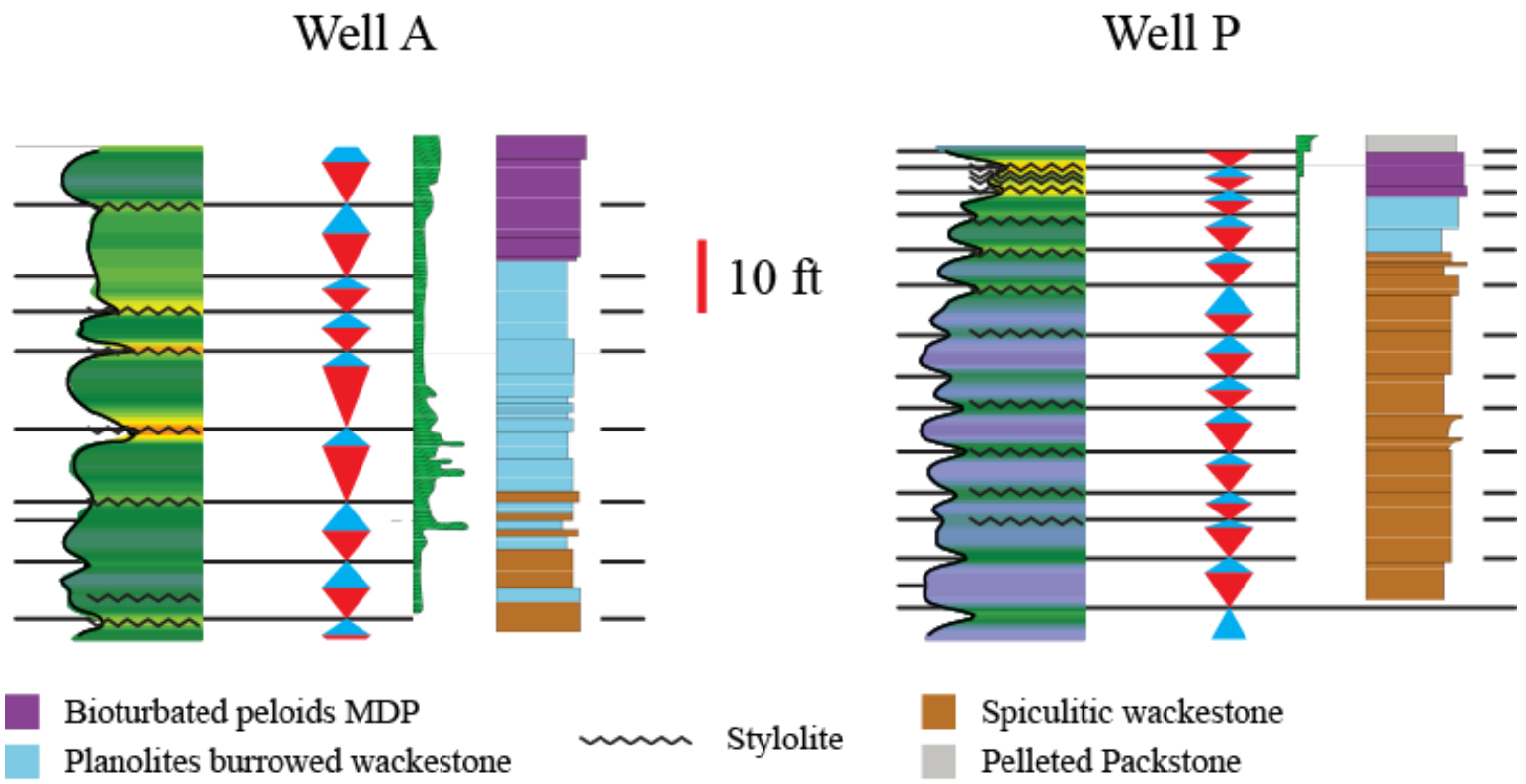

Figure 2. 1: Gamma ray response to spiculitic wackestones and *Planolites* burrowed wackestones. Cycle-scale flooding events are marked by increased gamma ray response at the site where stylolites develop due to changes in depositional conditions

Peloidal Mud-Dominated Packstone

The bioturbated peloidal mud-dominated packstone (MDP) consists of 0.3-2.5 m thick coarsening upward beds where *Thalassinoides* burrows extend from the overlying skeletal GDP (plate 2.4). The peloidal MDP lithofacies is differentiated from the skeletal GDP by the absence of current stratification and from the underlying wackestones by the predominance of peloids and absence of *Planolites*-burrows (plate 2.5). Both the upper and the lower contacts are gradual, where the upper contact marks the base of wave influence and the lower contact marks the increase of environmental stress indicated by the monospecific sponge fauna and *Planolites* bioturbated lithofacies.

The main allochems consist of peloids (10–35%) with common ostracods and echinoderms and rare brachiopods. *Thaumatoporella* and foraminifera (*Pfenderina, Valvulina, Miliolid*) assemblages are also present. The peloidal MDP has very low intraparticle porosity and, in some cases where dolomitized, intercrystalline porosity (2-5 %). The decrease in mud content and the increase of faunal diversity from the underlying beds are indicative of a relatively higher energy depositional setting (plate 2.5). In addition, the higher energy, associated with the increase of open marine fauna and *Thalassinoides* burrows, suggest a better oxygenated shallow marine environment, and thus interpreted as lower shoreface deposits within the fair-weather wave base (Pemberton et. al, 1992; Taylor and Gawthorpe, 1993). In addition, due to their development in the leeward of shelf crest (Rimthan Arch), they are protected from storm influence and hence the absence of any tempestite. The base of peloidal MDP lithofacies is marked by a distinctive gamma ray log response with a consistently higher API reading compared to the overlying skeletal GDP (figure 2.2).

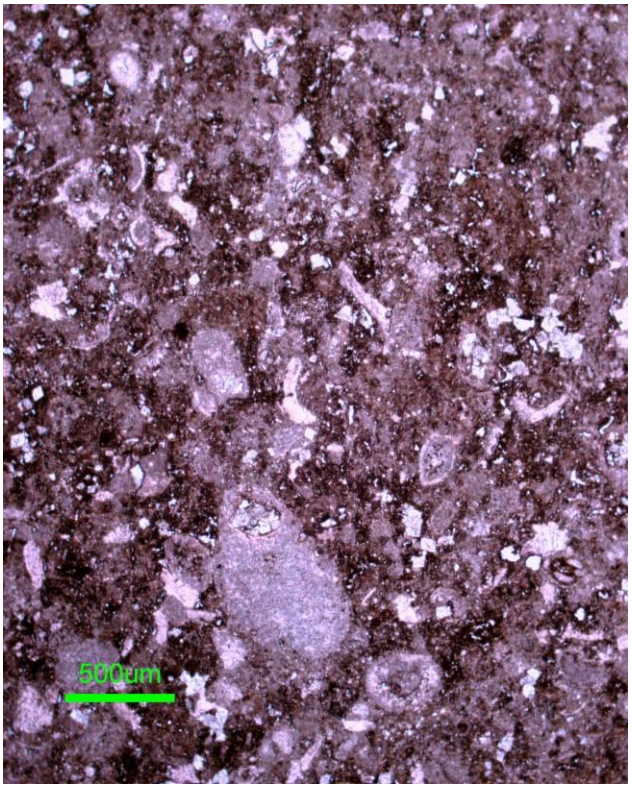

Plate 2. 4: Bioturbated Skeletal-Peloidal MDP core slab and photomicrograph. Core shows different cross sectional views of *Thalassinoides* burrows

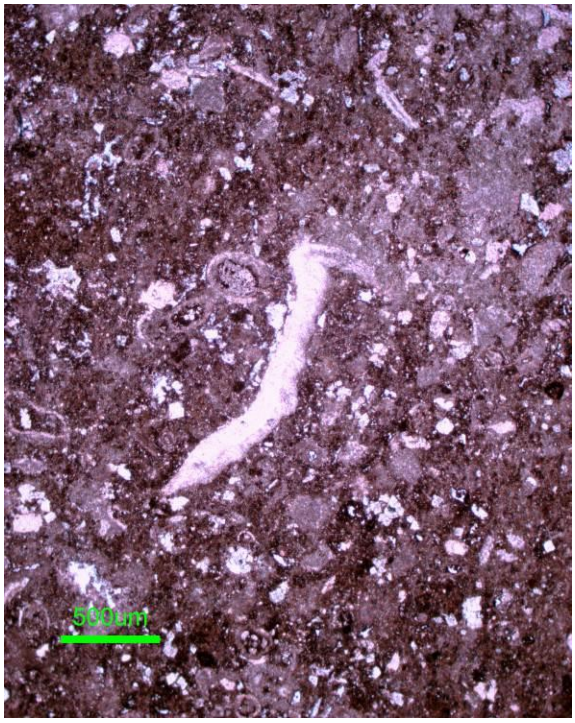

Plate 2. 5: Bioturbated Skeletal-Peloidal MDP photomicrograph and core slab

Skeletal Grain-Dominated Packstone

The skeletal grain-dominated packstone (GDP) consists of 0.3-3.7 m thick units that are planar stratified but weakly bioturbated (plate 2.6). The upper contact is gradational with overlying peloid-skeletal grainstones. Bioturbation is reduced significantly; while the basal contact of the skeletal GDP with the peloidal MDP is recognized by loss of current stratification, marking the lower limit of fair-weather wave base.

The skeletal GDP is composed of abundant, open marine skeletal allochems (15-50%) including abundant Thaumatoporella and common dasycladacean algae (*Clypeina*, *Salpingoporella*) and foraminifera (*Pfenderina, Valvulina, Redmondoides, miliolids*). Other accessory skeletal allochems include rare echinoderms, bivalves, brachiopods and Favreina. While the skeletal GDP constitutes up to 10% lime mud, peloids (15-40%) represent the dominant non-skeletal allochem.

The skeletal GDP lithofacies has 8-18% porosity, mainly well-preserved interparticle and intraparticle porosity as well as some intercrystalline porosity when dolomitized (plate 2.6). The increased sorting relative to underlying mud-dominated packstone and the rounding of open marine grains as well as the presence of bioturbated stratification and some lime mud suggest that this lithofacies was deposited in the middle shoreface environment (MacEachern and Pemberton, 1997). The gamma ray log response shows slightly higher API readings compared to the overlying skeletal grainstone especially if they were representing flooding events marking the base of depositional cycles (figure 2.2).

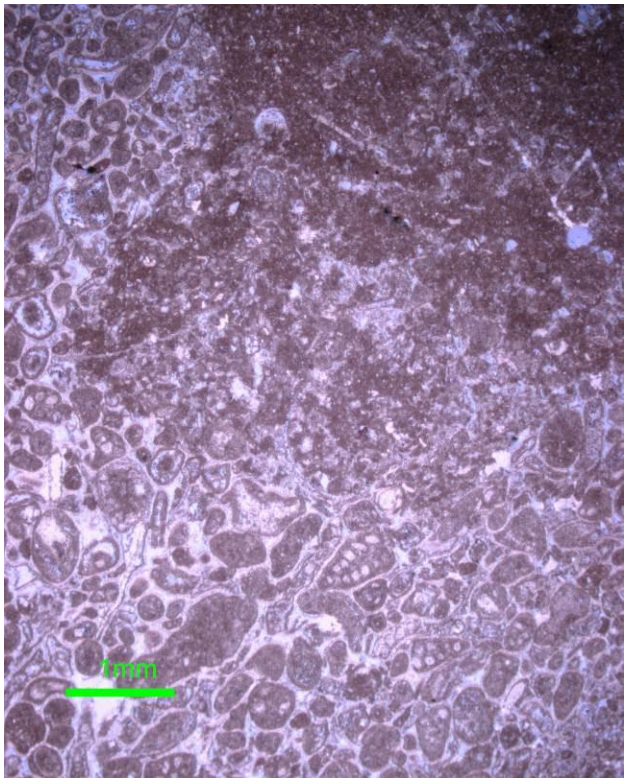

Plate 2. 6: Peloid-skeletal grain-dominated packstone photomicrograph and core slab. Thalassinoides burrows obliterate planar bedding.

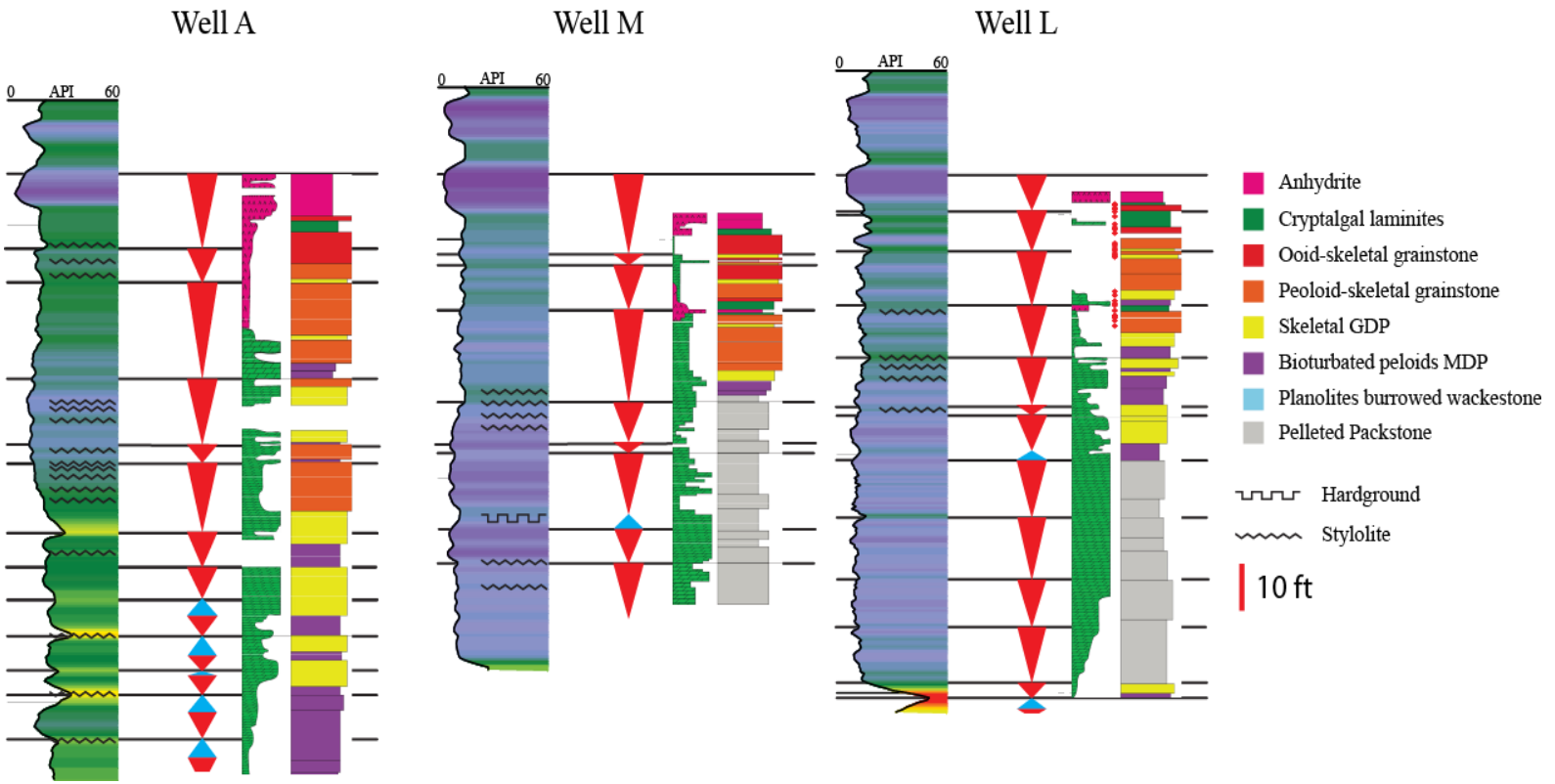

Figure 2. 2: Gamma ray response to different shallow water lithofacies. Gamma ray response increases when coinciding with stylolites. Anhydrite shows distinctive very low API values, while cryptalgal laminites have, generally, higher readings than the anhydrite and the underlying skeletal-ooid grainstone. Maximum flood surfaces within the intrashelf basin, in most cases, will show a slightly elevated API values.

Peloid–Skeletal Grainstone

Units of the peloid-skeletal grainstone lithofacies range in thickness from 0.6-6.5 m and represent the most abundant shallow subtidal lithofacies. These grainstones display well-developed planar lamination and low-angle ripple and trough cross-stratification (plate 2.7). The upper contact of the peloid-skeletal grainstone lithofacies with the ooid-skeletal grainstone is gradual, reflecting progressive shallowing and restriction. Also, the lower contact of the skeletal grainstone is gradational but it is characterized by gradual loss of energy and introduction of *Thalassinoides* burrows defining the underlying unit of bioturbated peloid-skeletal grain-dominated packstone (plate 2.6). The main non-skeletal allochems in the peloid-skeletal grainstone are peloids (30-50%), with accessory ooids (<8%) (plate 2.8). These grainstones contain a diverse assemblage of skeletal allochems including abundant dasycladacean algae (*Clypeina and Salpingoporella*) and *Thaumatoporella* with common foraminifera (*Pfenderina, Redmondoides, Valvulina, Mangashtia, Nautiloculina, Miliolid*) (figure 2.8). Accessory skeletal grains include rare echinoderms, bivalves, brachiopods, *Favreina* and *Prethocoprolithus*.

The peloid-skeletal grainstone lithofacies has 15-25% porosity, consisting of well-preserved interparticle porosity and lesser intraparticle and intraskeletal porosities. However, several diagenetic overprints including, cementation, dolomitization and compaction may ultimately result in significant decrease in original depositional porosity. At cycle tops, isopachous rim cement is commonly associated with vadose-compaction-related fitted-fabric, where grains interlock show concavo-convex contacts and result nullifying porosity (see discussion in diagenesis section). In addition, in the F, N, and O wells, these grainstones are completely dolomitized with well-preserved cross stratifications and intercrystalline porosity (plate 2.9).

The high degree of sorting and rounding as well as the well-developed cross-stratification suggests constant, high energy conditions above fair-weather wave base. Further, the abundance of open marine fauna suggests well-oxygenated conditions shallow marine setting analogous to mixed skeletal-oolitic beaches such as Long Bay beach or Dona Cut in Turks and Caicos (Morgan, 2008). The gamma ray signature of the peloid-skeletal grainstone shows generally low API readings throughout the field (figure 2.2).

Plate 2. 7: : Peloids- skeletal grainstone core slabs showing two different styles of stratification: higher energy cross stratification (A) and planar stratification (B)

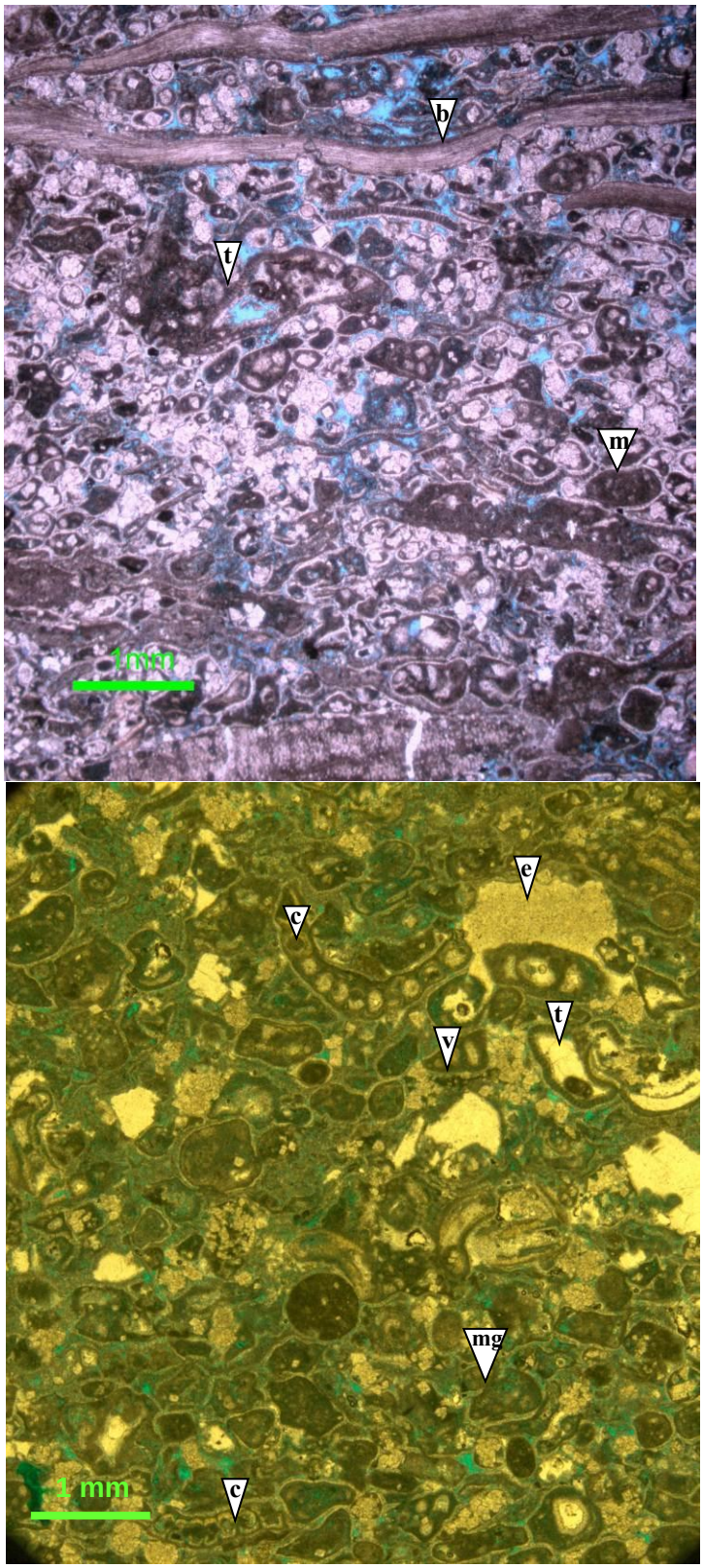

Plate 2. 8: Photomicrographs of the peloids-skeletal grainstone lithofacies displaying brachiopods (b), Thaumatoporella (t), Clypeina Jurassica (s), echinoderm (e), Valvulina (v), miliolid (m) and Mangashtia (mg). Deformation of grains during diagenesis makes the identification of different grains cumbersome.

Plate 2. 9: Completely dolomitized grainstone with well-preserved cross stratification

Pelleted Packstone

The pelleted packstone beds range in thickness between 0.3-1.5 m and represent barren deposits of a restricted basin. These packstones display moderately-developed, very fine parallel laminations and are restricted to the intrashelf basin part of the evolving system (figure 2.18, 2.19). Due to the nature of their distribution, they can be underlain by skeletal GDP or peloidal MDP (figure 2.10). Both the upper and lower contacts are transitional where the lower contact marks the onset of restriction of the intrashelf basin and the upper contact marks the fill of the intrashelf basin. The lower contact is underlain sharply by skeletal GDP and peloidal MDP at wells J, L and P (Plate 1). On the other hand, the sharp upper contact is overlain by cryptalgal laminites (well B), ooid-skeletal grainstones (well C), peloidal MDP and skeletal GDP at different locations in the field (master cross section).

The pelleted packstone lithofacies is typically heavily dolomitized, and non-dolomitized intervals lack the presence of burrows and other faunal assemblages suggesting that the environment was highly stressed. The highly dolomitized zones of the pelleted packstone lithofacies have intercrystalline porosity of 5-12% (figure 2.21). Examples of lath-shaped replacive anhydrite crystals occur in the pellet packstone as discrete crystal pseudomorphs after gypsum.

The absence of burrowing organisms or shelly fauna suggests that the depositional environment was highly stressed. The restricted water circulation and the development of very fine lamination suggest that accumulation of these sediments occurred in quiet waters, potentially in a setting where carbonates are precipitated from solution (Tucker and Wright, 1990). Stylolites are documented at the base of beds with finer grains and higher gamma ray API readings (figure 2.2).

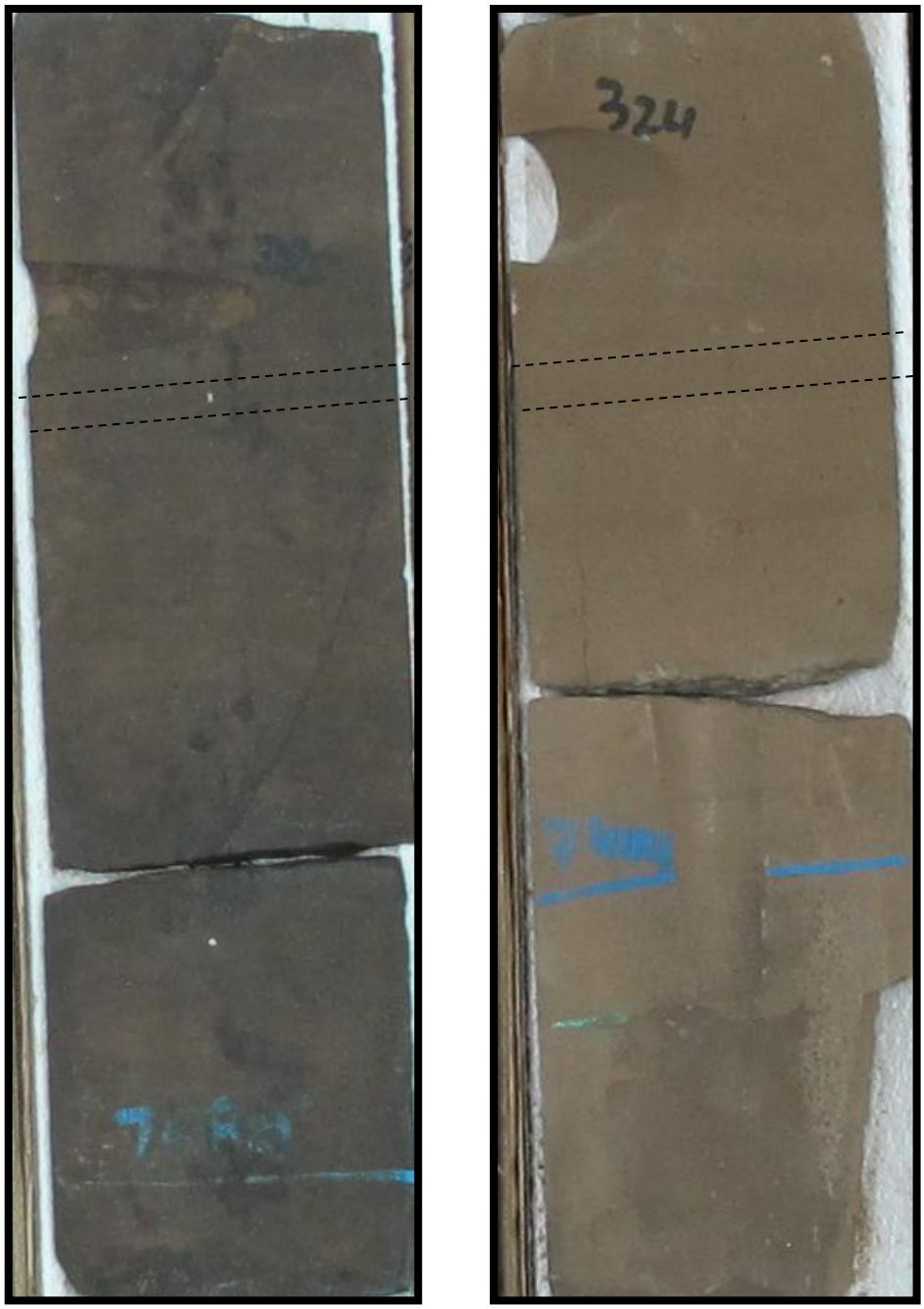

Plate 2. 10: Core slabs of finely laminated pelleted packstone.

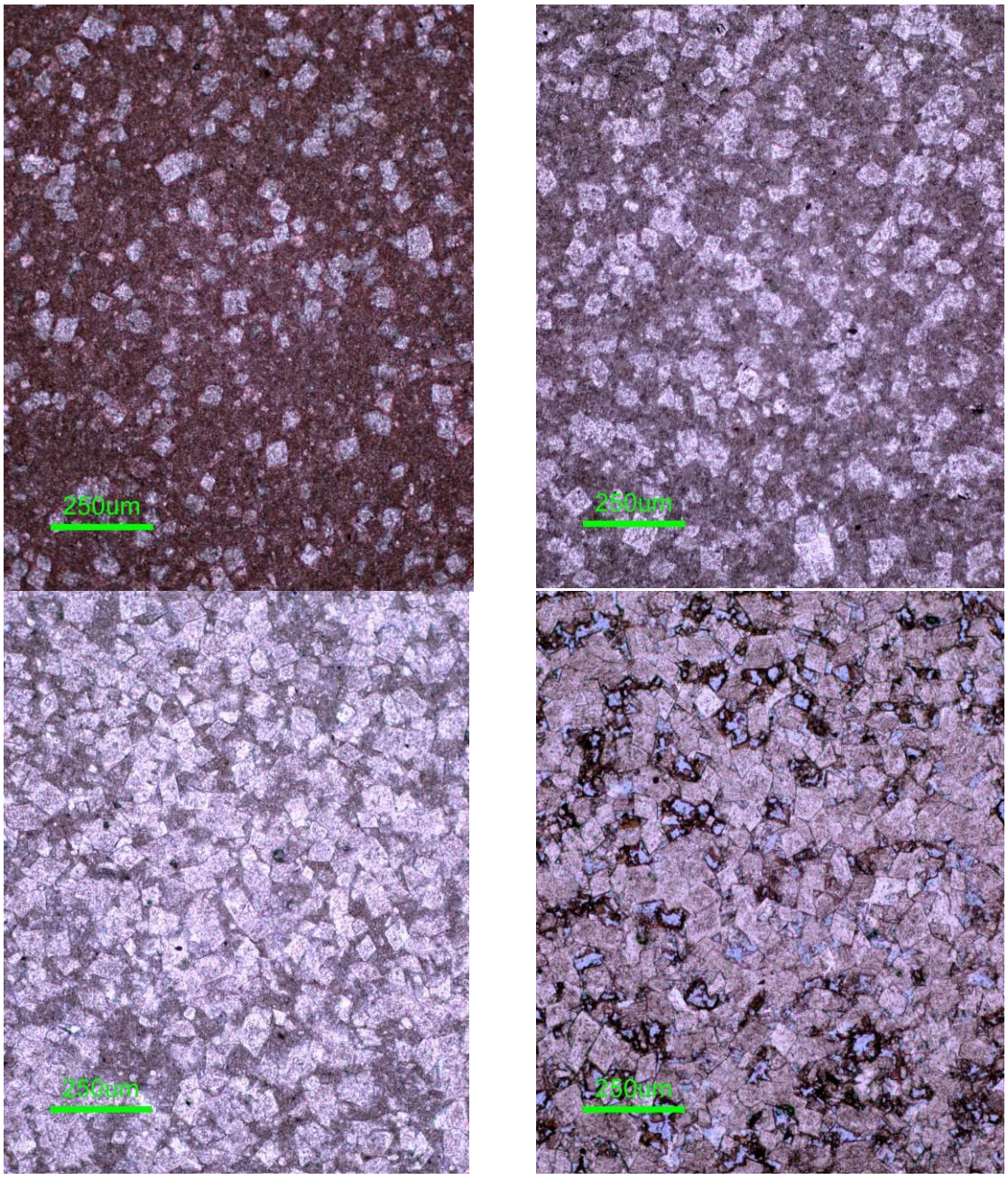

Plate 2. 11: Photomicrographs of the pelleted packstone showing different stages of dolomitization

Skeletal-Ooid Grainstone

Ooid-skeletal grainstone beds are restricted to the upper few cycles of the Arab D reservoir. These grainstones range between 0.3-1.5 m thick and lack well-developed sedimentary structures apart from faint parallel, low angle stratification. The skeletal-ooid grainstones are underlain by subtidal stratified peloid-skeletal grainstones and overlain by cryptalgal laminites. The upper contact shows progressive shallowing and restriction marked by the introduction of anhydrite laths (plate 2.13). Structureless intervals have mottled appearance that may reflect the presence of burrowing organisms, perhaps *Skolithos*, indicative of relatively high-energy settings developed in well-sorted, loose substrate (plate 2.13).

The main non-skeletal allochems in the skeletal-ooid grainstone are ooids which comprise up to 85% of this facies. Ooids in Qatif exhibit cortical leaching separated primarily by very thin, dark layers (plate 2.12). Due to extensive diagenetic overprint of ooids, typing these ooids using the classification of Strasser (1986), whether radial or tangential, cannot be determined with certainty. However, the closest fit is with the type 4, which is interpreted to represent restricted marine with intermittent high energy (figure 2.3) (Strasser 1986). The skeletal allochems including gastropods, foraminifera (*Pfenderina, Redmondoides, Trocholina alpina*) and dasycladacean algae (*Salpingoporella*) increase significantly downward.

The upper-fine to lower-coarse grain size of allochems is consistent with moderate wave energy as is the well-sorted and subrounded to rounded aspect of the grains. In general, the interparticle porosity is high (10-30%), while the intraparticle porosity, created by selective dissolution of the ooids nuclei or other skeletal components, is either open or filled with 50-90 micron dolomite (plate 2.12). Ooids have some intra-grain microporosity but the percentage has not been quantified. Isopachous rim cement,

equant, and syntaxial cements are all observed with this ooid-skeletal grainstone lithofacies. The ooid-skeletal grainstone does not show distinctive gamma ray response, but in general, it is lower than the overlying cryptalgal laminites and slightly higher than the underlying peloid-skeletal grainstones and anhydrites (figure 2.2).

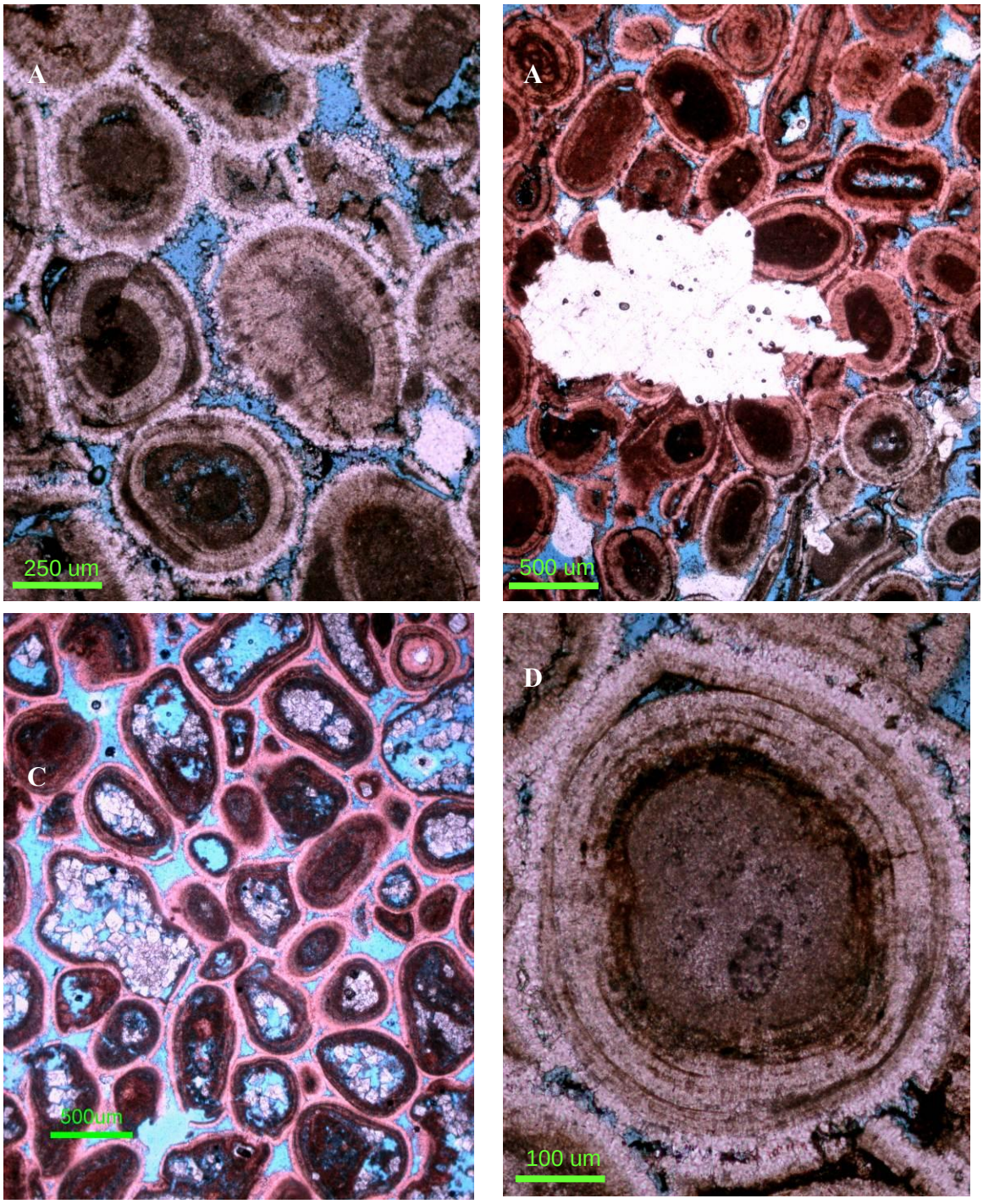

Plate 2. 12: photomicrographs of the skeletal-ooid grainstone. (A) Displays bladed cement and equant cements, (B) shows the precipitation of anhydrite close to exposure surface, (C) superficial ooids, (D) provides strong evidence for the radial fabric of ooids suggesting high Mg-calcite origin

Plate 2. 13: Skeletal-ooid grainstone core slabs showing mottled appearance due to burrowing activities. Salinities were very high and resulted in the precipitation of anhydrite laths (darker spots on core slab

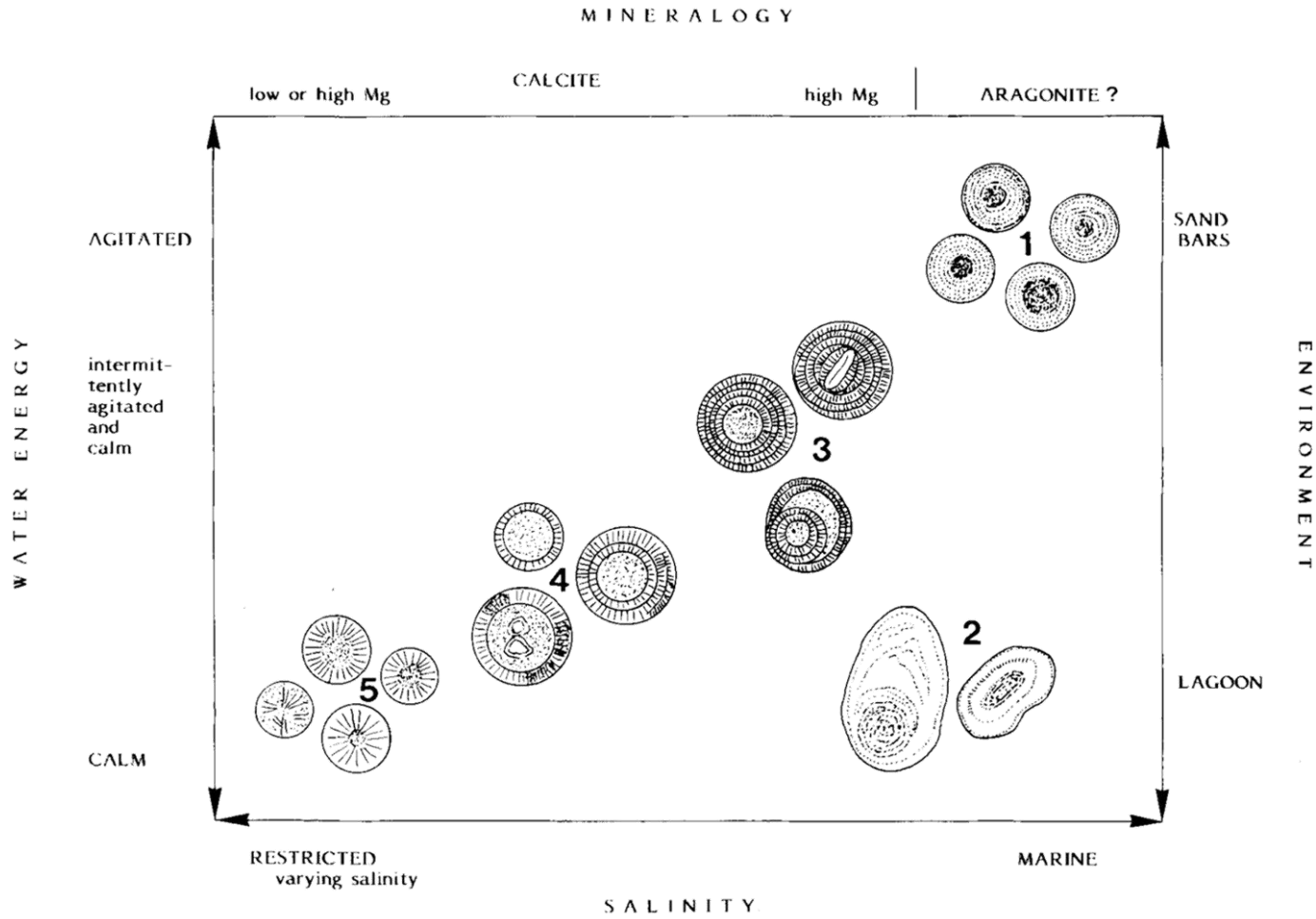

Figure 2. 3: Strasser (1986) classification of ooids forming under different environmental conditions.

Cryptalgal Laminites

The cryptalgal laminate facies consists of beds made up of 1–2 mm thick alternating light and dark-grey lamina, often oil stained (plate 2.14), micrite layers and can be interlayered with anhydrite to form 5–50 cm thick beds. These beds are typically underlain by ooid grainstones and overlain by nodular anhydrite, occurring in cycles of 0.5–2 m thickness. Both, basal and upper, contacts are gradual in nature with a decrease in carbonate at the base and increase in anhydrite at the top. In most cases, the cryptalgal laminites are composed of pure, barren, limestone but can, also, show fine-to-medium grain-sized peloids and ooids.

The cryptalgal laminites and their recognizable sedimentary structures including fenestral cavities and mud cracks place them in the intertidal-supratidal zone (plate 2.15) (Tebbutt et. al, 1965; Kendall and Skipwith, 1968; Assereto and Kendall, 1977; Shinn, 1983). Based on surficial morphologies, distinct vertical zonations can be recognized similar to recent algal mats documented in the Arabian Gulf (figure 2.4) (Kendall and Skipwith, 1968). These zonations in their vertical order include: a) polygonal zone, b) crinkle zone and c) flat zone (plate 2.14). The polygonal zone, intertidal, is characterized by desiccation polygons separating the algal mats where sediment can fill the space created by the curled-up polygons (plate 2.14). The crinkle zone, upper intertidal, has irregular, unsmooth, wrinkled algal mats where it sits above the polygonal zone and under the flat zone. The flat zone, upper intertidal–lower supratidal, has a smooth surface with no topographic that is overlain directly by the nodular anhydrite (plate 2.14).

In thin section, most of the algal mats show low measures of intercrystalline and microporosity in addition to the fenestral porosity. Other allochems observed only from thin section include predominantly *Prethocoprolithus* which further supports placing the

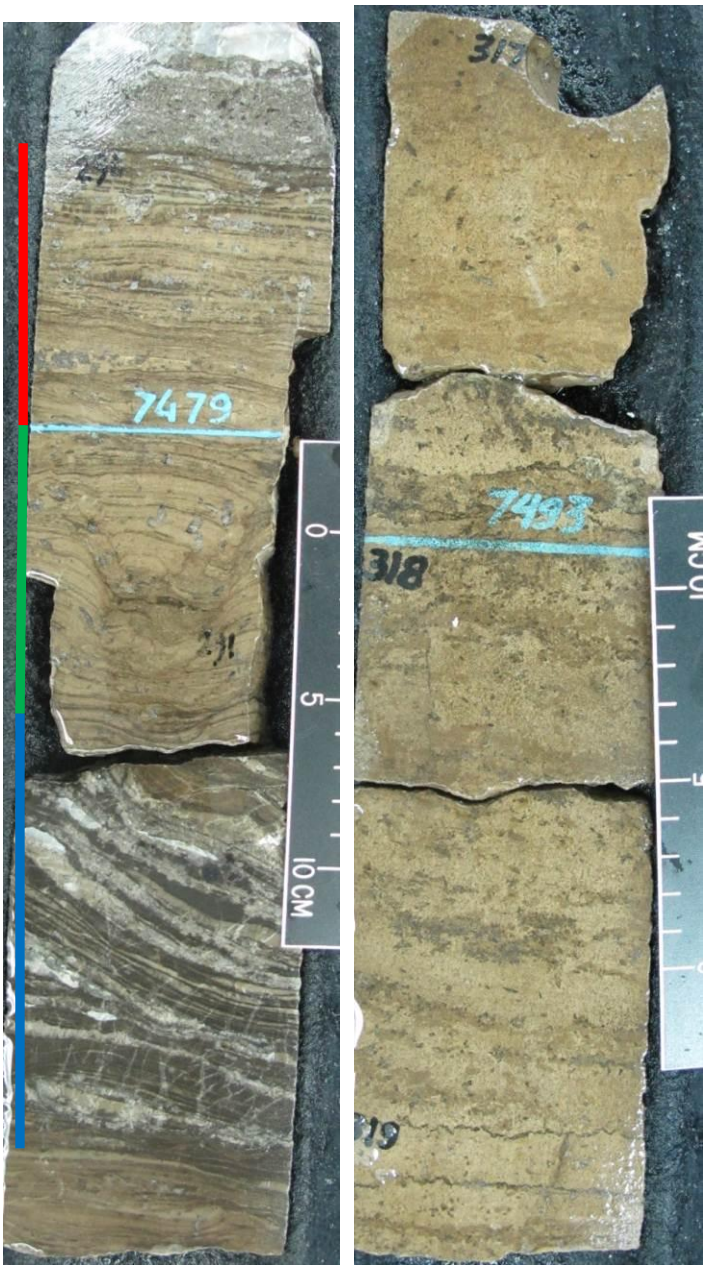

Plate 2. 14: Cryptalgal laminites lithofacies. Core A shows well developed laminite zones showing: *Flat Zone*, *Crinkle Zone* and *Polygonal Zone.* Core B show incipiently forming laminites.

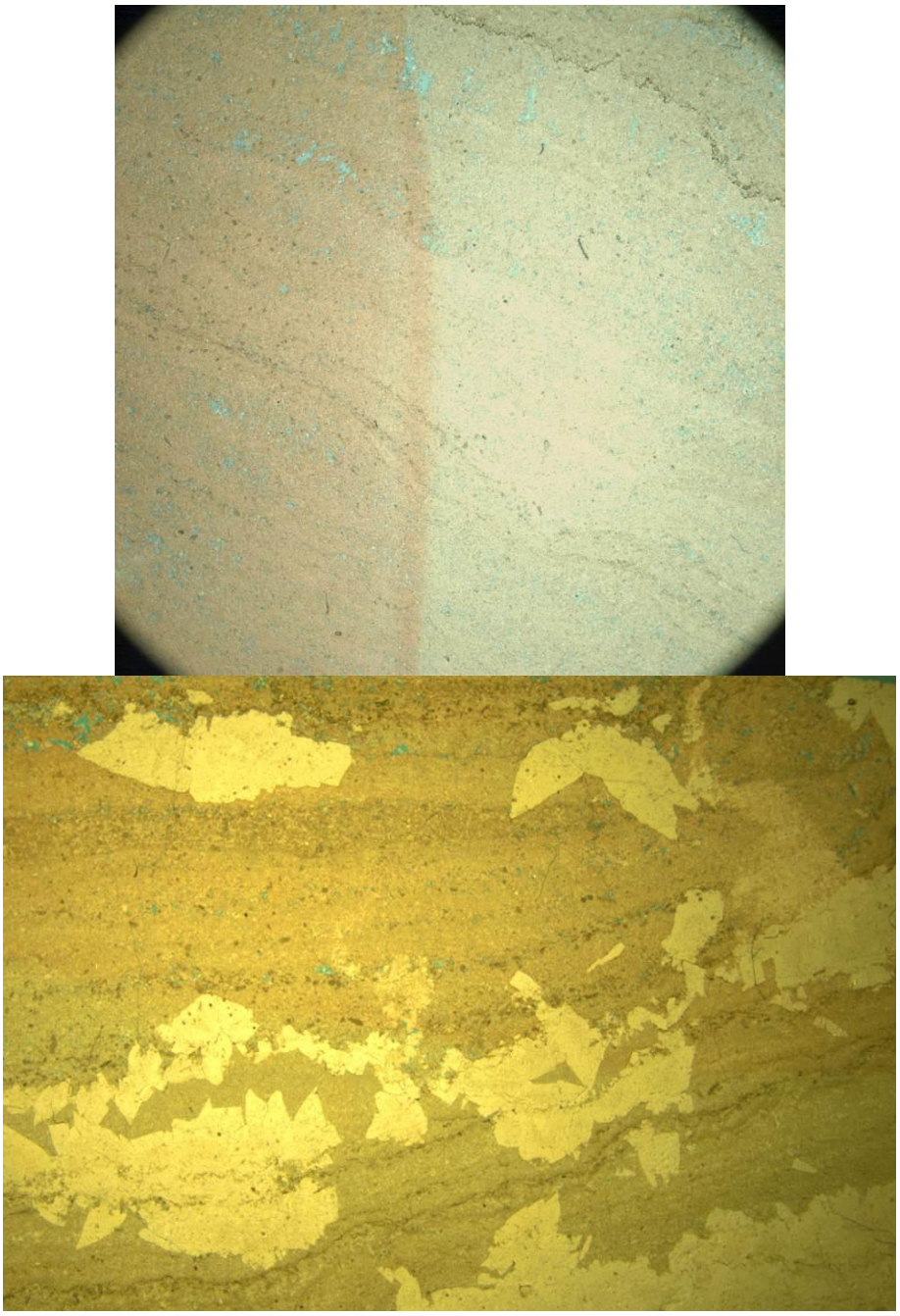

Plate 2. 15: Cryptalgal laminites photomicrographs showing fenestral pores and small scale stylolites (A: FOV=8mm) and displaying interlayering with amorphous anhydrite (B: FOV=15mm).

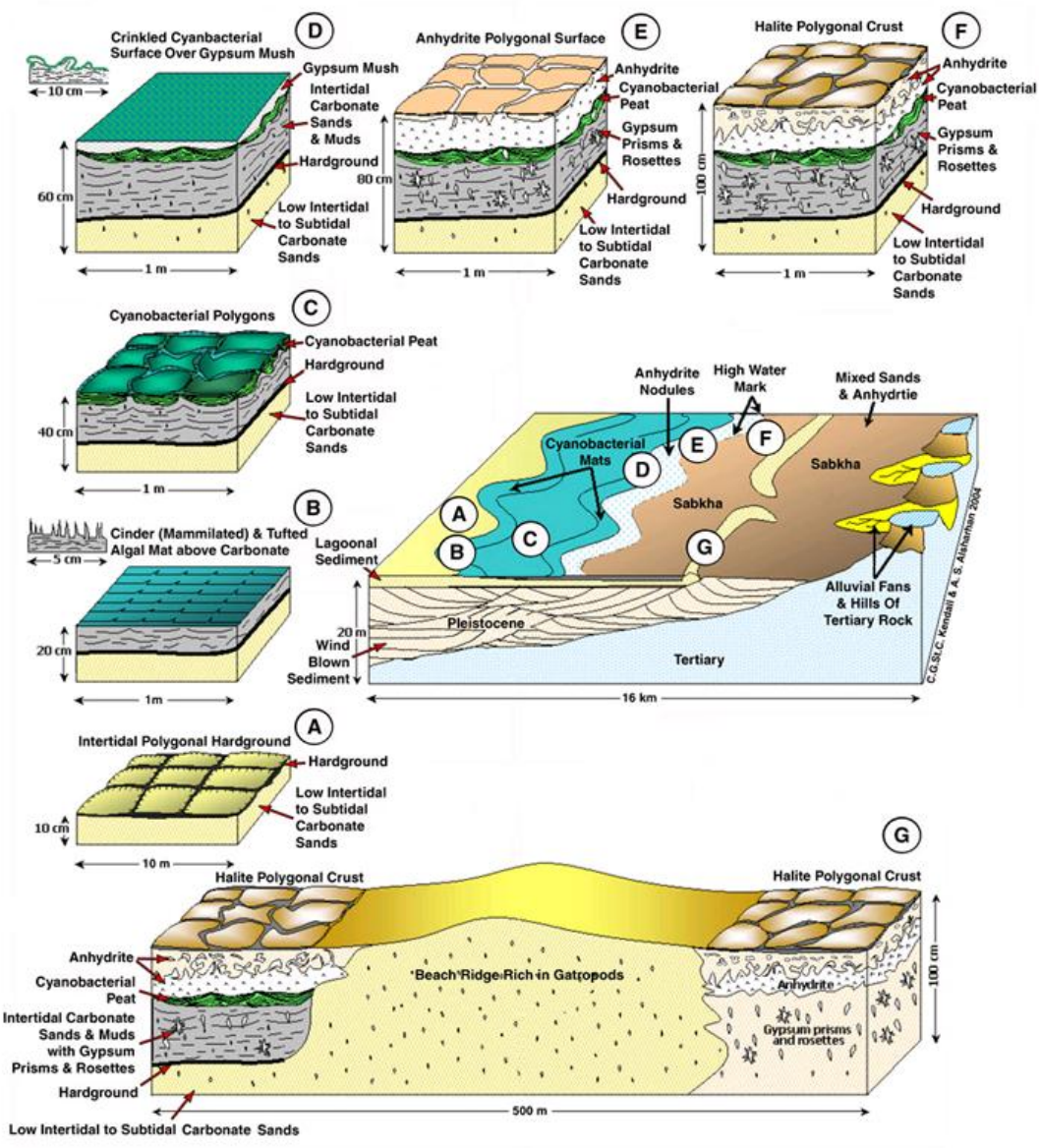

Figure 2. 4: Cryptalgal laminites classification of the Arabian Gulf (Kendall and Skipwith, 1968). In Arab D, a shallowing up cycle will show polygonal mats overlain by crinkle and flat laminites successively and capped by anhydrite (figure 2.25).

cryptalgal laminites lithofacies between the intertidal and lower supratidal settings (Hughes, 2010). The response of increased total gamma ray is locally useful in distinguishing tidal flat facies from more subtidal facies (figure 2.2).

Anhydrite

The anhydrite lithofacies consists of 1.2-3 m thick beds of nodular to palmate anhydrite occurring in the uppermost part of the Arab D reservoir section at Qatif. They are preceded by cryptalgal laminites in cycles of 0.5-2 m thickness. The bedded anhydrite is characterized by gradual contact at the base and sharp contact at the top. The nature of the basal contact signifies progressive, gradual shallowing, while the top contact reflects flooding. The anhydrite displays two distinctive fabrics: a) nodular-mosaic (chicken-wire) anhydrite (Imlay, 1940; Butler, 1970) (plate 2.16) and b) rarely preserved palmate crystals (bottom growth gypsum pseudomorphs) (plate 2.16B). The chicken-wire fabric represents a syndepositional, interstitial growth of displacive anhydrite developed primarily subaerially in a sabkha setting (Kasprzyk, 2003; Warren, 2006). This interpretation is supported by the increase in the size of nodules closer to the upper contact (plate 2.16A). The limited palmate anhydrite observed in the anhydrite develops as gypsum under shallow subaqueous settings and turned into anhydrite during burial by means of dehydration (Warren, 2006). The limited presence of the palmate anhydrite compared to the nodular anhydrite and their lateral continuity suggests that anhydrite developed in sabkha settings rather than salina, and the palmate anhydrite developed in localized depressions where bottom growth structure sometimes is preserved (Kendall and Skipwith, 1968; Warren, 2006).

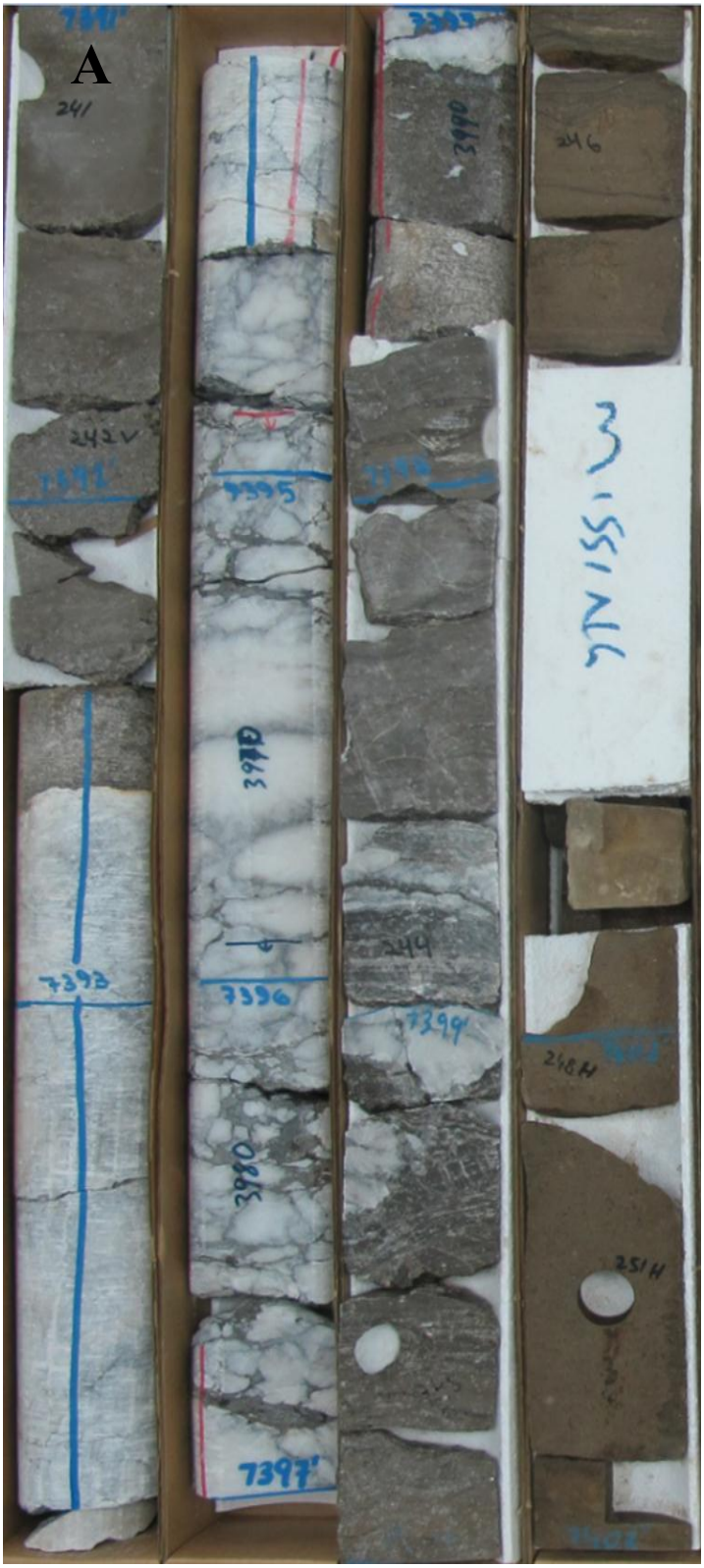

Plate 2. 16: Anhydrite lithofacies develop after progressive restricting conditions indicated by the increase of nodules size and the sharp contact at the top of the anhydrite. In B, it can be shown that some of the crystals may have developed under little depressions or hypersaline ponds.

The anhydrite nodules are separated by thin, dark films of dolomite representing the remnants of sediment in which the nodules grew. Anhydrite beds are recognized by low response on gamma-ray log, lower than limestone, dolomite or sandstone and a high neutron curve value, which indicates little fluid content and little porosity (Ellis and Singer, 2008).

ENVIRONMENTAL INTERPRETATION

DEPOSITIONAL MODEL

The Arab D reservoir at Qatif is composed of nine depositional facies that can be arranged spatially in several 2-dimensional models recording the gradual shoaling and restriction of the shallow ramp/intrashelf basin setting. Existing Arab–D depositional models (discussed in chapter 1) cannot be used directly for Qatif field due to its unique location on the platform. The lithofacies types reflect a range from high energy to low energy hydrodynamic conditions related to gradual increase in water depth. The lithofacies types and their equivocal interpretation of depositional environments, based on stratal context and related facies succession, are listed in table 1.

Four depositional environments are recognized for the previously described depositional lithofacies including: 1) sabkha, 2) foreshore, 3) shoreface, and 4) intrashelf basin.

Intrashelf Basin

The intrashelf basin had two phases of evolution: early and late. The early phase of basinal deposition is represented the spiculitic and *Planolites*- burrowed lithofacies,

while the late phase is represented by the pelleted packstone. The facies-specific phases represent gradual increase in restricted circulation of the intrashelf basin through time.

Early Intrashelf Basin Phase

Despite the fact that demosponges are found in many different environments from warm high-energy intertidal settings to quiet cold abyssal depths (Flugel, 2004), during the deposition of the spiculitic wackestones within the Qatif Arab D, the water depth of the stressed environment would have been between 20-25 m. The available core data reflect that during the early phase of the intrashelf basin, the Qatif field was at a site where the spiculitic facies dominated as the southern fields were prograding to the northeast (see chapter 3). Examples of Demospongia spicules have been documented in New Caledonia in a lagoonal setting where average water depths are 25 m (Clavier and Garrigue, 1999; Dupouy et al., 2010). The occurrence of monaxon and tetraxon sponge spicules in the absence of normal marine faunal assemblages is consistent with the interpretation that these spiculitic wackestone to mudstones were deposited in poorly oxygenated environments in moderately deep water(~25–35 m) (Saller et al., 1994; Elrick, 1996; Hughes 1996, 2004, 2009, Muller et al., 2004). Further, the presence of Kurnubia and brachiopods may indicate dysaerobic depositional zone never reaching anaerobic conditions (Savrda and Bottjer, 1987). In addition, the presence of *Lenticulina*, along with *Kurnubia*, suggests deep, mud dominated settings (Hughes, 2004).

Under the same depositional settings at slightly shallower depth, the *Planolites* lithofacies occurs above the spiculitic wackestone. The abundance of *Planolites* burrows along with the reduction of faunal diversity suggests opportunistic behavior pointing to some environmental stress. The presence of the *Planolites* in an intrashelf basin that

become progressively restricted (figure 2.7) suggests the bottom would have been hypersaline, stagnant and dysoxic, slightly more oxygenated than the spiculitic lithofacies. In addition, the environmental stress can be enhanced by lowered oxygenation in these dense, hypersaline, stagnant, bottom waters (Ekdale, 1984; Hughes, 1996; Milsom and Rigby, 2004; Miller. 2007). However, the cores do not contain *Chondrites,* which is common in poorly oxygenated fine-grained sediments (Bromley and Ekdale, 1984) which suggest that environmental conditions were much more important than water depth (~ 15-< 25 m) (Hasiotos personal comm.). Figure 2.5 provides an idealized depositional model showing the relationship between these two facies during this early phase.

Late Intrashelf Basin Phase

The late phase of the intrashelf basin is represented by a shallow depression (<20m) that extended from the North Dome of Abqiq Field to the central southern part of Qatif Field and was filled with barren, finely laminated pelleted packstone (figure 2.6). The absence of fauna suggests that the environmental setting has become too restricted and stressed to allow biomass diversity. In addition, in Fazran Field, southwest of Qatif Field, this unit is overlain by anhydrite that extends to the southern tip of Samin Field, west of Qatif Field, (Kerans personal comm.) which further suggests the existence of increased hypersalinity. As a result, the physiological efficiency of organisms is restrained under hypersaline conditions and can inhibit or limit the establishment and primary production of many species (Souza et al., 2003).

Three main hypotheses have been proposed to explain the origin of shallow-water carbonate mud/pelleted mud, 1) degradation of calcareous algae (Lowenstam and Epstein, 1957, Stockman et al., 1967), 2) degradation of other skeletal grains through

bioerosion, and 3) precipitation of aragonite needle muds directly from the water column "whitings" (Shinn et al., 1989; Milliman et al., 1993; Robbins et al., 1997). In the Qatif setting, the hypotheses that carbonate may originate by disintegration of calcareous algae (Lowenstam and Epstein, 1957; Stockman et al., 1967; Neumann and Land, 1975) or by the biomechanical breakdown of shell materials (Mathews, 1966) are rejected since there is no physical evidence that either calcareous algae or skeletal grains were present. For example, the fine-grained aragonite in nearshore sediments off the Trucial Coast is barren since calcareous algae do not grow in the Arabian Gulf (Kinsman, 1964). The direct precipitation hypothesis suggest aragonite needle muds precipitate out of seawater as whitings either inorganically (Black, 1933; Cloud 1962; Shinn et al., 1989; Steinen et al., 1988; Milliman et al., 1993, Friedman, 1994) or by biologically-induced precipitation from whitings (Robbins and Blackwelder, 1992). The inorganic precipitation of carbonates requires supersaturation with respect to calcium carbonate aided by high water temperatures and salinities (Milliman et al., 1969; Milliman and Müller, 1977).This proposition is rejected because the deposited that result from whitings will be preserved as mud rather than fossil-barren pellets.

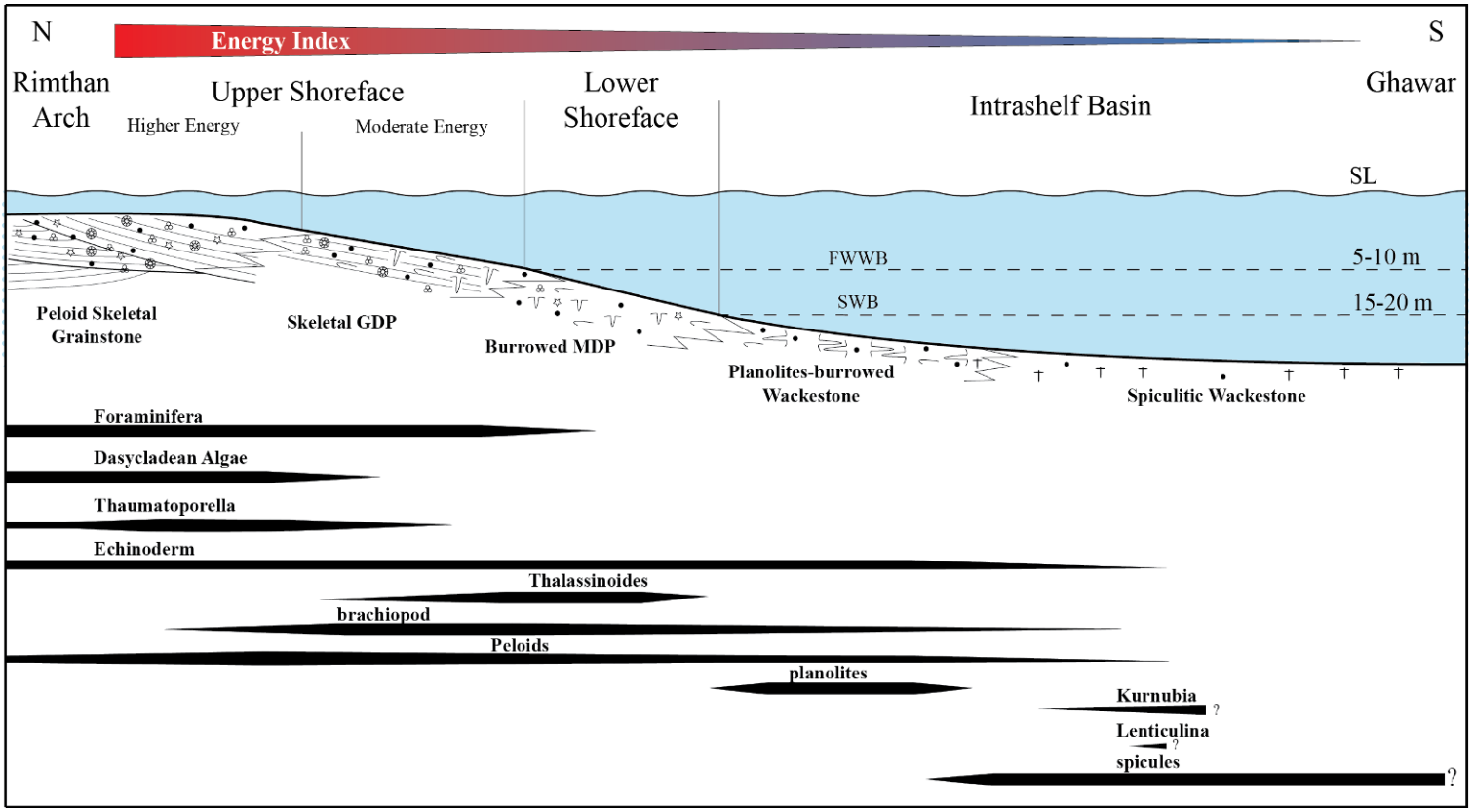

Figure 2. 5: Idealized depositional model during the early phase of the intrashelf basin displaying sea-level (SL), fair-weather wave base (FWWB), storm wave base (SWB) and the lateral relationship between

The third hypothesis suggests that barren carbonate deposits may be induced microbially. Similar deposits were reported from a Messinian hypersaline setting in the Caltanissetta Basin, Sicily (Oliveri et al., 2009) and the modern hypersaline Al-Khiran Lagoon in Kuwait (Gunatilaka et al., 1984). The precipitation of these carbonate deposits is attributed to microbially induced and controlled processes (Riding, 2000). Bacteria play a key role in carbonate precipitation in a broad range of environmental settings (Chafetz and Folk, 1984; Chafetz 1986, 1994) which has been proven by laboratory experiments (Krumbein, 1979). Stromatolite microfabrics resembling peloids and micritic pellet grainstones (Buczynski and Chafetz, 1991; Riding and Tomás, 2006) reflect a combination of microbial growth, decomposition and lithification (Grotzinger and Knoll, 1999; Reid et al., 2000) in both ancient (Sun and Wright, 1989) and modern environments (plate 2.17) (Montaggioni and Camoin, 1993).

In hypersaline, arid environments, a high evaporation rate will provide Mg^{2+}, Ca^{2+}, CO_3^{2-} and SO_4^{2-} ions in solution, in which Mg^{2+} and SO_4^{2-} are held together in space like a single particle (Bagotzky, 1993) as strong ion pairs (Vasconcelos and McKenzie, 1997). Sulfate reducing bacteria (SRB) are "essentially anaerobic micro-organisms that oxidize simple organic compounds using sulfate as an electron acceptor resulting in the formation of sulfide" (Stal, 2000). The SRB promotes calcium carbonate precipitation through sulfur metabolism in low oxygen level conditions (equation 1) and in anoxic conditions (equation 2) where sulfur reduction through anoxygenic phototrophs produces carbonate. On the other hand, the reverse is true, aerobic heterotrophs (equation 3) and sulfate oxidizing bacteria (SOB) (equation 4) promotes calcium carbonate dissolution and the system tends to form evaporites (Dupraz and Visscher, 2005).

$3HS^- + 4O_2 + CaCO_3 + HCO_3^- \rightarrow 2[CH_2O] + Ca^{2+} + 3SO_4^{2-}$

$(1 - SO_4^{2-}$ Oxidizers)

$3HCO_3^- + Ca^{2+} + HS^- \rightarrow [CH_2O] + CaCO_3 + SO_4^{2-}$

(2–Anoxygenic Phototrophs)

$2[CH_2O] + SO_4^{2-} + OH^- + Ca^{2+} \rightarrow CaCO_3 + CO_2 + 2H_2O + HS^-$

$(3 - SO_4^{2-}$ Reducers)

$[CH_2O] + CaCO_3 + O_2 \rightarrow HCO_3^- + Ca^{2+}$

(4–Aerobic Heterotrophs)

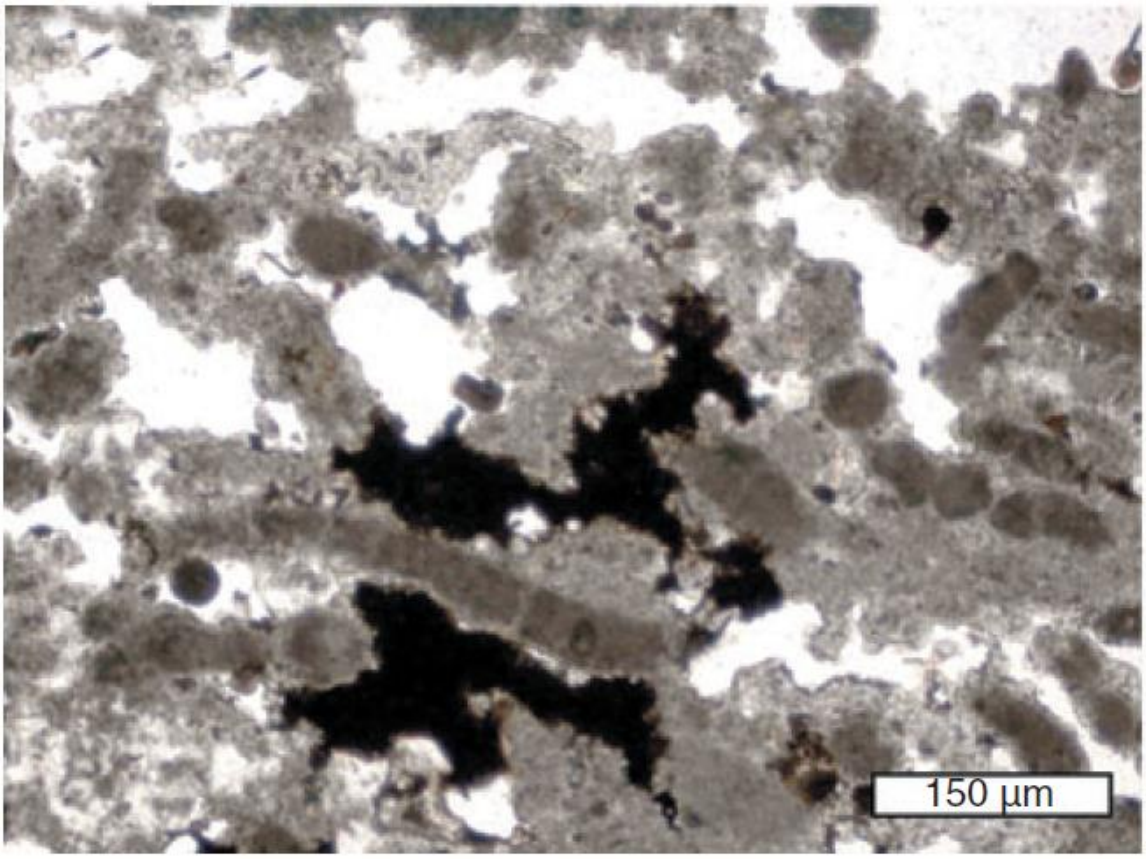

Plate 2. 17: Stromatolites in thin section showing dolomicrite and filaments, with voids partially filled by black amorphous matter and displays the development of pellets (from Oliveri et al., 2010)

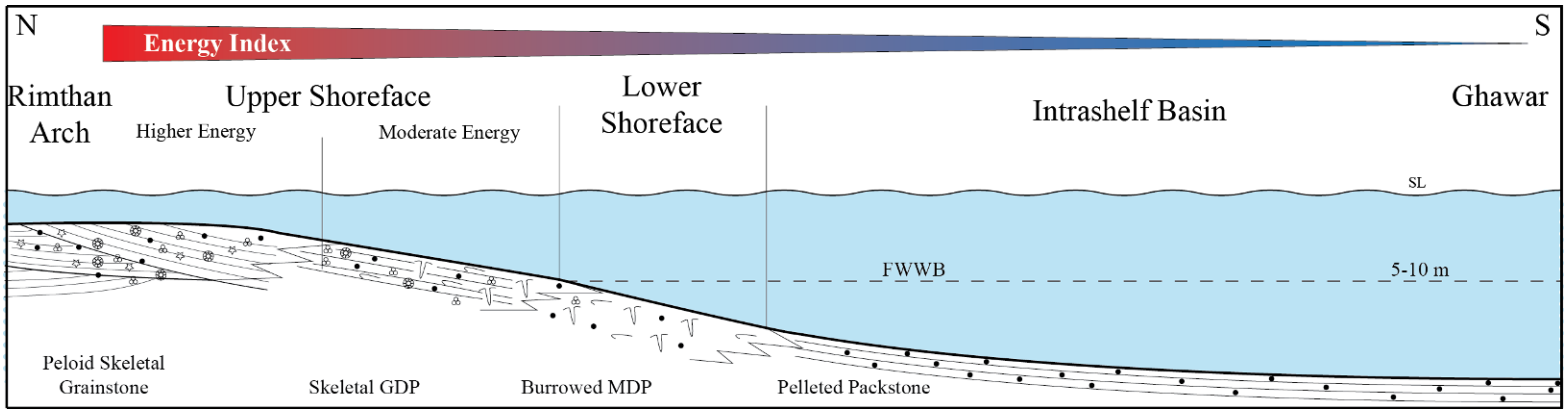

Figure 2. 6: Late phase of restriction of the intrashelf basin where the intrashelf basin is dominated by finely laminated pelleted packstone

The Lower Shoreface

The lower shoreface setting represents the area where the effect of waves is very limited so the effect of storms and offshore process may also be of significant importance (Einsele, 2000). The lower shoreface represents the depositional site of the bioturbated skeletal-peloidal MDP. On a depositional profile, this lithofacies would be located above average storm wave base (SWB) so that it would be influenced by storms occasionally (Buatois et al., 1999). However, the site where peloidal MDP was deposited in Qatif field was not affected by storms. This is due partly to the shelf configuration but also to existence of these lithofacies in intrashelf basin settings where storms would break at the shelf margin hundreds of kilometers to the east (figure 2.7) and its energy is further dispersed at the Rimthan Arch. The skeletal peloidal MDP shows a significant increase in mud content, deterioration of sorting and flourishing of *Thalassinoides* burrowing (figure 2.5, 2.6). The allochems present including echinoderms, foraminifera (*Pfenderina, Valvulina, Miliolid*), brachiopods and ostracods are indicative of open marine conditions. Moving further down-dip and seaward, the diversity of the biocomponents becomes limited to some brachiopods and echinoderms while *Thalassinoides* persist throughout. This suggests that the ecological niche is becoming more restricted. Storm beds are present in few wells. The paleobathymetry of these facies is estimated to be between 10–15 meters of water depth.

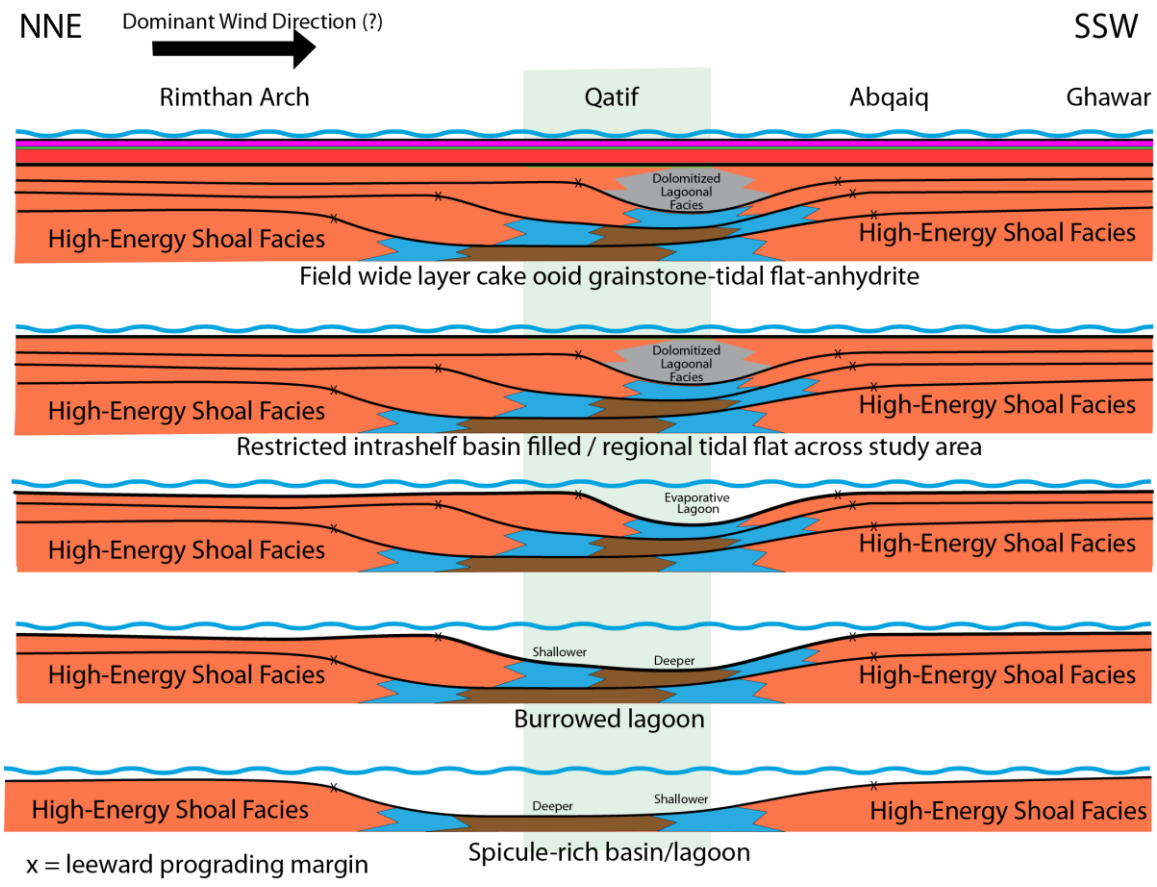

Figure 2. 7: Schematic representation of the evolution of the Arab D in Qatif. It shows the progressive restriction of the intrashelf basin

The Upper Shoreface

The upper shoreface represents the zone that is constantly affected by wave action and currents' activity under normal conditions (figure 2.5, 2.6). It is characterized by trough or high angle (<15˚) cross stratification resulting of bed migration in the direction of longshore current, while perpendicular to the beach accretion direction (Stricklin and Smith, 1973). Due to the high energy nature of the upper shoreface, the depositional lithofacies often lack mud. The upper shoreface is represented by a vertical succession of skeletal GDP lithofacies that are overlain by peloidal-skeletal grainstones. A diverse open marine fauna including dasycladacean algae (*Clypeina* and *Salpingoporella*), *Thaumatoporella* and agglutinated foraminifera is indicative of well circulated, shallow waters. However, *Clypeina, Thaumatoporella, Pfenderina* and *Mangashtia* are specific organisms that occur relatively at deeper settings relative to *Trocholina alpina* (Hughes personal comm.).

The maximum fair weather wave energy decreases as depth increases until its influence is absent below the intersection of the wave base with the submarine topography, i.e. at the FWWB. Thus, the relatively moderate energy, upper shoreface is characterized by low-angle planar stratified beds that are often obliterated by bioturbation and trace fossils (Prothero and Schwab, 1996; Buatois et al., 1999). This zone is marked by first appearance of *Thalassinoides* burrows such that irregularly inclined to vertical cylindrical network of burrow components cross cuts developed stratification (figure 2.5, 2.6). The faunal communities are similar to the higher energy upper shoreface except that burrowing activities result in a reduced sorting and mud introduction. However, despite the introduction of mud through digestion of sediment and excreting them as finger sediments, the rock petrophysical properties are not affected significantly from the peloidal-skeletal grainstone.

The abundance of the *Pfenderina, Clypeina* and *Thalassinoides* as well as the absence of *Mangashtia* suggests that these beds where deposited at 5 – 10 meters of water depth (Hughes, 1996, 2004, personal comm.).

Foreshore

Foreshore sediments are characterized by low angle, seaward dipping, planar-stratified beds (Figure 2.8) affected by the swash and backwash of the breaker comprising the zone between low and high tides (McCubbin, 1982). The reduction in water column height, as the wave front approaches the shore, results in a decrease of wave's speed and length and an increase in its height. As the wave enters the zone of wave buildup, the crest of spilling wave slide down the face of the wave as it breaks on the shore. Thus, the foreshore zone deposits will be dominated by wave swash. In the Late Kimmeridgian, the energy levels of waves were probably very high due to the long fetches they had resulting in high energy shorelines despite the energy dissipation rate (Markello et al., 2008). The foreshore is represented by finely laminated, skeletal-ooid grainstones. In addition, it is important to note that the presence of *Skolithos*, vertical cylindrical dwelling burrows occupying very shallow, high energy depositional environments, has a profound effect on primary depositional features, obliterate stratification and other detailed lithological variations giving rise to the mottled appearance (Frey, 1975; Bromley, 1996; Pemberton et. al, 2001; McIlroy, 2004; Miller, 2007). Moreover, sporadic presence of *Salpingoporella, Trocholina* and *Redmondoides* with oolitic coating suggests freshening episodes, allowing normal marine fauna to exist, or current energy was sufficient to transport them to the foreshore. The presence of *Trocholina* species is indicative of very

shallow marine environment 0-3 meters of water depth (Clifton et. al, 1971; Inden and Moore, 1983; 1996, 2004, Hughes personal comm.).

The Early Cretaceous Cow Creek is a classic example where similar sedimentary structures and carbonate beach facies relations can be observed, except that the back-beach berm, landward dipping beds, is not developed, or not recognized, but rather equivalent to the sabkha deposits (Kerans and Loucks, 2002).

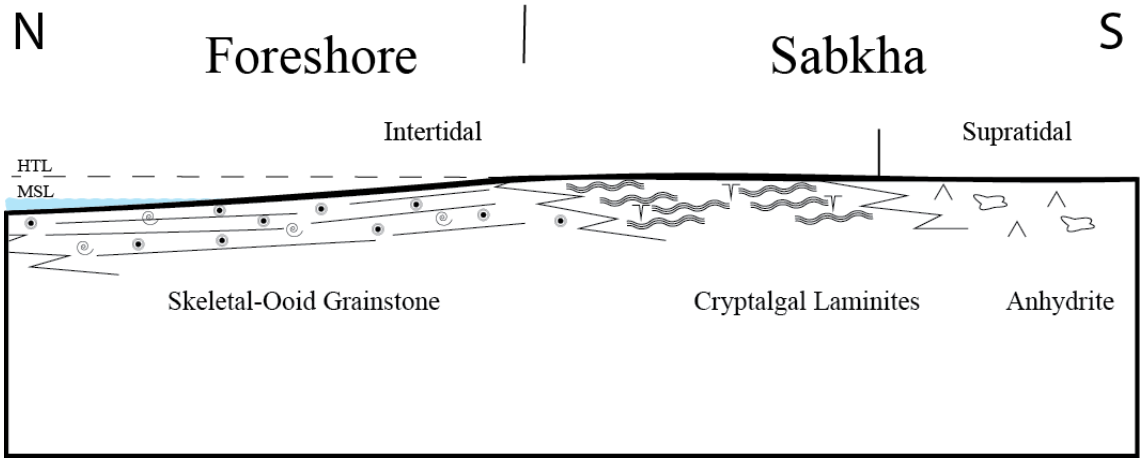

Figure 2. 8: Hypothetical depositional model of the foreshore and sabkha environments in Qatif. The correlation panel shows an apparent layer-cake stratigraphy

Sabkha

In Qatif field, the sabkha environment is composed of two basic subenvironments: 1) supratidal, and 2) intertidal. The supratidal deposits are represented by the nodular anhydrite lithofacies where it is deposited above mean high tide and subaerially exposed most of the time, except during spring and storm tides. The intertidal zone represents the sediments deposited in the area between mean low tide and mean high tide which is exposed once or twice daily.

***Sabkha:* Intertidal Zone**

The intertidal environment represents the zone between the low and the high tide that is exposed twice a day. It represents the site at which cryptalgal laminites were deposited. At this site, three sedimentary structures suggest the interpretation that the cryptalgal laminites lithofacies were deposited under intertidal settings: 1) stromatolitic laminations, 2) mud cracks and 3) fenestral pores. The stromatolites are laminated benthic microbial deposits (Riding, 1999) and are a product of both physical sedimentation and biological processes (Ginsburg, 1991). Three distinct zones have been recognized as analogous to the algal mats of the Trucial Coast (Kendall and Skipwith 1968) including: a) flat zone, b) crinkle zone and c) polygonal zone (figure 2.4). Although, core slabs examined under binocular microscope appear to lack faunal communities, in thin sections rare abundances of *Prethocoprolithus* fecal pellets are present. The *Prethocoprolithus* is indicative of lower supratidal to intertidal settings (Hughes 2010) and stromatolites are used to infer a shallow, stressed environment where these salinity-tolerant microbial forms were growing (Kershaw, 1994).

Mud cracks are not very common but they are found coexisting with the flat-cryptalgal laminite zone. Mud cracks develop due to the desiccation and shrinkage of

carbonate mud related to wetting and drying of tidal processes. They are commonly filled with anhydritic cement. This suggests that these structures develop in supratidal to upper intertidal settings. The last sedimentary structure is the fenestral pores which are associated with algal mat deposits and are thought to form by organic decay along laminations, a common feature in the upper intertidal zone (Shinn 1968, Tucker & Wright 1990). In general, the fenestral pores preservation is variable, but most of the time they are filled anhydrite or calcite cements.

***Sabkha:* Supratidal Zone**

This setting represents the shallowest facies of the succession, and is composed of two main subenvironments that cap the last few shallowing-up cycles: supratidal and intertidal. The supratidal zone refers to the zone above the mean sea level or high tide level. It is exposed most of the time and only becomes submergent during spring tides or storm floods. In the Arab D, this setting is represented by a sabkha depositional setting where the predominant depositional lithofacies are nodular anhydrites with chickenwire textures occurring above the water table (Warren, 2006). These depositional facies typify the supratidal setting of a coastal sabkha in modern analogs such as the Trucial Coast, where minimal submergence and frequent exposure and evaporation occur (Kendall and Skipwith, 1968; Shinn, 1983; Kendall et. al 1994; Kirkham 1997). The chickenwire texture of the nodular anhydrite is believed to form as gypsum mush in soft mud that is later displaced by anhydrite and the trapped sediments between the nodules give the specific texture (Butler, 1970). Thin carbonate layers maybe present within the anhydrite and these maybe attributed to dissolution episodes during minor transgressions or flooding events. In addition, the dissolution surfaces may be explained by continuous

growth of anhydrite nodules which raises the sabkha surface out of the capillary zone into the vadose zone leaving erosional surface onto which carbonate sediments are left (Warren, 2006). The other depositional texture is the palmate anhydrite which is described as bottom-growth gypsum that forms in salina setting (supratidal pond) that later dewaters to anhydrite (Lowenstein, 1987; Warren, 2006). Gypsum can dehydrate to anhydrite at the surface by solar heating in a very arid climate or in capillary zones of sabkhas where gypsum crystals are bathed in highly saline brines. Anhydritization occurs during early burial when gypsum is dehydrated, releasing large volumes of water, and converted to nodular anhydrite at ambient temperatures above 50ºC (Warren, 1991). The coexistence of these two textures suggests the possibility that they had formed in a supratidal environment that has combinations of salinas and sabkha flats (Lock et. al, 1983).

Chapter 3: Sequence Stratigraphic Architecture

SEQUENCE STRATIGRAPHIC TERMINOLOGY

Sequence stratigraphy is a method to impose the dimension of time on the relationships of rock units in space (area and depth) (Kerans lecture note). It deals with strata that obey Walther's Law (Middleton, 1973) where the distribution of the depositional environments in a conformable succession will shift with relative sea-level fluctuations. The emerging units in response to sea-level fluctuations are termed "sequences". A sequence represents a conformable succession of genetically related strata bounded by unconformities (erosion or non-deposition) and their correlative conformities (Vail et al., 1977).

This study adopts the terminology used by Kerans and Fitchen (1995) which was first introduced by Mitchum and Van Wagoner (1991) modifying the Exxon-type sequence stratigraphic terminology (Vail et al., 1987). The hierarchy of chronostratigraphic cyclicity is documented at three distinct scales including composite sequences (CS) that are made up of high-frequency sequences (HFS) which in turn composed of high-frequency cycles (cycles) (Kerans and Fitchen, 1995; Kerans, 1995, Kerans and Tinker, 1997).

Genetically related lithofacies are the building blocks of high-frequency cycles sometimes formed during a specific stage of relative sea-level cycle. The cycles record specific relative sea-level cycles defining a set of system tracts (Posamentier et al., 1988). According to the terminology Kerans and Fitchen (1995) lowstand system tracts (LST) and highstand system tracts (HST) cycles are deposited during relative sea-level fall (or decreasing rate of sea-level rise), while transgressive system tracts (TST) cycles are

deposited during relative sea-level rise. A complete depositional cycle comprising LST, TST and HST defines a single high-frequency sequence (HFS). Sets of high-frequency sequences stack into lowstand, transgressive and highstand sequence sets defining the system tracts of the seismically resolvable composite sequences (CS). Despite the fact that the terminologies used are not time-specific, the high-frequency cycles, high-frequency sequences and composite sequences are broadly analogous to 5th, 4th and 3rd orders respectively (Haq et al., 1987; Goldhammer et al., 1990; Kerans and Fitchen, 1995; Kerans, 1995).

Shallowing upward cycles are very common and have been recognized and documented in many carbonate successions reflecting varying degrees of the overall paleoenvironmental trends (James, 1979, 1984, Wright, 1984, 1986, Grotzinger, 1986). In this study, cycle (c.f. high-frequency cycle) refers to the smallest, mappable division across multiple depositional environments of genetically related lithofacies deposited during a single sea-level rise (Kerans and Fitchen, 1995; Kerans and Tinker, 1997).

Mitchum and Van Wagoner (1991) have recognized several unconformity-bound sequences within Vail's seismic sequence using detailed stratigraphic analysis of core and well log data and thus assigned the term composite sequence (3rd order) to capture the nested cyclicity. Thus, the composite sequence consisted of several higher order (4th order) sequences termed high-frequency sequences that include lowstand, transgressive and highstand system tracts that are recognized by retrogradational, aggradational and progradational cycle stacking patterns (Kerans and Fitchen, 1995; Kerans and Tinker, 1997).

The composite sequence, the lowest order of stratigraphic package documented in this study, is comparable to depositional sequence of Vail's (1987) and includes lowstand, transgressive and highstand system tracts that are composed of

retrogradational, aggradational and progradational high-frequency sequences (Kerans and Fitchen, 1995; Kerans and Tinker, 1997).

SEQUENCE STRATIGRAPHIC ANALYSIS TOOLS

The sequence stratigraphic analysis tools used in this study were originally described by Goldhammer et al. (1990) and Gardner et al. (1992) and were summarized by Kerans (1995). In this study, the sequence stratigraphic analysis tools used include one- and two-dimensional analysis tools. The one-dimensional tools are utilized to establish an initial cycle framework where lithofacies data from cores are the only data source. The lithofacies data can then be quantified and integrated with wellbore data, including wireline logs, to be used in constructing a two-dimensional stratigraphic framework and ultimately the three-dimensional geological model (Kerans and Tinker, 1997). The end product of the one-dimensional analysis is depositionally and petrophysically significant packages allowing a two-dimensional stratigraphic correlation framework.

The one dimensional stratigraphic analysis tools include: a) cycle stacking patterns, b) facies proportions, c) cycle symmetry, d) strata preservation, and e) facies tract offset. On the other hand, the two dimensional stratigraphic analysis tools include: a) correlation of cycles, b) stratal geometry, and c) recognition of sequence boundaries versus cycle boundaries.

Cycle Stacking Pattern

Cycle stacking pattern analysis examines the systematic 1D variations of cycle thickness, facies proportions within a cycle, or symmetry of transgressive versus

regressive hemicycles within a cycle (Kerans, 1995; Kerans and Tinker, 1997). It was first introduced using *Fischer Plots* (Read and Goldhammer, 1988) which represented the thickening and thinning of cycles, as normalized to a constant subsidence rate. Accommodation, i.e. the space available for potential sediment accumulation, trends are associated with systematic upward thickness variations of cycles. Upward thickening cycles reflect a general increase in accommodation on the platform top which is diagnostic of transgressive system tract deposition, where maximum accommodation space coincides with maximum flooding. On the contrary, upward decrease in cycle thickness in a prograding system reflects gradual shallowing and filling of the available accommodation (figure 3.1). Nonetheless, variations in cycle stacking pattern is sensitive to changes in sea-level amplitude, sedimentation rate, and subsidence rate and thus may not provide a unique solution.

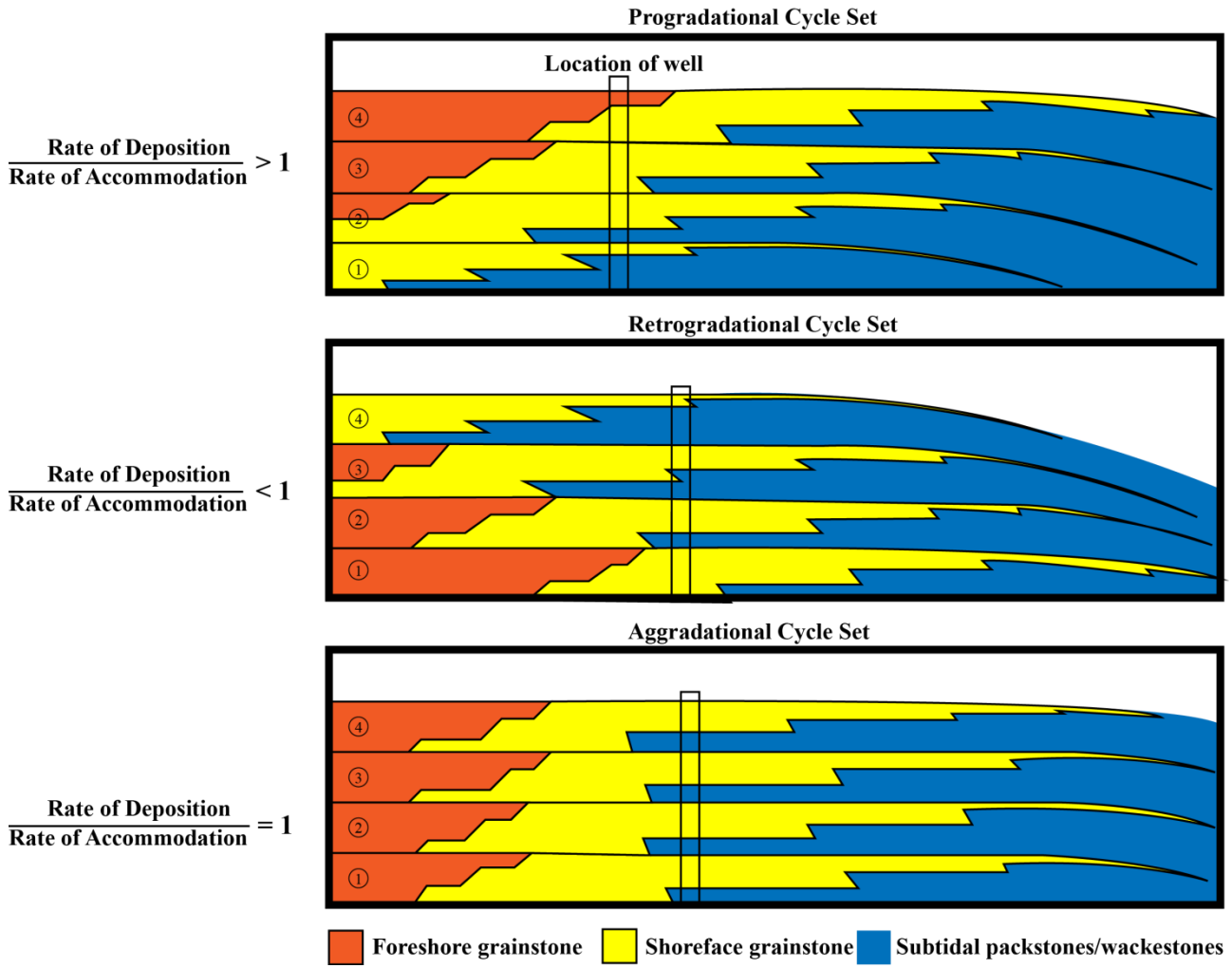

Figure 3. 1: High-frequency cycles stacking patterns in cycle sets. While, progradation is marked facies amalgamation of shallower facies upsection, shallower facies become progressively thinner with thicker more subtidal facies during transgression. During aggradation, style and thickness of cycles stay similar (modified from Van Wagoner et al., 1990)

Facies Proportions

Facies proportion, in association with cycle stacking patterns, can reflect a more realistic picture of accommodation trends. Facies proportion analysis is achieved when comparing the ratio of peritidal and shallower facies to the more subtidal ones within a single cycle, or across multiple cycles. Thus, in regressive or highstand cycle sets, the decrease in accommodation is reflected both in the upward thinning of cycles and in the increased proportion of peritidal facies relative to subtidal facies (figure 3.2). The converse is also true, where in transgressive cycle sets with increasing accommodation, thickening of the cycles, is associated with an increase in thickness of the subtidal facies compared to the shallower ones. The use of facies proportions analysis alongside with cycle stacking pattern provide a powerful tool for paleobathymetry and sequence boundaries.

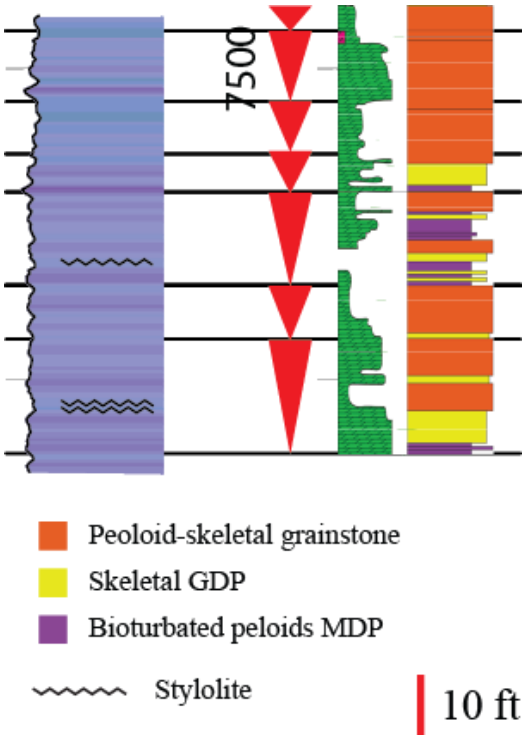

Figure 3. 2: Shallowing upward cycle in well O displaying the change in facies proportion. Basal two cycles show the progradation, where cycle is dominated by the grainstone, followed by a transgression event where subtidal facies dominate. The last three cycles show amalgamated shallow-water grainstones reflecting progradational stacking pattern during the fill of accommodation space

Cycle Symmetry

Cycle symmetry is a method used for describing vertical stratigraphic trends by splitting each cycle into the portions that record transgression and the portion that records regression. After transgression, there is a lag time before the carbonate factory heals and regains its full potential (Schlager, 1981). Under greenhouse Milankovitch settings, low-amplitude sea-level fluctuations are needed for deepening to occur (Read et al., 1986). Short transgressions will have short lag times and hence will produce cycles with thin subtidal portion and thicker peritidal caps. Increasing lag time allows more deepening without sediment aggradation that will produce cycles with thicker subtidal bases and thinner peritidal caps.

Stratal Preservation

This analysis emphasizes the importance of documenting regressive and transgressive erosional surfaces whenever observed. When they are integrated with other observations, their distribution should provide additional information indicative of accommodation creation or loss associated with facies change.

Facies Tract Offset

Sequence stratigraphy, in most cases, honors Walther's Law and hence the lateral distribution of facies is expected to be reflected in ideal vertical successions. For instance, in a restricted platform where the upper intertidal – lower supratidal cryptalgal laminites are located in front of the supratidal sabkha anhydrite and behind the intertidal oolites, the oolites are expected to overlain by the cryptalgal laminites which are overlain by the sabkha anhydrite. Thus, non-ideal vertical facies transitions provide an important

signal resulted in response to base-level shift. An oolitic grainstone overlain directly by sabkha anhydrite suggests that the two lithofacies have been juxtaposed by a major base-level fall, causing the system to step seaward prior to accumulation of laminites. The recognition of "out of sequence" lithofacies successions indicates significant events and surfaces, such as sequence boundaries.

Correlation of Cycles

Using the set of one-dimensional analysis tools including cycle stacking pattern, facies proportions, cycle symmetry, strata preservation, and facies tract offset allows the ranking of key chronostratigraphic surfaces that can be defined and correlated. Recognition of the turnaround from transgressive to regressive cycle stacking pattern allows the mapping of ranked chronostratigraphic horizons across different lithofacies. The maximum flooding surface is a conceptual surface marking such turnaround and marks the separation between retrogradational and progradational cycles and its onlap point represents the most landward position of shoreline resulted from the transgression. Similarly, the high-frequency sequence boundaries coincide with the surfaces marking the greatest basinward progradation.

Recognition of Sequence Boundaries versus Cycle Boundaries

The most reliable indicators of sequence boundaries are exposure surfaces that may be expressed as karst surfaces, large facies tract offset, and stratal terminations. The absence of such indicator makes the definition of sequence boundaries more difficult. The change in stacking pattern from upward-thinning cycles with well-developed peritidal facies components, into upward-thickening cycles with decreased peritidal to

subtidal facies ratio marks the turnaround from regressive, progradational cycles to transgressive, retrogradational cycles that can be used to constrain sequence boundaries (analogous to Vail's type 2 sequence boundary).

SEQUENCES ARCHITECTURE

The use of high-frequency cycles as fundamental chronostratigraphic elements for correlation represents the most practical scale of correlation that unravels the sequence stratigraphic framework of the Arab D reservoir in Qatif field. Cycle amalgamation, local depositional topography and autocyclic processes (Ginsburg, 1971) represent the most important issues that may hinder cycle correlation. The correlation of the cycles was conducted using one- and two-dimensional sequence stratigraphic approaches (Kerans, 1995) described previously.

Although Qatif Field Arab D lithofacies are not equivalent to those observed in other fields, including Ghawar, Abqaiq and Khurais, they are in fact time-equivalent and understanding the regional setting aids the understanding of the causative reasons behind the development and differentiation of lithofacies.

The absence of the regional sequence stratigraphic context resulted in chronostratigraphic-units-deficient nomenclature. Previous studies document that the Arab D reservoir includes the upper part of Jubaila Formation and the Arab D member of the Arab Formation. However, conventional naming of high-frequency sequences mapped in the Ghawar, Abqaiq, Khurais and other Jurassic fields is still under review in Saudi Aramco. As a result, this study will refer to the three high-frequency sequences mapped in Qatif field as the *QSEQ1, QSEQ2, and QSEQ3* sequences.

SEQUENCE STRATIGRAPHIC FRAMEWORK

The sequence stratigraphic framework for the Arab D in the Arabian Basin published by several authors (review Chapter 1) highlights a significant level of controversy in stratigraphic interpretation. The main reason for this controversy arises from the disparate datasets worked by the different authors, with some focusing on large regional datasets and others having examined only a portion of a field. Limiting the stratigraphic work to field-windows can be misleading especially if there is a regional antecedent topography that could amplify or degrade localized depositional topography.

This study considers the position of the Qatif Arab D within the context of the broader Jurassic carbonate ramp extending from the Arabian Shield to the Rimthan Arch and further to the northeast. I identify one-long term, composite-sequence within the Qatif Arab D section, which in turn is composed of three high-frequency sequences representing a succession encompassing the upper Jubaila and the Arab D member (Meyer et al., 1996; Lindsay et al., 2006). The QSEQ1 high-frequency sequence (HFS) which consists of 6 high-frequency cycles (HFCs) represents only the highstand portion of the HFS. The other two HFSs, QSEQ2 and QSEQ3, are symmetrical sequences composed of 12 and 11 HFCs respectively. In both sequences, the HFCs are broken down into transgressive system tracts and the highstand system tracts of the HFS. The correlation of the high-frequency cycles produced a high-resolution sequence stratigraphic framework representative of the evolution of the Arab D in Qatif Field.

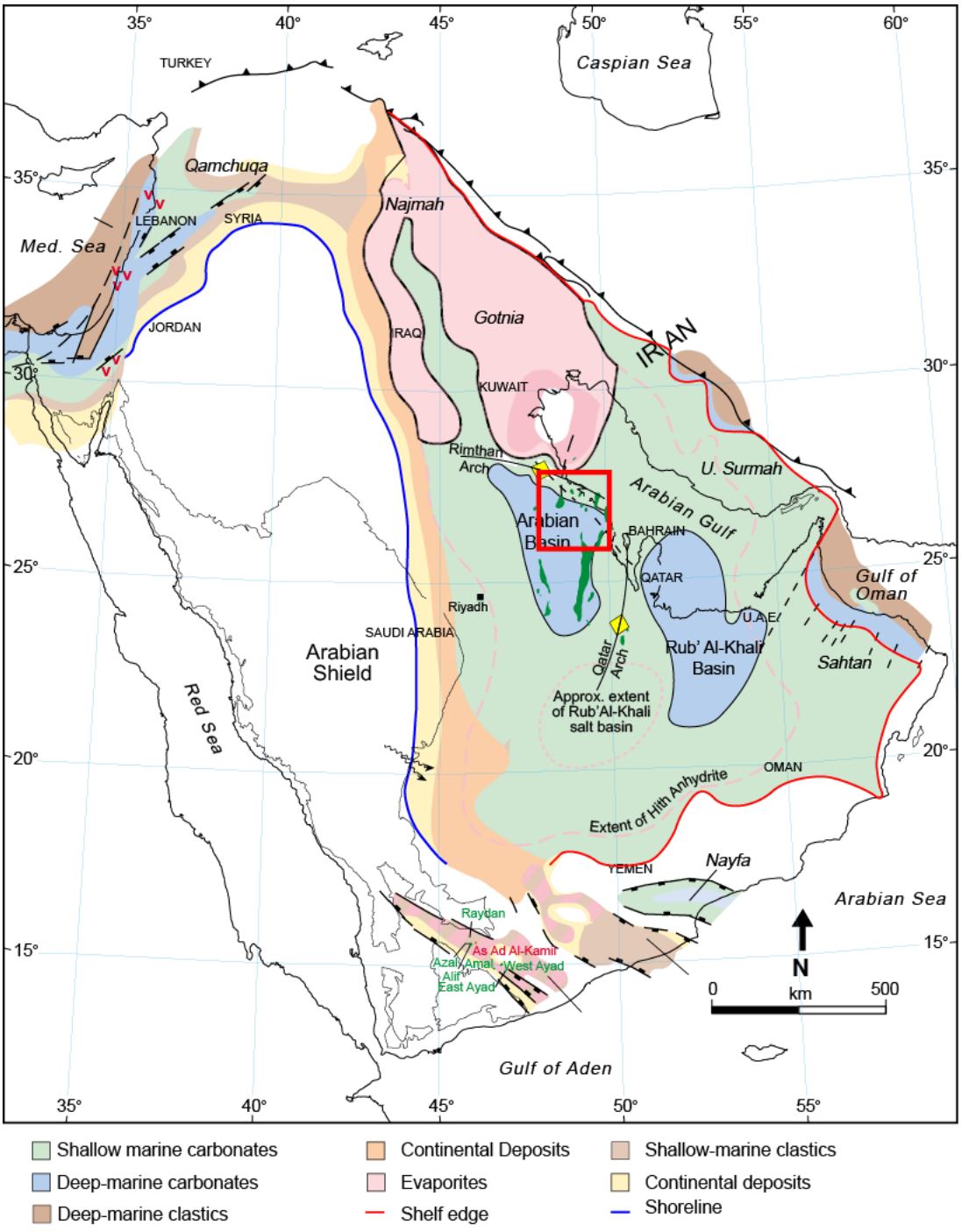

Figure 3. 3: Regional distribution of paleo-facies during Late Jurassic. Qatif field was several hundreds of kilometers from the shoreline (blue) and the shelf

OVERVIEW

The Upper Jurassic Arab D rocks of Qatif field were deposited in a wide, gently sloping carbonate ramp. The field was bounded by Rimthan Arch to north and by an intrashelf basin to the south (figure 3.3) (Ziegler, 2001). Although, the pioneer work of Wilson (1981, 1985) in Qatif provided a sedimentologic overview of depositional facies and environments, his work did not consider the influence of antecedent topography on the type of sediments or their cyclic depositional pattern. This study uses the detailed observations made from cores and limited wireline log data and integrates these with the regional and local structural setting (i.e. Rimthan Arch) to build high-resolution sequence stratigraphic framework of the Arab D in Qatif field.

Using the described cores, gamma ray logs and petrographic analysis, a southwest-northeast cross section is constructed illustrating isochronous lithofacies relationships within the Arab D composite sequence (~3rd order). Through this, multiple conceptual geological models are created to represent the evolution of the Arab D reservoir considering temporal and spatial variability. These stratigraphic models provide an explanation of the chronostratigraphic evolution of the Arab D system and its relation to the lithostratigraphic units. The actual distribution of lithofacies at a given point in time is a function of accommodation, eustasy, climate, and tectonics. For example, ramp-crest lithofacies are generally better developed during sea level highstands and lowstands than during transgression.

The depositional environments of the Arab D represent a succession of intrashelf basin, lower and upper shoreface, foreshore (beach facies), and sabkha environments (see Chapter 2 for details). The fine scale of cyclicity observed in the Qatif Arab D is best illustrated using well O (figure 3.4). The models will describe the Upper Kimmeridgian

Arab D in terms of 3 high-frequency sequences (HFS) as discussed above and shown figure 3.4. The HFSs are broken in terms of characteristic facies stacking pattern and cycle thickness changes into several high-frequency cycles. The high-frequency cycles (HFCs) can be bundled, where applicable, into transgressive system tracts (TSTs) and highstand system tracts (HSTs). The TST includes all the deposits that accumulate during the rise of sea-level till the time of maximum flood resulting in a retrogradational stacking pattern, whereas the HST includes the deposits that accumulate above the maximum flooding surface (MFS) during decreasing rate of rise of sea-level, stillstand or falling stage of sea level associated with maximum efficiency of carbonate factory (Loucks and Sarg, 1993).

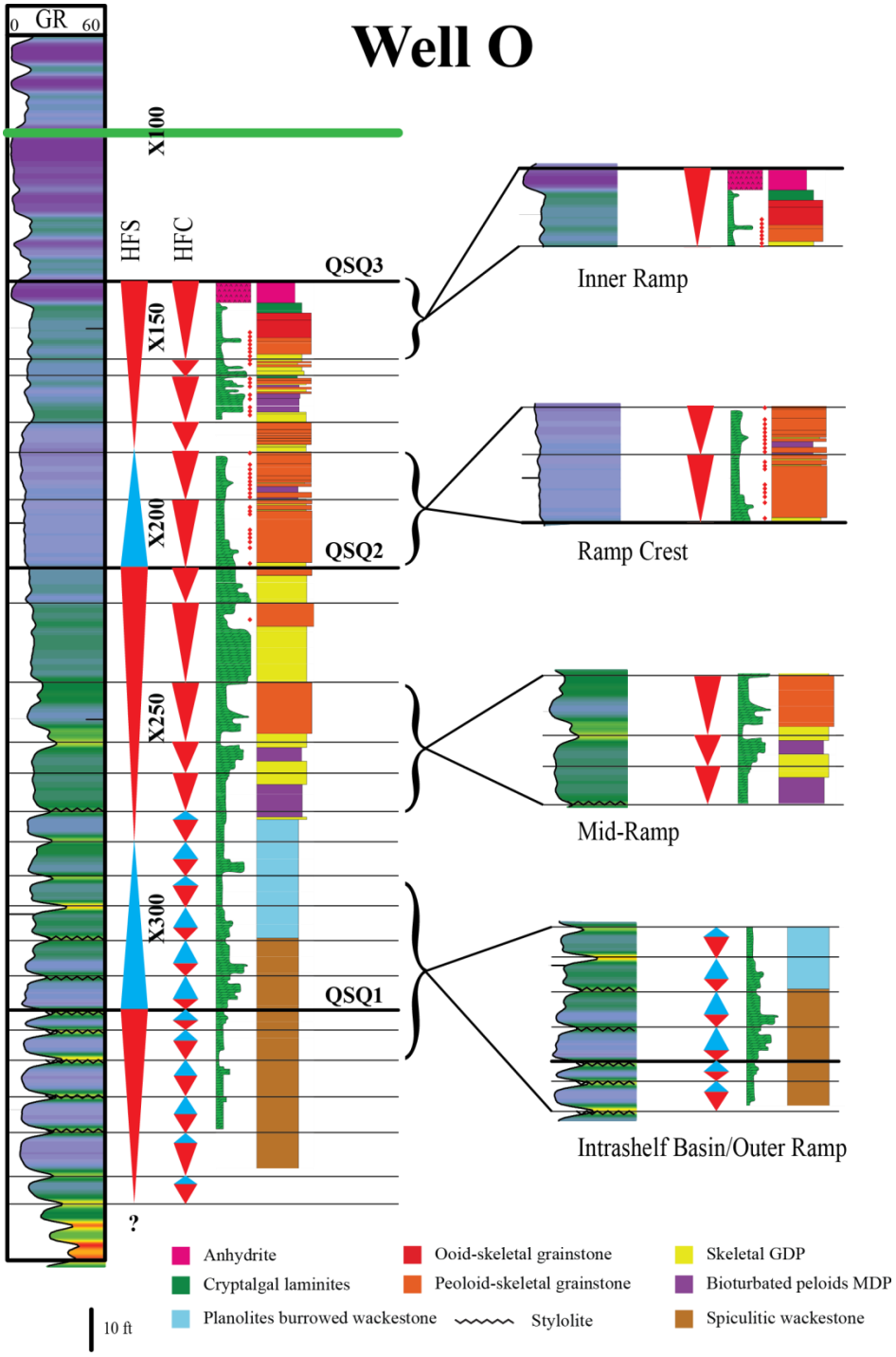

Figure 3. 4: Well O with interpretation of finest scale of cyclicity. Insets show typical high-frequency cycles of intrashelf basin, mid-ramp, ramp-crest and inner ramp.

The asymmetric QSEQ1 HFS only shows the highstand system tracts consisting of 0.5-2 m thick high-frequency cycles of amalgamated spiculitic wackestone. The absence of core control below the interpreted HST precludes definitive mapping of the TST. The QSEQ2 is characterized by 1) a basal transgressive system tracts composed of spiculitic wackestone overlain by *Planolites*-burrowed wackestones and 2) highstand system tracts of shallow water peloidal MDP, skeletal GDP and peloid skeletal grainstones with an average cycle thickness of less than 2 m. The QSEQ3 transgressive system tract consists of high-frequency cycles are 1–4.5 meter thick that are dominated by peloidal MDP-skeletal GDP-peloid-skeletal grainstone associations in the north, and by barren pelleted packstone in the southern segment of the field. The early highstand cycles of the QSEQ3 HFS are generally 1.5–3.7 meter thick and have a typical peloidal MDP-Skeletal GDP-Peloid-Skeletal grainstone-cryptalgal laminites-anhydrite facies succession. In the late highstand QSEQ3 HFS, high frequency cycles are usually 1–5.5 meter thick and consist of a succession of skeletal GDP–peloid–skeletal grainstone-skeletal–ooid grainstone–cryptalgal laminites–anhydrite facies succession.

The study documents the stratigraphic evolution of the Arab D ramp from relatively deep intrashelf basin facies to shallow water, high-energy facies. Facies patterns and stacking also illustrate the influence of the Rimthan Arch on the more rapid shoaling of the northern end of the field as well as the south-directed progradation (figure 3.5, 3.6).

The distribution of lithofacies can best be understood when considered in light of conceptual geological models. Four models are constructed to depict lateral facies/paleo-environmental relationships and depositional patterns of the Arab D, addressing their evolution.

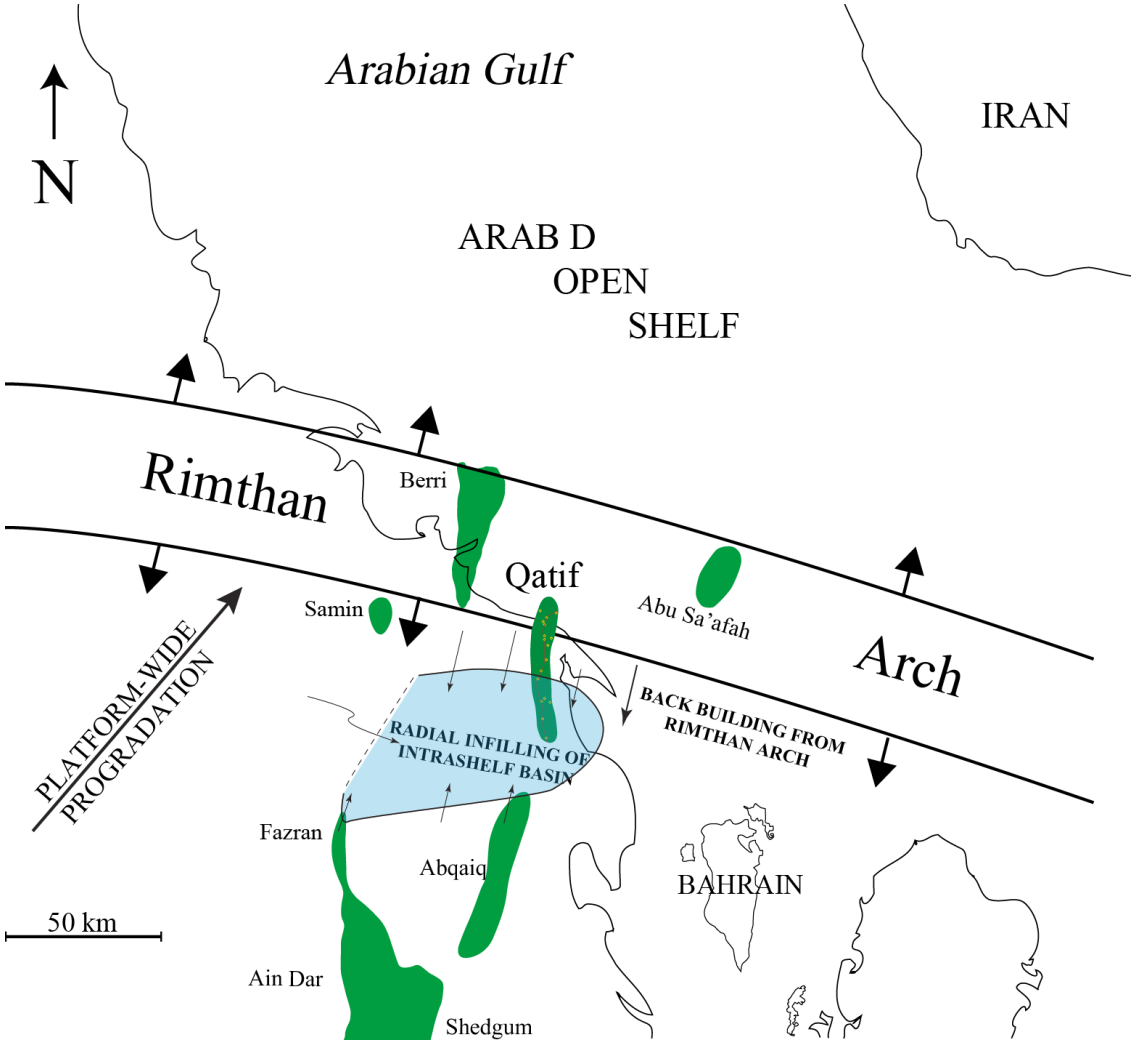

Figure 3. 5: Regional overview of the ramp configurations during Arab D time and Rimthan Arch strutural-conrol the sedimentation styles recorded in Qatif field.

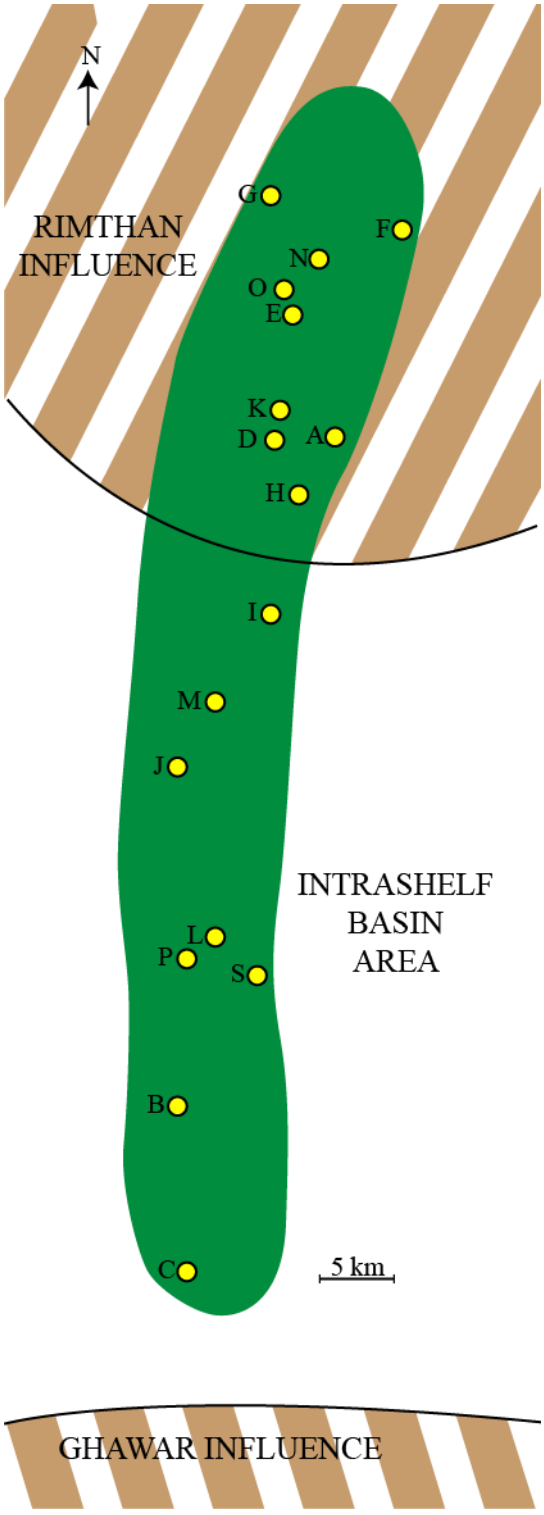

Figure 3. 6: Qatif field map showing well locations and areas of influence of Rimthan Arch and Ghawar anticline.

The anhydrite and cryptalgal laminites represent deposition on the inner ramp in a sabkha-tidal flat setting. The ooid-skeletal grain-dominated packstone-grainstone lithofacies is typical lithofacies deposited in a high-energy ramp-crest setting. The peloidal MDP documents middle-ramp, lower shoreface lithofacies interbedded with ramp-crest and intrashelf basin facies. The barren pelleted packstone lithofacies is restricted to the southern segment of the field and its close association with the peloidal MDP indicates that it was deposited in a relatively deep lower energy, circulation-restricted depocenter.

Architecture of the QSEQ 1 Arab D HFS at Qatif

The QSEQ1 HFS is only represented by the HST consisting of 6 high-frequency cycles (HFC 1.1–HFC 1.6) which, where core is available, can be shown to be composed mainly of spiculitic wackestone. The HFCs in this deeper-water outer ramp setting are symmetrical and show thinning from south to north with an average thickness of about 1 meter. The trend of thinning of the HFCs to the south is reflected in GR log correlations in figure 3.7 and 3.8 which is believed to indicate an earlier Arab-D progradation direction sourcing from the Ghawar platform area have been influenced by the Ghawar and Abqaiq structures which were structurally higher at that time

The trend of thinning of the HFCs to the south is reflected in GR log which is believed to have probably been influenced by the Ghawar and Abqaiq structures which were structurally higher at that time (figure 3.7-3.8). The top of the QSEQ1 is a sequence boundary (top HFC 1.6) running through the amalgamated section of symmetrical spiculitic wackestone cycles. The top QSEQ1 is defined from recognizing the turnaround from seaward-stepping (upward thinning) to landward-stepping (upward cycle

thickening) patterns. In this deeper part of the ramp in a greenhouse setting, we do not expect to observe an exposure surface or major facies tract offset.

For QSEQ1, core data which is only available for the K and O wells; however, the consistency of the gamma ray signature is clear and is interpreted as correlatable across the field. In cores, the GR high response is developed, in most cases, where stylolites are concentrated in somewhat more organic-rich intervals (figure 3.9), likely to represent orbitally driven oxygenation cycles e.g. the Bridge Creek Limestone Member (Cenomanian-Turonian) and Smokey Hill Chalk Member (upper Turonian-lower Campanian) (Research on Cretaceous Cycles Group, 1986). Stratigraphically, stylolites commonly mark the base of a transgression signal coinciding with maximum flooding surfaces dividing the transgressive deposits from the highstand deposits (Raspini 2001). Furthermore, the stylolites coincide with high GR response and the spectral GR logs show that the signal is modulated by uranium; thorium and potassium which further support the interpretation that GR signifies a condensed section associated with a concentration of organic matter that would favor complexing of uranium. Such radioactive zones associated with condensed sections during maximum floods are common in many regions (Galloway, 1989). In addition, the observed trend is analogous to condensed sections of deeper marine deposits where production rates can be as low as 1 to 10 mm/yr (Vail et al., 1984; Loutit et al. 1988) and hence the cycle thickness is generally reduced, explaining the observed trends. Thus, the high-frequency cycles are interpreted as symmetrical cycles (figure 3.9) that represent the correlative conformities of higher energy, upward-shallowing cycles observed in Abquiq and Fazran fields to the south (Kerans and Smith personal comm.). At this time, the northern dome of Qatif Field was situated just seaward of the southern flank of the Rimthan Arch where relatively deep facies predominated.

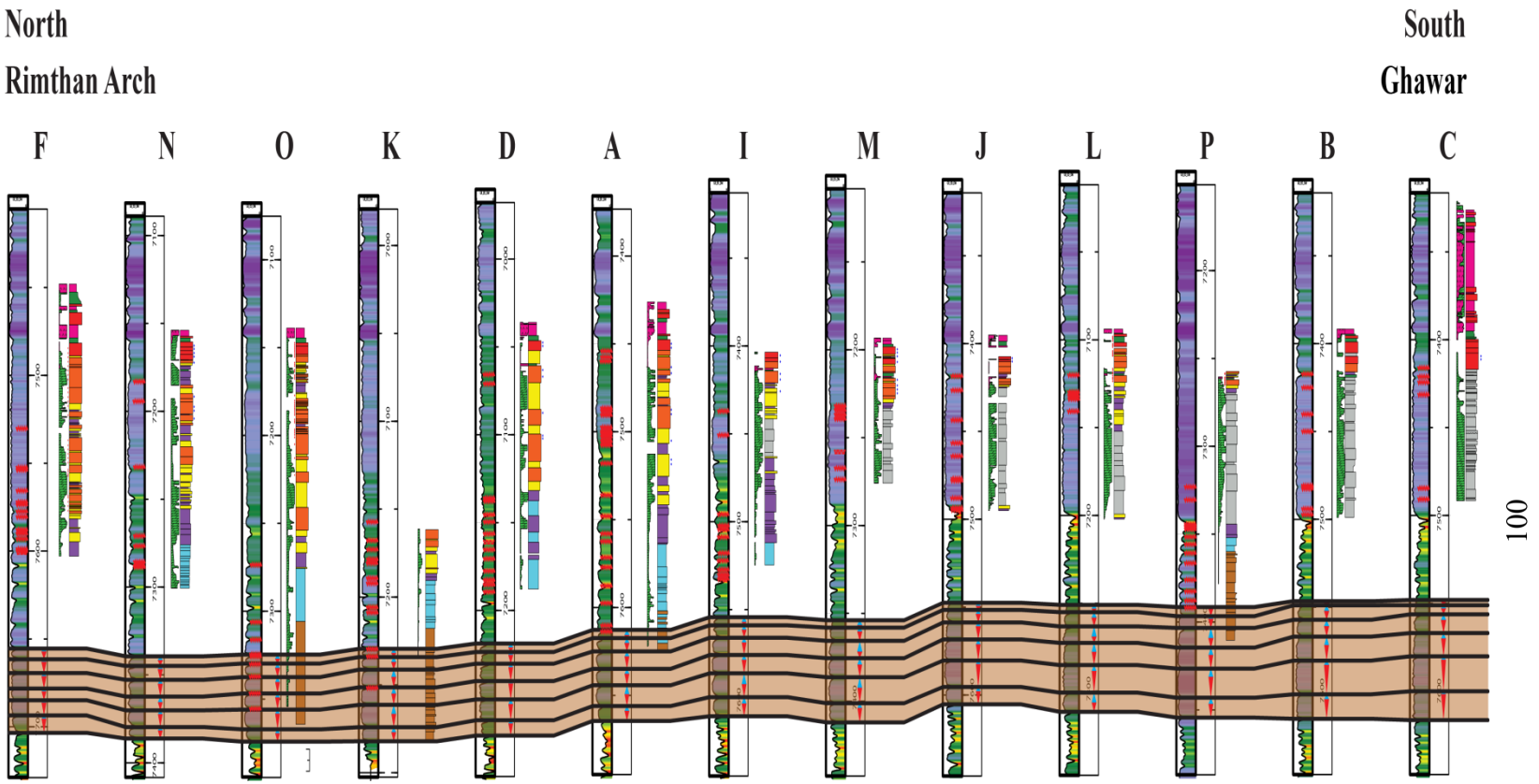

Figure 3. 7: mapping core/wireline log data of HSTof QSEQ1 which the influence of Ghawar anticline was the most prominent and the cycles thin towards the north into deeper basinal conditions.

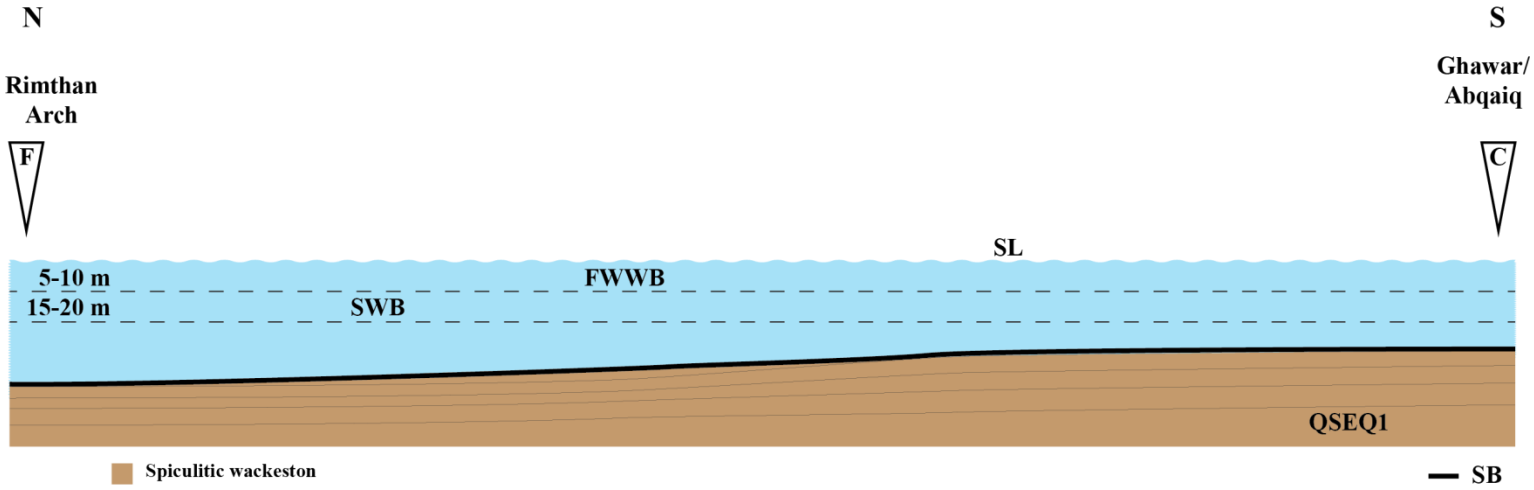

Figure 3. 8: Schematic representation of the highstand of QSEQ1 which the influence of Ghawar anticline was the most prominent and the cycles thin towards the north into deeper basinal conditions.

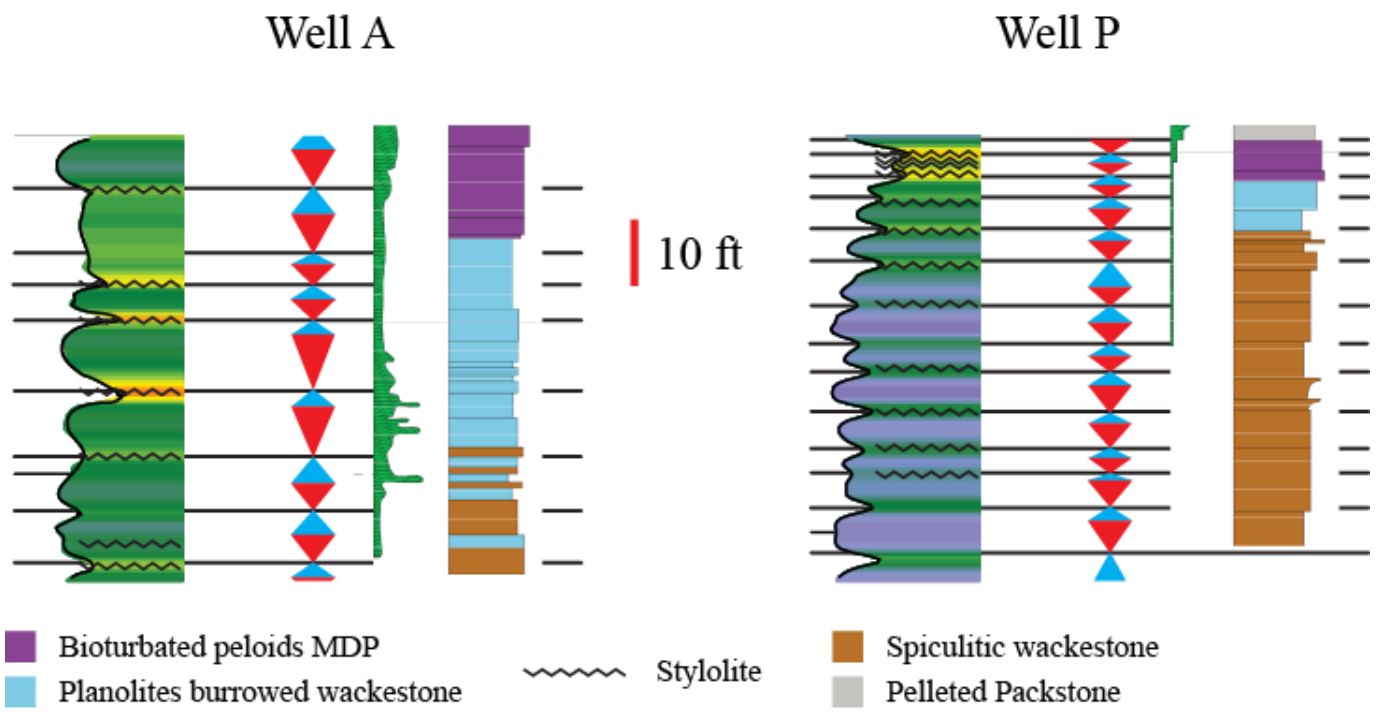

Figure 3. 9: Typical gamma ray response for different lithofacies. Stylolites coincide with correlative flood

Architecture of the QSEQ 2 Arab D HFS at Qatif

The QSEQ2 HFS consists of intrashelf basin, spiculitic and *Planolites*-burrowed subtidal wackestones, middle-ramp peloidal MDP and ramp-crest skeletal-ooid grain-dominated packstones and grainstones. The QSEQ2 is a symmetrical high-frequency sequence that documents transgression and backstepping, maximum flooding of the platform, progradation and back building of the Rimthan Arch to the south, and finally, platform exposure (figure 3.5). The symmetry is inferred from the 1D stacking patterns and facies proportion of the HFC within the QSEQ2 HFS. QSEQ2 is composed of 12 high-frequency cycles (HFC 2.1 – HFC 2.12) that can be subdivided on the basis of stacking patterns into transgressive and highstand system tracts. The transgressive system tract is characterized by an intrashelf basin succession resulting from slow transgression and probably aggradation and/or backstepping during sea-level rise. The aggradational bundles maintain a constant thickness (1.5-2 m) of amalgamated subtidal *Planolites* burrowed lithofacies (figure 3.4). The highstand system tract of QSEQ2 HFS is characterized by the development of relatively higher energy depositional conditions as reflected by the presence of peloid-skeletal grain-dominated packstones and grainstones.

The QSEQ2 TST is composed predominantly of subtidal lithofacies in the area of the Qatif Field, including: 1) spiculitic wackestone and 2) *Planolites*–burrowed mudstone. The presence of only the sponge spicules and scarcity of Kurnubia foraminifera are indicative of a deeper environment (Barczyk et. al, 1988), the overlying *Planolites* lithofacies is indicative of disoxic conditions above which the sediments are progressively oxygenated upsection (Bromley and Ekdale, 1984; Ekdale, 1992; Savrda and Bottjer, 1986, 1989). The rarity of storm beds in the lower section indicates, despite not being in normal marine conditions, that the location of Qatif field was in an energy shadow zone caused by Rimthan Arch deflecting energy approaching from the north

(figure 3.12). Storms had a more pronounced effect on southern fields (Ghawar, Abqaiq and Khurais) (Kerans personal comm.) compared to Qatif.

The maximum flooding surface (MFS) is identified from careful correlation of the high-frequency cycles using their well-defined GR character. The MFS of the QSEQ2 HFS is placed on top of HFC 2.4 as it represents the maximum accommodation space created associated with the predominance of subtidal lithofacies during sea level rise. The initial seaward shift of lithofacies and platform-wide progradation to the north-northeast was associated with radial infill of Qatif intrashelf basin south of the Rimthan Arch (figure 3.5). Above the maximum flooding surface, the HFCs become progressively thinner from north to south (figure 3.10, 3.11). In the north, above the maximum flooding surface, shallower water, thick, peloids-skeletal packstones and grainstone successions cap the QSEQ2 HFS. Lower energy, thinner, muddy facies in the south segment of the field are symmetrical HFCs where their maximum flooding surfaces represent the correlative conformities of the asymmetric HFCs deposited on the ramp crest. These correlative conformities exhibit an elevated GR log response that could be correlated easily in the southern segment of the field all the way to the northern segment of Abqaiq field (Read, Smith, Musa and Thompson personal comm.). Overall, the maximum flooding surface, HFCs correlation lines of QSEQ2 HFS show a reciprocal thickening trend compared QSEQ1 HFS from progressively narrowly-spaced to the north to progressively narrowly-spaced to the south. The general progradation direction of the QSEQ2 sequence is reversed from that of QSEQ1, with thinning occurring in a north to south direction as opposed to the south to north thinning observed in QSEQ1.

The QSEQ2 HST is represented by the high-frequency cycles HFC 2.5 – HFC 2.12. In the intrashelf basin, the typical upward-shallowing cycle is characterized by basal, bioturbated skeletal peloidal MDP, overlain by peloidal-skeletal GDP and capped

by skeletal grainstones. On the ramp crest typical HFCs consist of asymmetric shallowing-upward cycles. The tops and bases of the cycles are defined by thin mud-dominated beds or exposure-indicative fitted fabrics (see chapter 4). The fitted fabrics are indicative of subaerial exposure surfaces formed when shoal grainstones built to and above sea-level.

The stacking pattern analysis for well O (figure 3.4) reveals the following: 1) cycle thickness trends from thick basal cycles of 3.6 m average thickness to 5 cycles (HFC 2.8–HFC 2.12) of average 2.5 m thickness, 2) cycle symmetry evolves from fully symmetrical lower in the well to distinctly asymmetrical in the top 5 cycles (HFC 2.8–HFC 2.12), and 3) facies proportions grade from 100% deeper subtidal to an average of 65% peritidal. These trends in key stacking parameters clearly illustrate a transition from higher accommodation lower TST cycles to gradually decreasing accommodation in the upper 5 cycles (HFC 2.8–HFC 2.12).

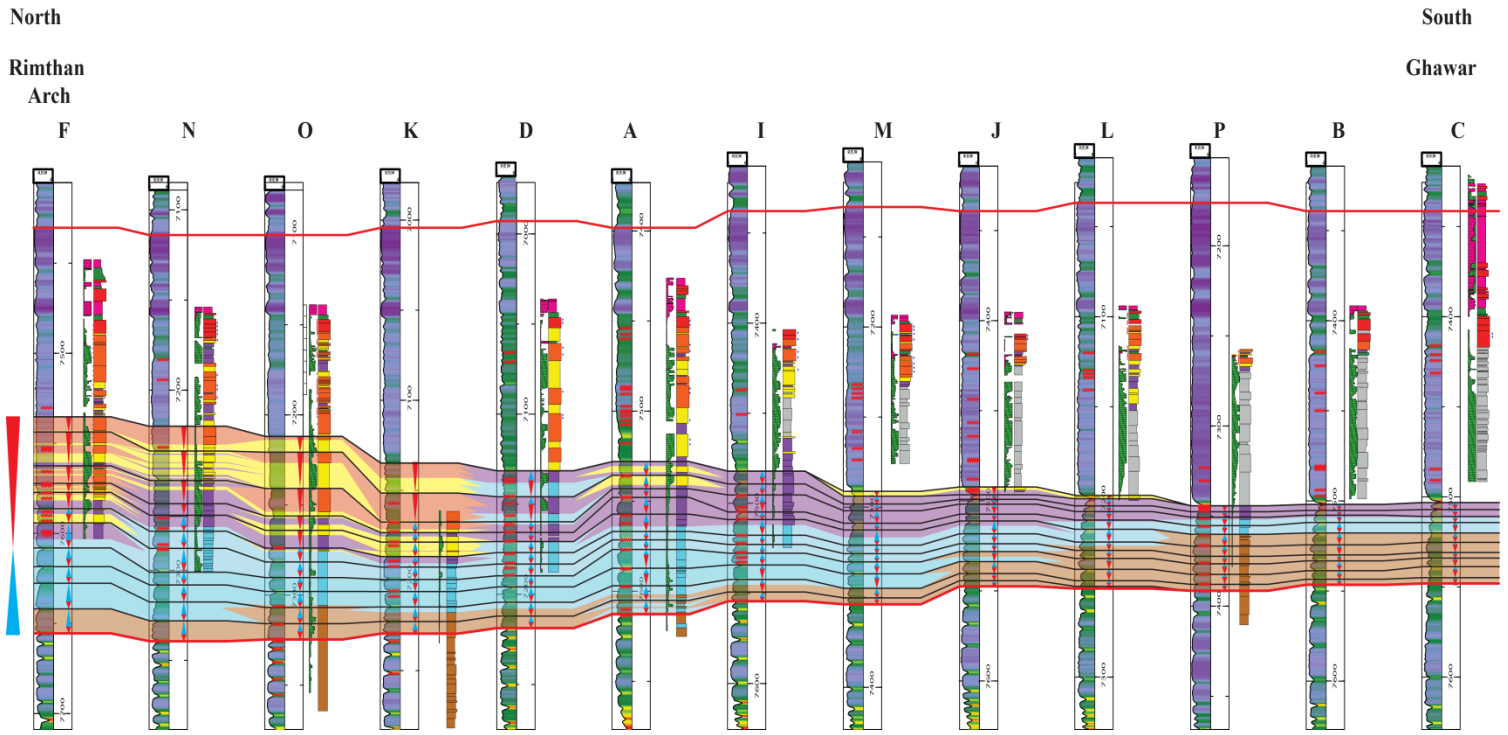

Figure 3. 10 QSEQ2 HFS during which the influence of Rimthan Arch was the most prominent and the leeward margin of the Rimthan Arch progrades to the south towards the intrashelf basin.

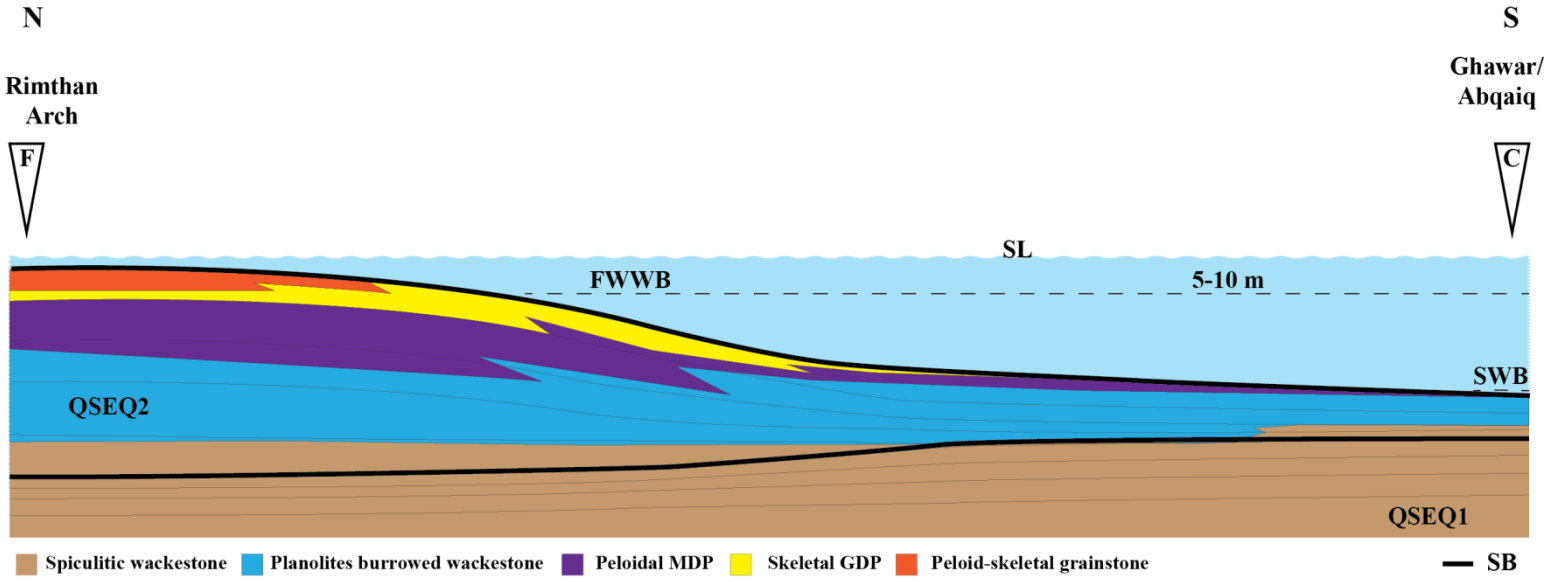

Figure 3. 11: Schematic representation of the QSEQ2 HFS during which the influence of Rimthan Arch was the most prominent and the leeward margin of the Rimthan Arch progrades to the south towards the intrashelf basin.

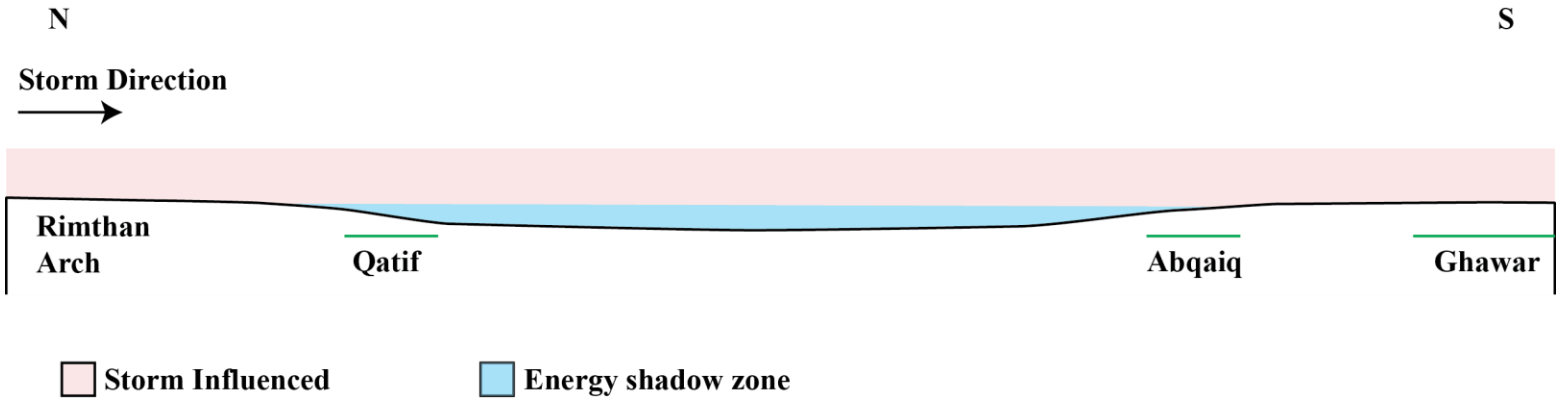

Figure 3. 12: Storms approaching from the north have little effect on Qatif field as it falls in energy shadow zone created behind the Rimthan Arch

The SQEQ2 sequence boundary (SB) is marked by a distinctive high gamma ray spike (figure 3.13) in the southern segment of the field at the intrashelf basin zone (main cross section) but the gamma ray response becomes progressively lower and more diffuse to the north as it climbs toward the Rimthan Arch. The high gamma ray character in the intrashelf basin is interpreted to represent periods of restricted bottom-water circulation and/or with a time of reduced sediment supply. In general, these periods indicate the formation of condensed sections or a time-gap associated with a non-depositional hiatus (disconformity) during the exposure of the ramp crest. The gamma ray "spike" in the intrashelf basin zone corresponds to potassium (K), thorium (Th) and uranium (U) in spectral gamma ray log. The importance of U is that it can exist in solution as uranyl carbonate as oppose to K and Th which are mostly detrital (Combaz, 1986; Wignall and Myers, 1988). Organic matter plays an active role in the extraction of U from dilute solutions (seawater) under reducing conditions (Postma and Veen, 1999). Under reducing conditions or in the presence of organic matter and/or phosphate the uranium is fixed at the water-sediment interface (Wignall and Myers, 1988). In the lower parts of the succession, the correlative conformities are believed to have occurred during cycle-scale condensed section during maximum floods. However, at the sequence boundary the GR spike was probably the result of strongly condensed facies, likely related to sediment starvation as well as restricted bottom-water circulation associated with uranium fixation at water-sediment interface (figure 3.13).

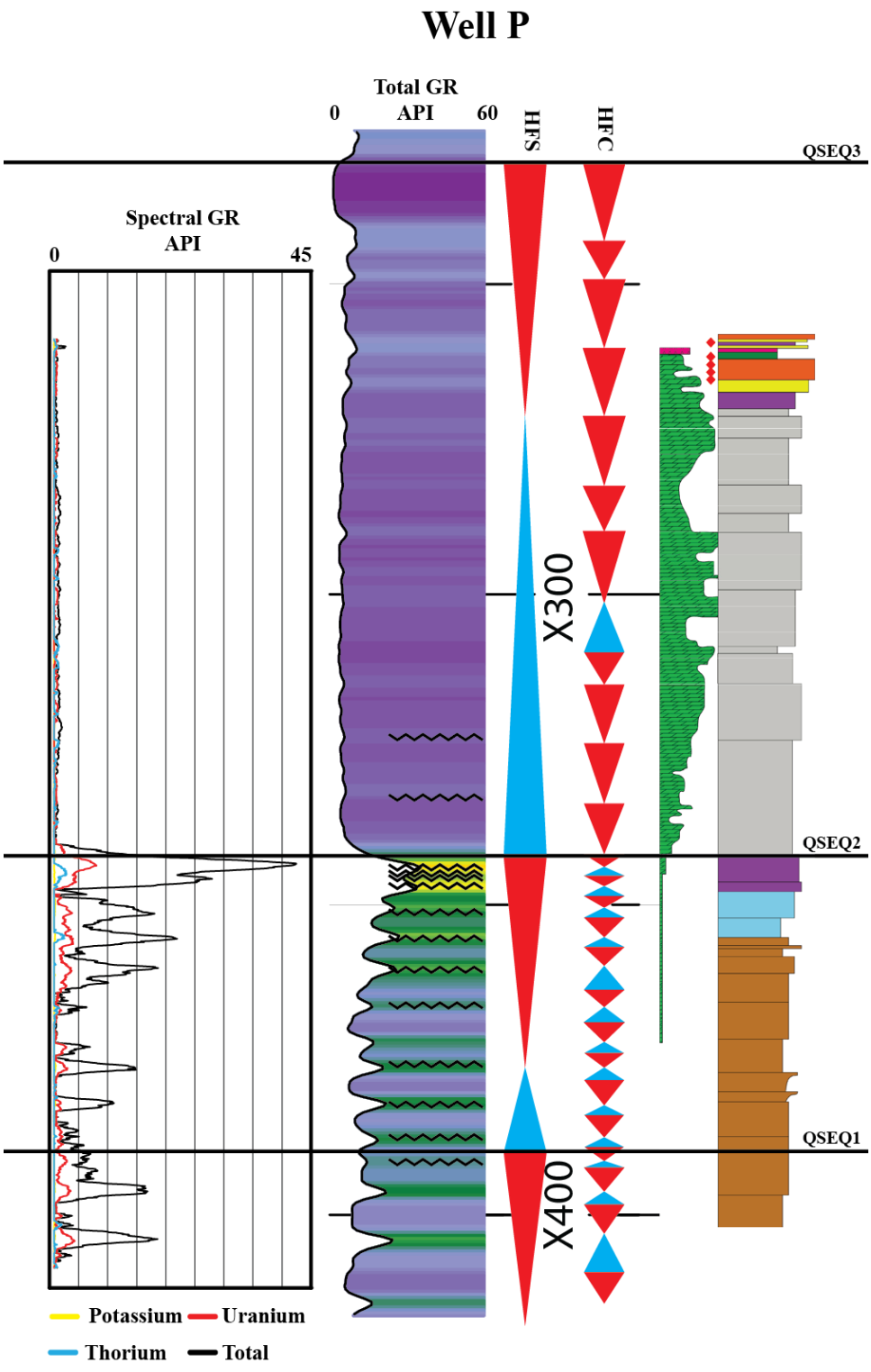

Figure 3. 13 Total and spectral GR of well P showing uranium has the most influence modulating the total GR

Architecture of the QSEQ 3 Arab D HFS at Qatif

The QSEQ3 HFS consists of 11 HFCs (HFC 3.1– HFC 3.11) and records a time of initial aggradation on the platform followed by a marked sea-level fall and basinward progradation with possible forced regressive character (figure 3.14). QSEQ3 consists of transgressive system tract (HFC 3.1– HFC 3.8) dominated by grain-dominated facies in the northern segment of the field, and by barren, pellet-dominated facies in the southern segment of the field (figure 3.16). The typical HFC contains a succession of peloidal MDP overlain by skeletal grain-dominated packstones and grainstones. TST high-frequency cycle thickness is variable ranging from 1.2 m to 4 m on the ramp crest to the north, and up to 6 m thick in the intrashelf basin in the southern segment of the field. Highstand system tract (HFC 3.8–HFC 3.11) facies consist of accumulated lower shoreface, upper shoreface, foreshore grainstones and sabkha algal mats and anhydrite (figure 3.17). Typical HST high frequency cycle thickness ranges between 1.5 and 6.5 m thick throughout the field.

The QSES3 TST is marked by a series of aggradationally-stacked skeletal-peloidal grainstones and grain-dominated packstones in the northern segment of the field (wells F and A, figure 3.15). TST cycles include intercalated bioturbated skeletal (foraminifera, brachiopods, echinoderms) mud-dominated packstone. During transgression, shoal water areas surrounding the intrashelf basin were dominated by peloid-skeletal grainstones whereas the deeper intrashelf basin setting was occupied by low-energy pelletal packstones. During high-frequency, cycle-scale sea level fall, continued-deep water conditions in the intrashelf basin are recorded by a thick, wedge of dolomitized pelleted packstone (figure 3.18, 3.19) while updip at the ramp-crest shoreface and foreshore deposits were developed. Along the ramp crest and intrashelf basin, evidence for upward deepening is very subtle, but is in indicated by an increase in

cycle thickness increase and an associated shift in facies proportions in which an increase in the abundance and diversity of bioclasts within the subtidal unit is observed. The thinning of cycles to the north during transgression is controlled by geomorphology of Rimthan Arch where accommodation space created closer to Rimthan Arch is significantly less than accommodation space created away from it.

The maximum flooding surface is not easily recognized, but is interpreted to best placed within HFC 3.8, which is associated with the maximum accommodation space created and the incursion of subtidal lithofacies to proximal areas towards the Rimthan Arch. The maximum flooding surface is placed within subtidal facies with a remarked elevated GR signature that could be correlated across the field. At this time, the intrashelf basin was almost filled and the transgression allowed the grainstone to step landward further to the south (figure 3.15).

The highstand system tract is characterized by subtidal packstone grading into peloid-skeletal grainstone and capped by well-sorted foreshore skeletal-ooids grainstones and/or sabkha algal mats and anhydrite. The highstand system tract demonstrates two-order hierarchy in stacking patterns; that is, progradational cycle-stacking patterns within a bundle characterize the overall progradational pattern of the platform to the north-northeast. During the deposition of HFC 3.8 peloid-skeletal grainstones sit basinward of the cryptalgal laminites and are best interpreted to represent a low-energy shoreline similar to beach facies immediately seaward of the tidal flats, similar to the facies association observed in northeastern Turks and Caicos Islands (Morgan, 2008). HFC 3.9 was deposited as a lowstand wedge marking the final stage of filling of the intrashelf basin. As a result, HFC 3.10 started to prograde to the north with more open marine conditions to the north indicated by the peloid-skeletal grainstone and grain-dominated packstone. The late highstand is marked by layer-cake cycle/facies distribution marking

the final infilling of the intrashelf basin. HFC 3.11 is characterized by peloids-skeletal grain-dominated packstones and grainstones and capped by skeletal-ooid grainstones and/or incipient cryptalgal laminites. The progressive restriction, flattening and loss of accommodation as well as the sharp top of the anhydrite overlain by skeletal rudstone (plate 3.1) makes the top of HFC 3.11 the sequence boundary for QSEQ3 HFS.

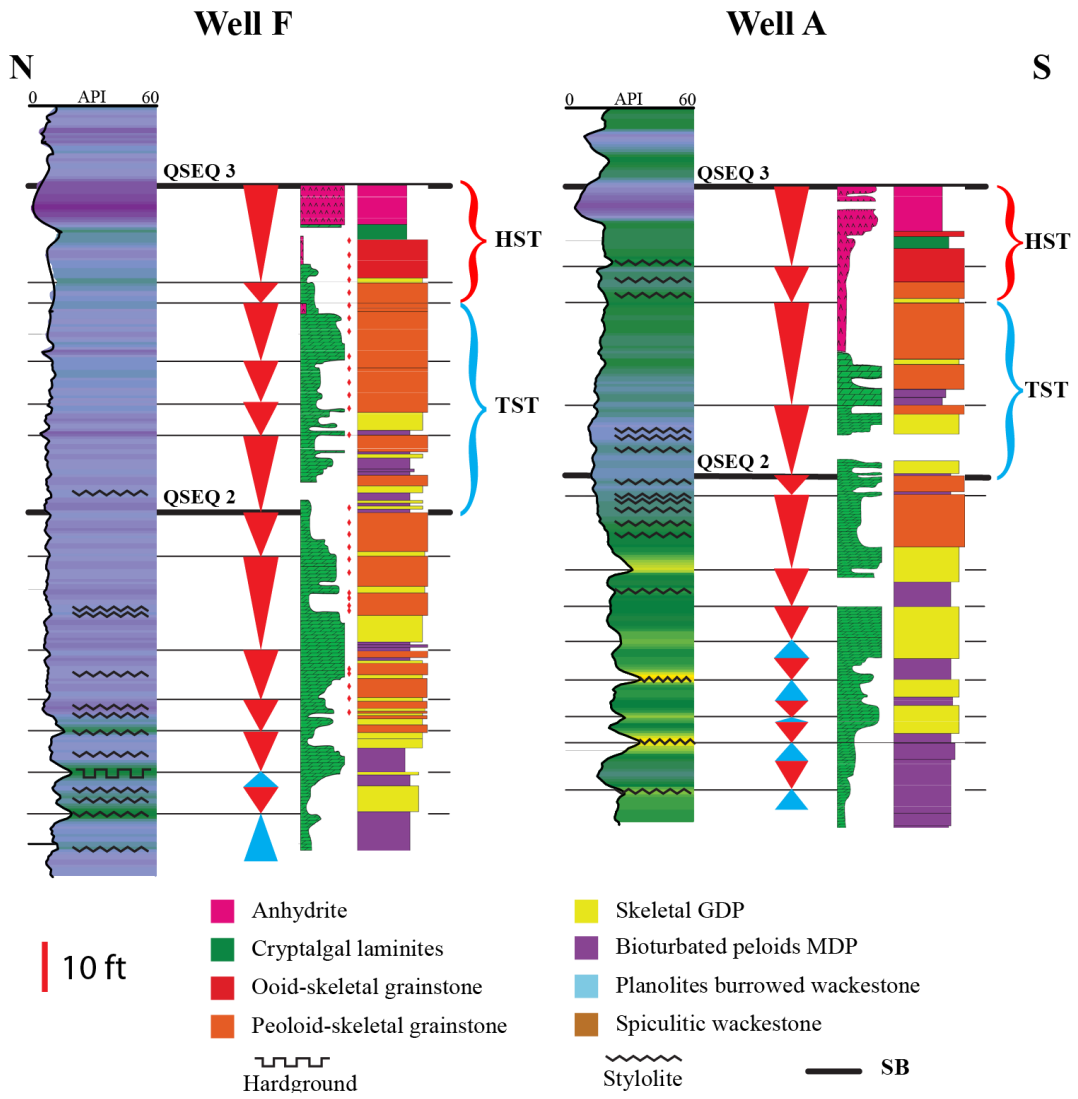

Figure 3. 14: Stacking patterns and facies proportion of QSEQ3 in well F and well A.

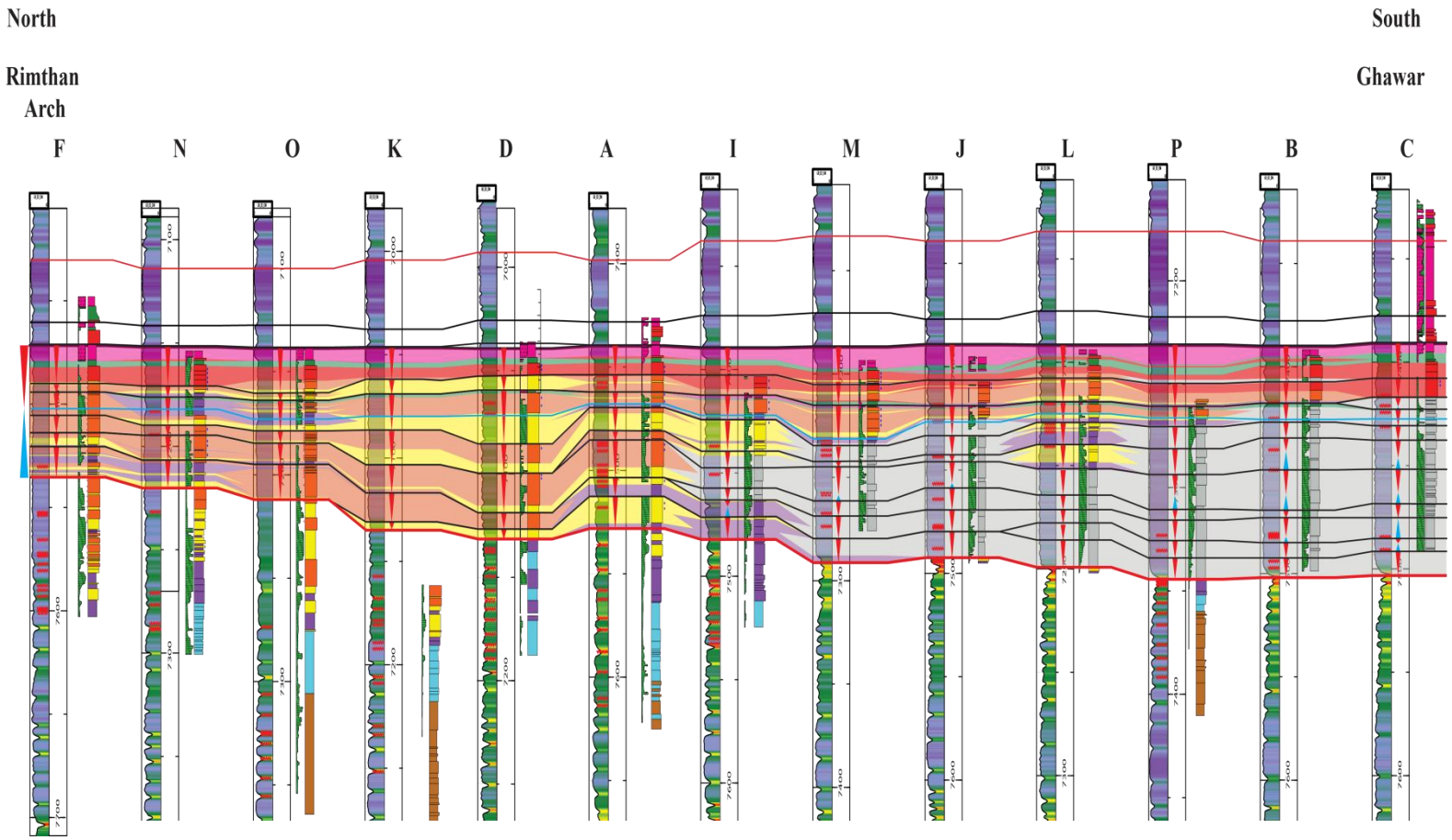

Figure 3. 15 : QSEQ3 architecture where the TST pelleted packstone filling the intrashelf basin during the progradation of the southern margin of Rimthan Arch and HST progradation is synchronized with platform direction

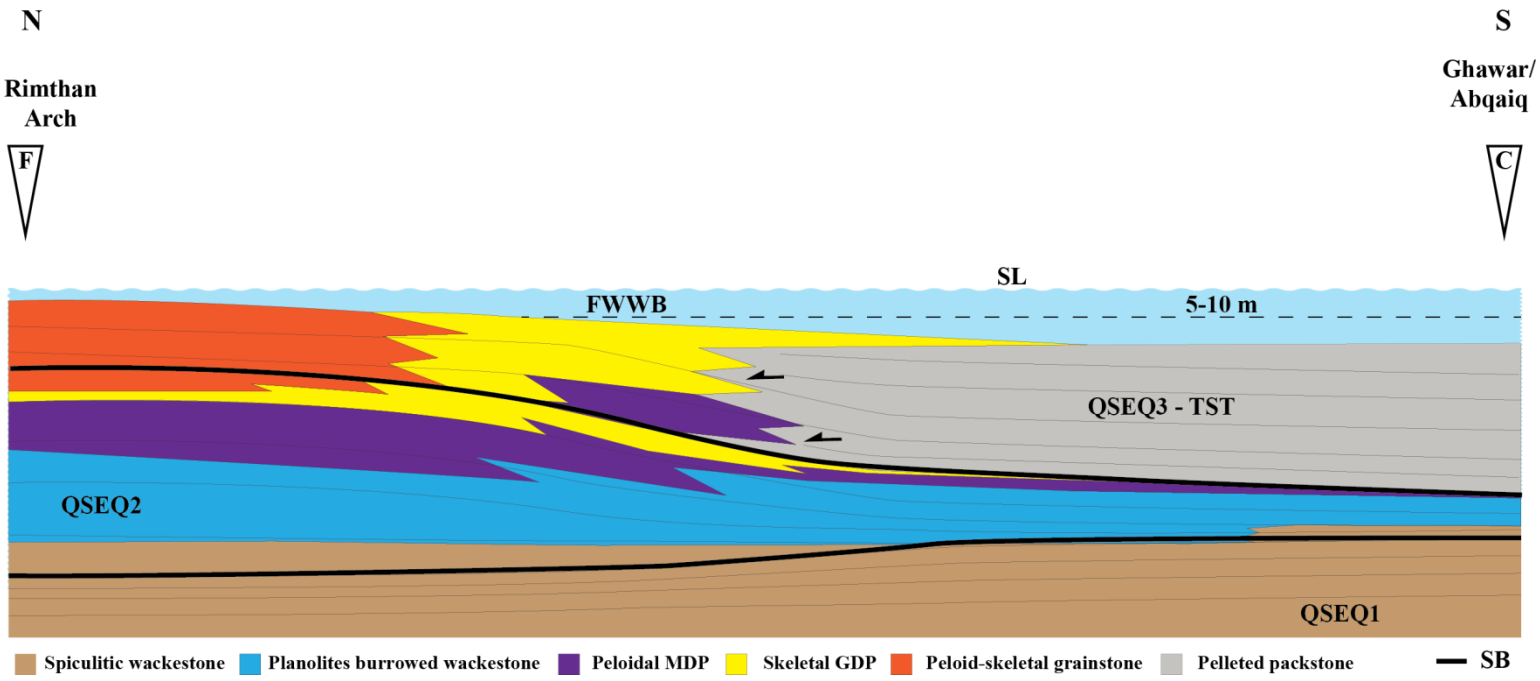

Figure 3. 16: Schematic represenation of the TST of QSEQ3 where the pelleted packstone filling the intrashelf basin during the progradation of the southern margin of Rimthan Arch

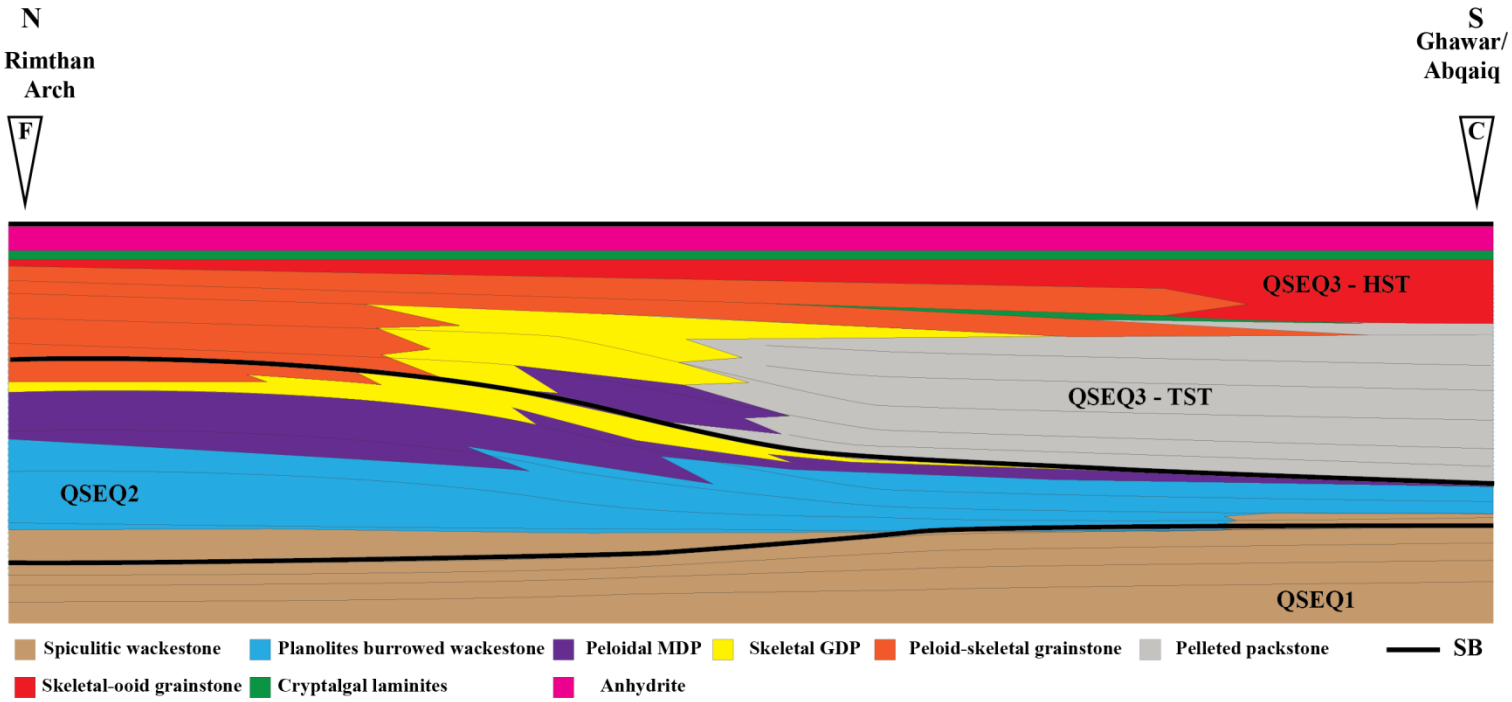

Figure 3. 17: Evovled depositional model and the filling accommodation space. Once the intrashelf basin was filled during TST and early HST progradation direction changes from south towards the north-northeast

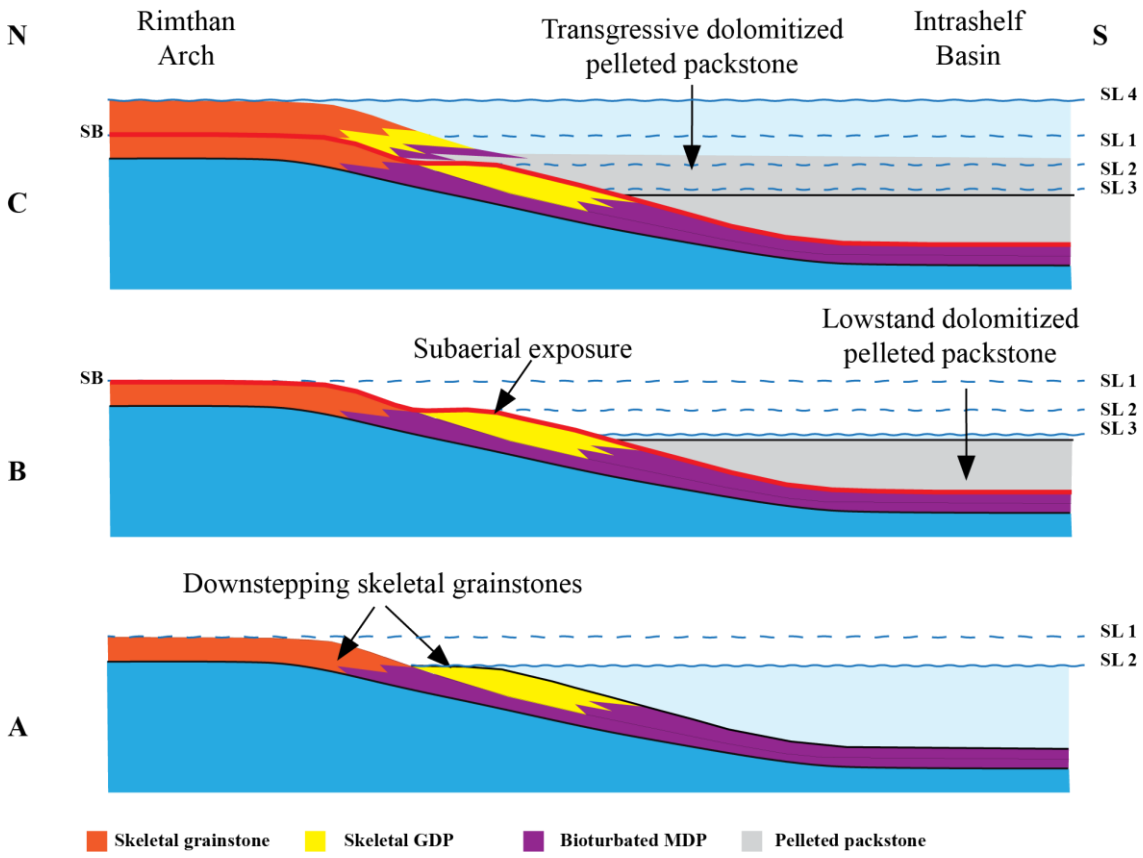

Figure 3. 18: Schematic representation of the continuous deposition of the pelleted packstone recording transgressive, lowstand and highstand sea level high-frequency oscillations.

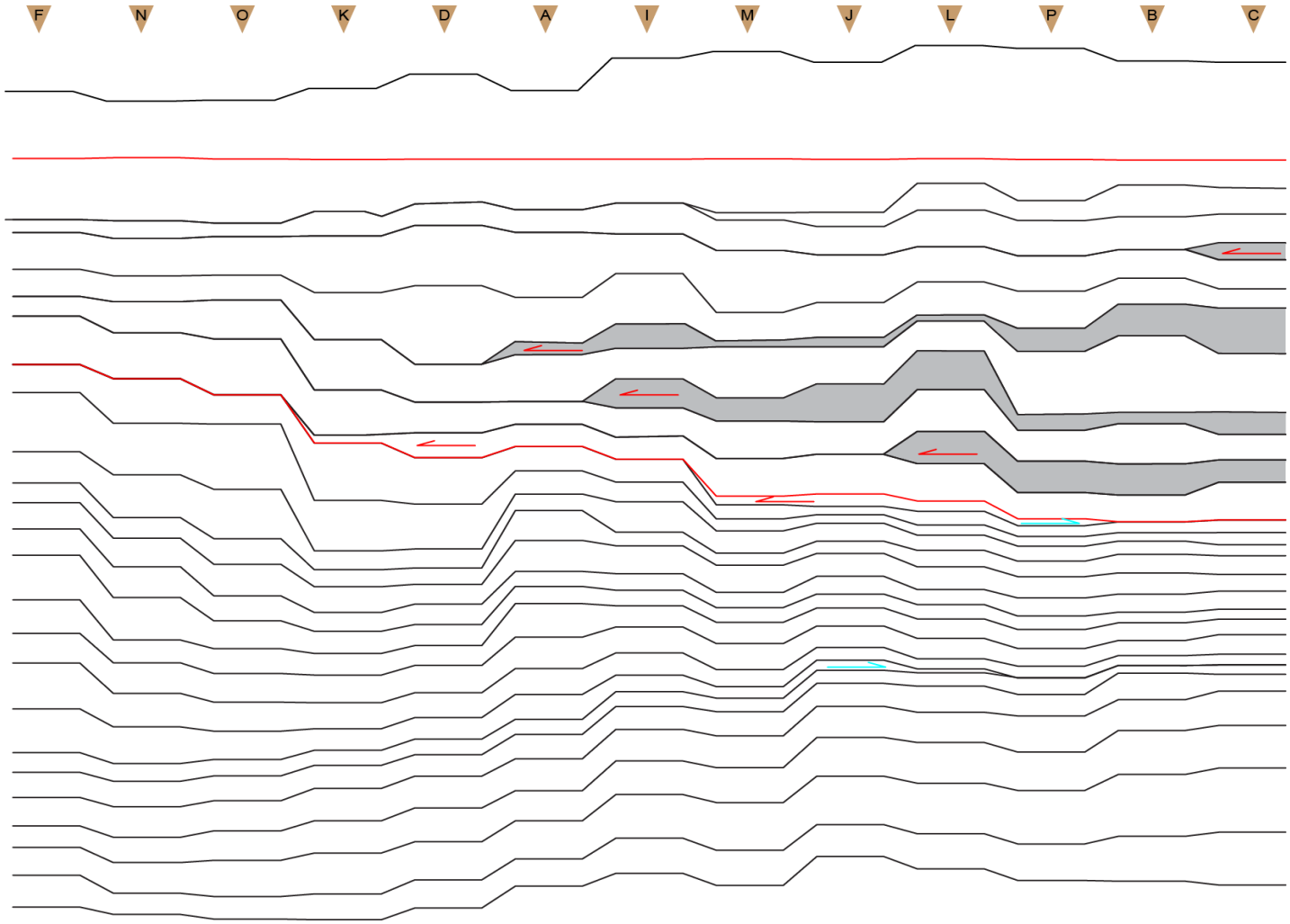

Figure 3. 19: Actual data showing well location and lowstand wedges of pelleted packstone (in grey) displaying onlap geometries

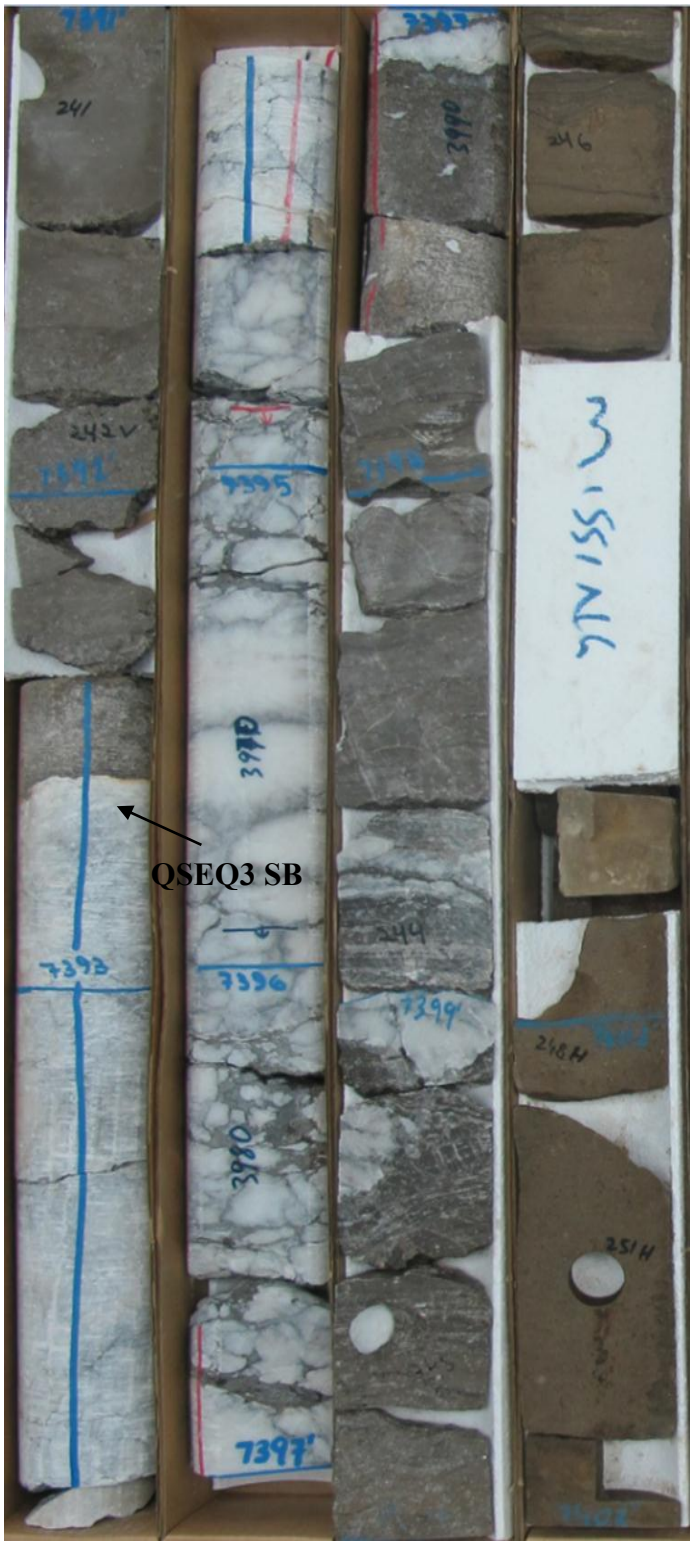

Plate 3. 1: The progressive shallowing, shallowing and filling of accommodation space with anhydrite marks the QSEQ3 sequence boundary. The following transgression resulted in a sharp contact with the overlying skeletal rudstone.

Discussion

The Arab D member in Qatif Field provides important insights into styles of cyclicity, sequence development and stratigraphic architecture of Kimmeridgian carbonate platform. Cycles and high-frequency sequences are typically fully aggraded, many being capped by exposure-related lithofacies. However, cycles rarely display evidence of karst-related diagenetic features compared to icehouse counterparts (cf. Read, 1995). Unlike composite sequences (aka 3rd-Order), which are best developed platform margin and slope, patterns of TST and HST development in high-frequency sequences define the basic depositional facies architecture that most likely to develop on such carbonate platform top.

These sequences are composed of laterally continuous high-frequency cycle that can be correlated across the entire field. The high frequency cycles are probably produced by high frequency sea-level oscillation typical of greenhouse settings. Documented greenhouse setting has sea level oscillation of an amplitude that range between 4-5 m e.g. Lower Jurassic of Morocco (Crevello, 1991) and up to 10 m e.g. the Late Cambrian peritidal cycles of the Appalachians (Koerschner and Read, 1989).

The facies distribution is primarily controlled relative sea-level change and associated accommodation space as well as water chemistry, especially in the intrashelf basin. High-frequency cycles and sequences are affected by local topographic features, namely the Rimthan Arch. QSEQ 1 is low relief, asymmetric sequence which was not affected greatly by the Rimthan Arch and was dominated by subtidal lithofacies. The overlying QSEQ 2 is a symmetrical sequence which its highstand tract was represented by shallow water facies developed at the southern limb of Rimthan Arch. The building of shallow water facies developed a back-arch margin where a break in depositional profile

develops where shoreline and shelf edge trajectories (Johannessen and Steel, 2005) may be applied.

Chapter 4: Diagenesis

Diagenetic modification of petrophysical properties in carbonate reservoir has a significant impact on reservoir quality and its productivity. The Arab D reservoir has four stages recording the succession of the diagenetic environments and processes. Our study shows that diagenetic processes resulted in either reduced or enhanced reservoir characteristics. Major diagenetic processes of the Arab D reservoir include cementation, dissolution, chemical compaction and dolomitization. The precipitation of cements and dissolution of carbonates is primarily controlled by original mineralogy, primary porosity and flow rate of water through pores, the salinity of solutions, composition of pore fluid, Mg/Ca ratios, rate of precipitation, composition of organic matter and geological history of sediments in terms of burial/uplift and prevailing climate (Folk, 1974; Friedman et al., 1974; Mucci and Morse, 1984; Given and Wilkinson, 1985; Tucker and Wright (pp. 314-340), 1990; Hardie, 1996). Similar to burial compaction, chemical compaction associated with burial (but of dissolution rather than mechanical process) can reduce porosity substantially (Schmoker and Halley, 1982; Brown, 1997; Tucker and Wright, 1990).

DISSOLUTION AND CEMENTATION

The sequence of cements observed at Qatif is probably related to the stratigraphic position of the rocks relative to sea-level and to burial history. The main dissolution event predates cementation of isopachous and equant cements. The isopachous cement is the most common throughout the grainy lithofacies of the Arab D, whereas syntaxial and blocky calcite cements are present, but to a lesser extent.

The Late Jurassic (when Qatif Arab D carbonates were deposited) is considered a greenhouse period of earth history (Read, 1990). One attribute of greenhouse carbonates

is that because they were formed in seawater with lower Mg/Ca ratios and higher atmospheric ρCO2, the precipitation of high-Mg calcite (HMC) and low-Mg calcite (LMC) was favored over aragonite (figure 4.1) (Hardie, 1996). Thus, it can be argued that the original mineralogy of most non-skeletal allochems such as ooids and peloids primarily consisted of high-Mg calcite. The ooids have well-preserved radial microstructure (plate 4.1) and this argues that the primary mineralogy was HMC (Sandberg, 1983, 1985). Several examples have documented the HMC mineralogy of the radial ooids in modern environments including Baffin Bay, Texas (Land et al., 1979) and the Amazon Shelf (Milliman and Barretto, 1975).

Isopachous cement may form in shallow-marine settings as high magnesium calcite (HMC) (Schroeder, 1973; Schroeder and Purser, 1986; Aissaoui et al., 1986) or as aragonite (Walls and Burrows, 1985). Folk (1965) classified isopachous cement based on carbonate crystal relative length to width ratios, including crystal size terms and terms describing the relationship between cement and substrate, into three categories: a) fibrous, highly elongated, crystals have length to width ratios greater than 6 to 1, b) equant crystals have length to width ratios of less than 1.5 to 1, and c) bladed crystals have length to width ratios intermediate between those of fibrous and equant crystals. Measurements of axial ratios from several samples where isopachous cement is well developed (plate 4.2) revealed that the most common cement is neither equidimensional nor fibrous but rather bladed (table 4.1). In addition, the isopachous cement does not show square-ended terminations such as typical of aragonite, or the typical noemorphism to blocky spar. One the basis of crystal morphology and greenhouse setting, the isopachous cements are interpreted as relic high-magnesium calcite (HMC). Crystal size is up to 10 μm in width and between 8 and up to 50 μm in length where the width increases with the increase of the crystal's length. There is a general acceptance that the

bladed HMC is of marine origin (Ginsburg et al., 1971; Schroeder, 1972; James and Ginsburg, 1979; Harris et al., 1985; Aissaoui, 1988). The isopachous nature of the cement is due to uniform radial crystal growth from grain surfaces into sea-water-filled pores. However, bladed isopachous cements have also been reported from the mixing zone (Moore, 1977) and from active meteoric phreatic settings where cement nucleates on crystals on the surfaces of grains and grows outward to produce such forms (Halley and Harris, 1979; Longman, 1980). Nonetheless, the bladed isopachous cement lacks polygonal boundaries indicating marine phreatic origin and thus further support the interpretation of meteoric phreatic precipitation (Longman, 1980).

The earliest phase of cementation is represented by the isopachous cement (plate 4.2) composed of euhedral to subhedral bladed calcite crystals which form a significant volume of the total cement. This cement precipitated between grains in facies which were accumulating in the very shallow, warm water grainstones and grain-dominated packstones. The presence of equivalent isopachous cement within leached aragonitic grains (plate 4.1 D), while absent within small intragranular cavities of calcitic grains e.g. *Salpingoporella annulata* suggest two episodes of dissolution: 1) predates isopachous cement precipitation, and 2) postdates isopachous cement precipitation. Thus, the precipitation of the bladed cements must have occurred between two dissolution events.

The dissolution would have occurred in a meteoric phreatic zone where waters are undersaturated with respect to magnesium or during relative sea level fall, which cause the introduction of undersaturated waters and promote the dissolution of the metastable HMC and aragonite grains and precipitation of LMC. HMC is sensitive to saturation state and due its solubility, which can exceed that of aragonite, it will be the “first responder” to these changes (Morse et al., 2006). However, the presence of isopachous bladed cement lining intragranular pores created by dissolved aragonitic grains (plate 4.2 D) and

its absence within pores of dissolved HMC grains (plate 4.1-A,- C,- D) supports the argument of a minor dissolution event predating the isopachous cement precipitation. The second dissolution event probably occurred during exposure, where meteoric waters lead to dissolution and eventual replacement by stable LMC (Friedman 1964, Land et al. 1967, Richter 1979).

The precipitation of the bladed and the equant cements must have occurred between two dissolution events. This probably occurred in a meteoric phreatic zone where waters are under saturated or during relative sea level fall, eustatically or induced by subsidence (unlikely because it would take too long to happen), allowing the percolating freshwaters promoting the dissolution of the metastable HMC and aragonite grains and precipitation of LMC. The HMC is sensitive to saturation state and due its solubility, which can exceed that of aragonite, it will be the "first responder" to these changes (Morse et al., 2006). The presence of isopachous bladed cement within pores created by dissolved aragonitic grains (plate 4.2) and its absence within pores of dissolved HMC grains argues that a minor dissolution predates precipitation of the isopachous cement and was followed by another dissolution event The second dissolution event had probably occurred during times of exposure, where meteoric waters lead to dissolution and eventual replacement by stable low Mg calcite (Friedman 1964, Land et al. 1967, Richter 1979).

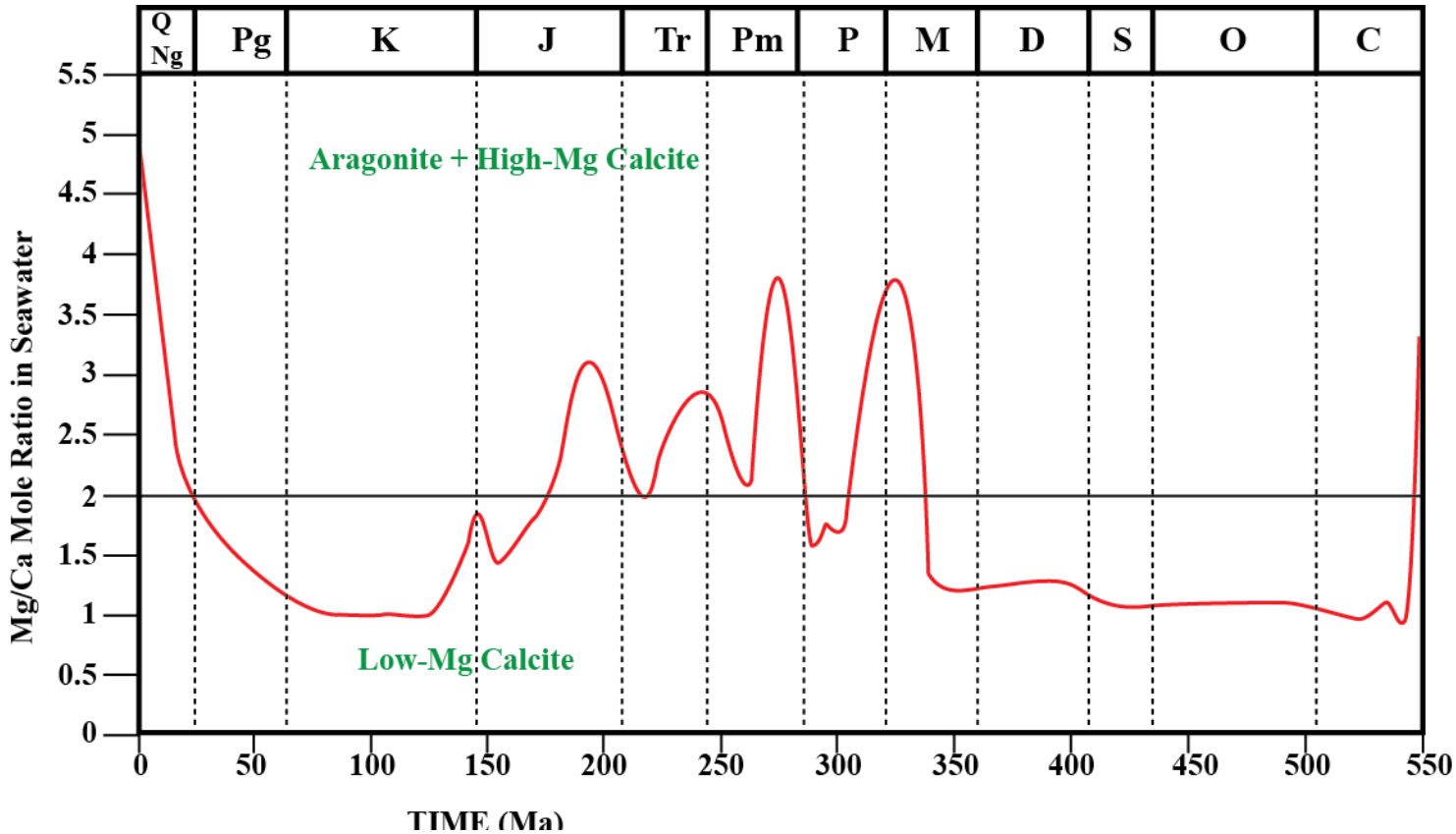

Figure 4. 1: Prediction of secular variation in mineralogy of non-skeletal marine carbonates during Phanerozoic from Mg/Ca vs. time modeled by Hardie 1996. The late Jurassic is predicted to be dominated by LMC.

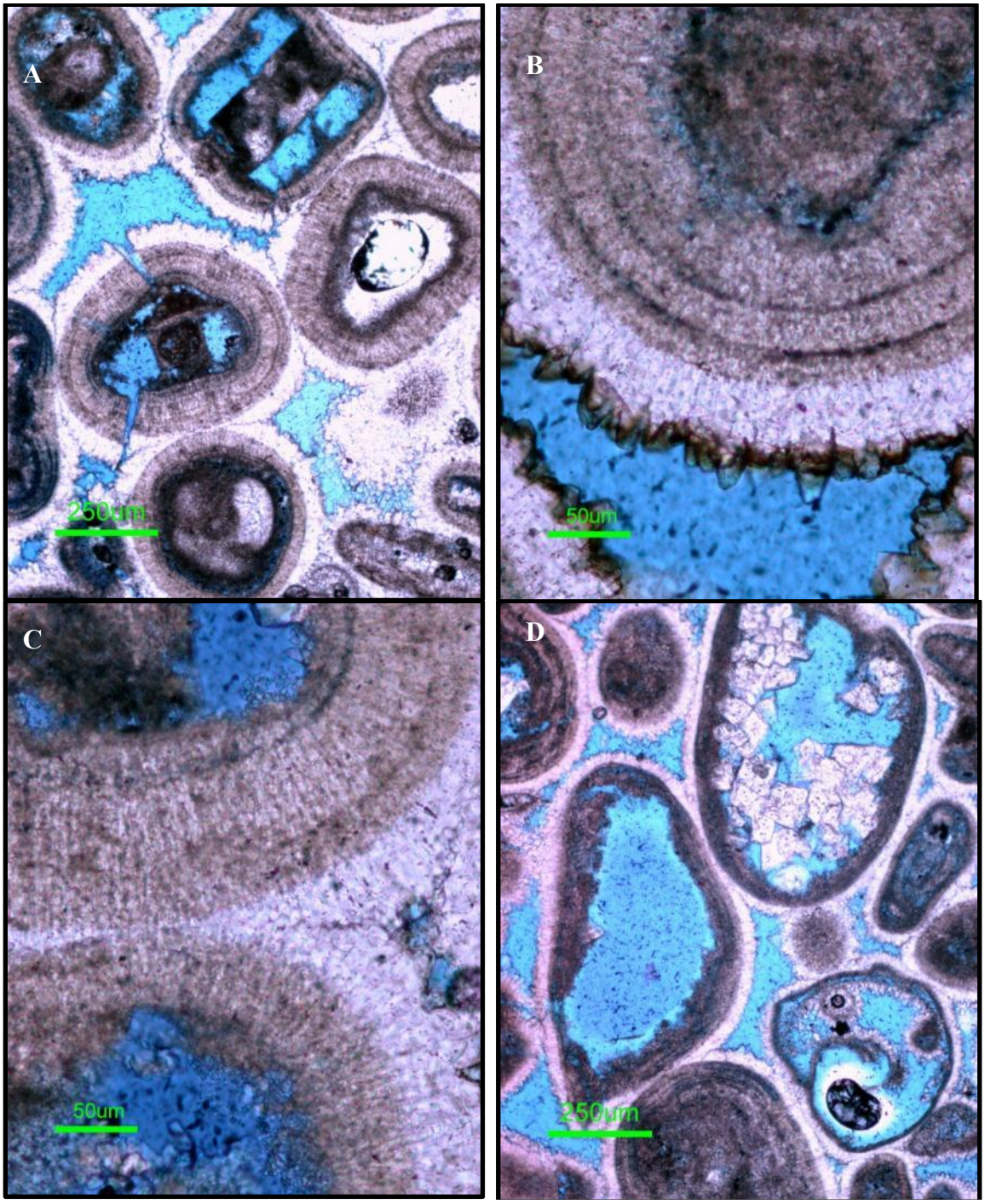

Plate 4. 1: Ooids displaying well preserved radial microstructure suggesting that they have HMC mineralogy (A-C). In D, the isopachous bladed rim cement occurs inside the gastropod (aragonitic) which had to dissolve prior to precipitation of the cement.

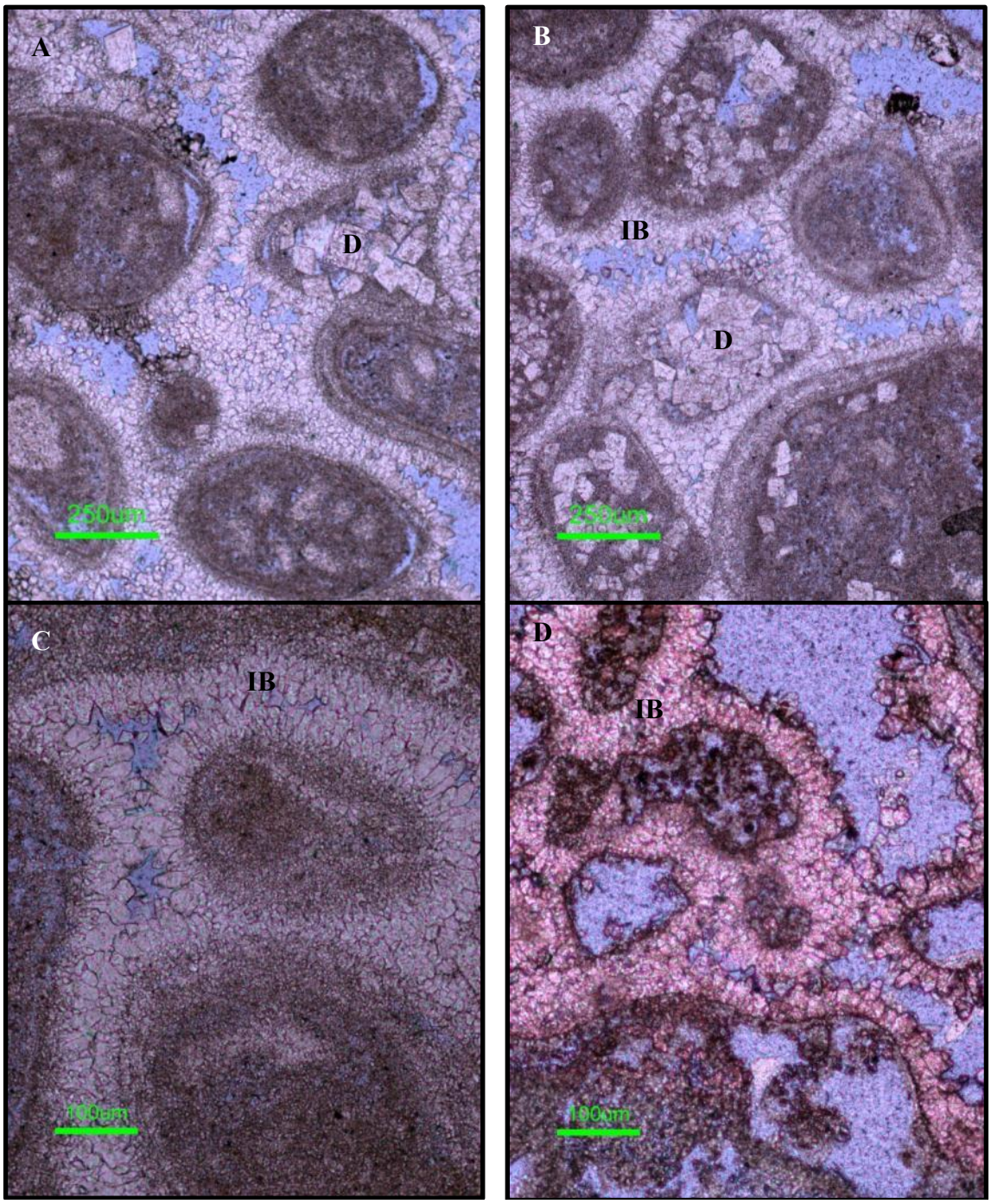

Plate 4. 2: diagenetic sequence starts with slow dissolution, followed by the precipitation of isopachous bladed (IB) cements, followed by a second dissolution and was concluded by the replacing dolomite (D).

Sample # 1		Axial Ratio		Sample # 2		Axial Ratio		Sample # 3		Axial Ratio	
Length	Width	Length	Width	Length	Width	Length	Width	Length	Width	Length	Width
14.64	3.09	5	1	14.77	6.56	2	1	12.92	2.55	5	1
14.15	3.23	4	1	16.82	8.41	2	1	20.51	3.69	6	1
14.15	2.54	6	1	16.00	5.33	3	1	14.36	3.79	4	1
16.31	3.69	4	1	13.33	5.13	3	1	21.64	5.33	4	1
15.54	6.61	2	1	13.74	4.10	3	1	9.27	4.00	2	1
15.38	9.86	2	1	15.80	3.49	5	1	8.41	2.98	3	1
14.31	6.00	2	1	12.10	3.49	3	1	11.69	3.79	3	1
10.87	3.03	4	1	12.92	7.18	2	1	9.13	2.87	3	1
13.69	3.69	4	1	18.15	7.18	3	1	8.10	3.59	2	1
8.62	1.69	5	1	12.51	6.15	2	1	17.49	7.23	2	1
20.62	7.69	3	1	9.44	3.69	3	1	26.67	4.82	6	1
9.08	4.15	2	1	13.54	6.97	2	1	32.61	9.23	4	1
10.77	3.69	3	1	12.72	3.90	3	1	20.41	4.31	5	1
16.15	7.23	2	1	13.13	4.31	3	1	14.77	5.03	3	1
14.00	6.46	2	1	11.28	5.95	2	1	12.10	1.95	6	1
12.46	6.61	2	1	16.41	4.92	3	1	18.46	5.13	4	1
13.85	6.61	2	1	20.72	6.47	3	1	17.64	3.79	5	1
15.23	3.08	5	1	14.97	5.95	3	1	21.54	5.33	4	1
10.92	4.77	2	1	11.28	4.41	3	1	21.13	4.20	5	1
13.23	5.08	3	1	11.28	3.18	4	1	12.92	2.92	4	1
9.84	2.15	5	1	13.54	2.87	5	1	10.31	4.36	2	1

Table 4. 1: Measurements of axial ratios of the isopachous cement from 3 samples indicate that they are mostly fall in the range between 6:1 and 2:1 which is typical of bladed cement (Folk, 1974).

FITTED FABRIC

The term "fitted fabric" refers here to a carbonate diagenetic texture where grain contacts are distinctively concavo-convex (plate 4.3). The arrangement of grains in this distinctly close-fit nature is thought to be a result of chemical compaction related to dissolution rather than the result of mechanical compaction, mainly because it can be shown that this fabric develops within the first meter of burial (refs). In addition, the concavo-convex grain contacts do not show suturing, expected to be observed in mechanical compaction, but rather corroded grain contacts. Several examples have been documented including the Jurassic Dogger Oolites (Cussey and Friedman, 1977), Mississippian Great Oolite Group, Hampshire (Sellwood et al., 1985), and Mississiippian Brofiscin Oolites, south Wales (Hird and Tucker, 1988) (plate 4.4). The distortion of the grain shapes while being fitted results during the dissolution process as leaching of internal structures of the grains aids the flowing of the outer part and results in the extreme fitting observed (Hird and Tucker, 1988). Importantly, the isopachous meteoric cements found in association with this fitted fabric are not deformed, indicating that dissolution which was followed the precipitation of the cements. An illustration of the variables resulting the in development of this fitted fabric is shown in figure 4.2.

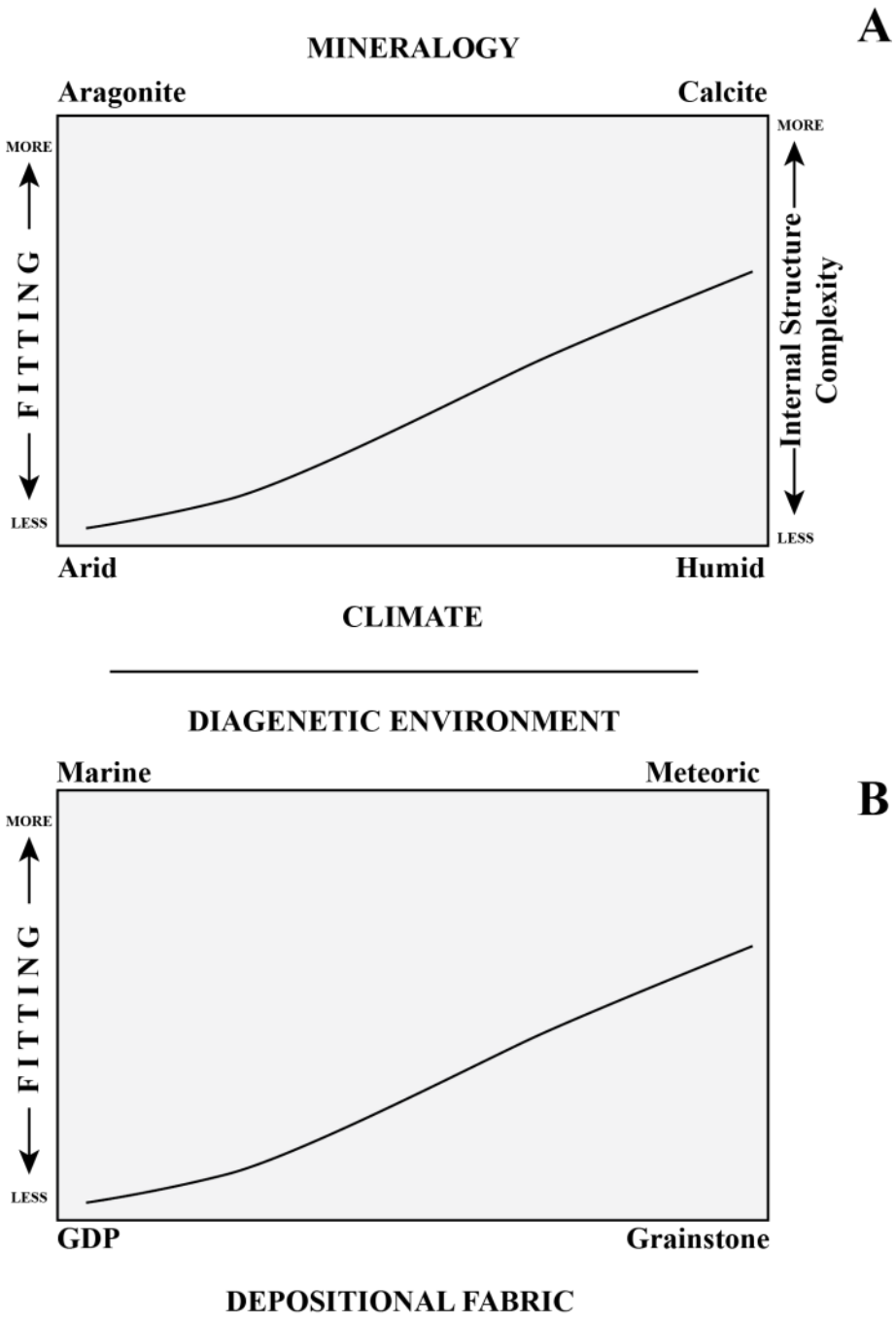

Figure 4. 2: Two figures showing different variables controlling the development of fitted fabric. A) A small degree of leaching of internal structure is needed to aid the fitting of grains which then is followed by precipitation of isopachous cement favored in semi-humid environment (Hird and Tucker, 1988). B) Calcitic grains are more likely to experience the leaching in the undersaturated meteoric setting, favored in grainstones.

Dunham (1969) classified the compaction as chemical, suggesting that it occurred in vadose zone and termed the resultant fabric as fitted fabric. In extreme cases, a complete loss of interparticle porosity occurs when grains are completely closely packed (plate 4.3). He reported the occurrence in the intertidal zone of a very young beach rock. Recent examination of recent beachrock from Turks and Caicos, Bahamas (plate 4.5) show an initial fitting phase where grains start to corrode and interlock with each other prior to complete development of the rim cement. This observation agrees with Hird and Tucker's (1988) interpretation that leaching of internal structures of grains is what allows them to "flow" and interlock. In cores, this fabric is observed to coincide with grainstones near the top of shallowing up cycles; this diagenetic process is associated with vadose conditions, which is observed at the tops of cycles. Sellwood et al. (1985) have reported that these fabrics are best developed at the capping horizons of in shallowing upward oolitic cycles while their intensity of development diminishes downward from such surfaces. Similarly, the fitted fabric observed in the Arab D is restricted to grainstones capping or close to the cap of shallowing upward cycle (plate 4.6, 4.7).

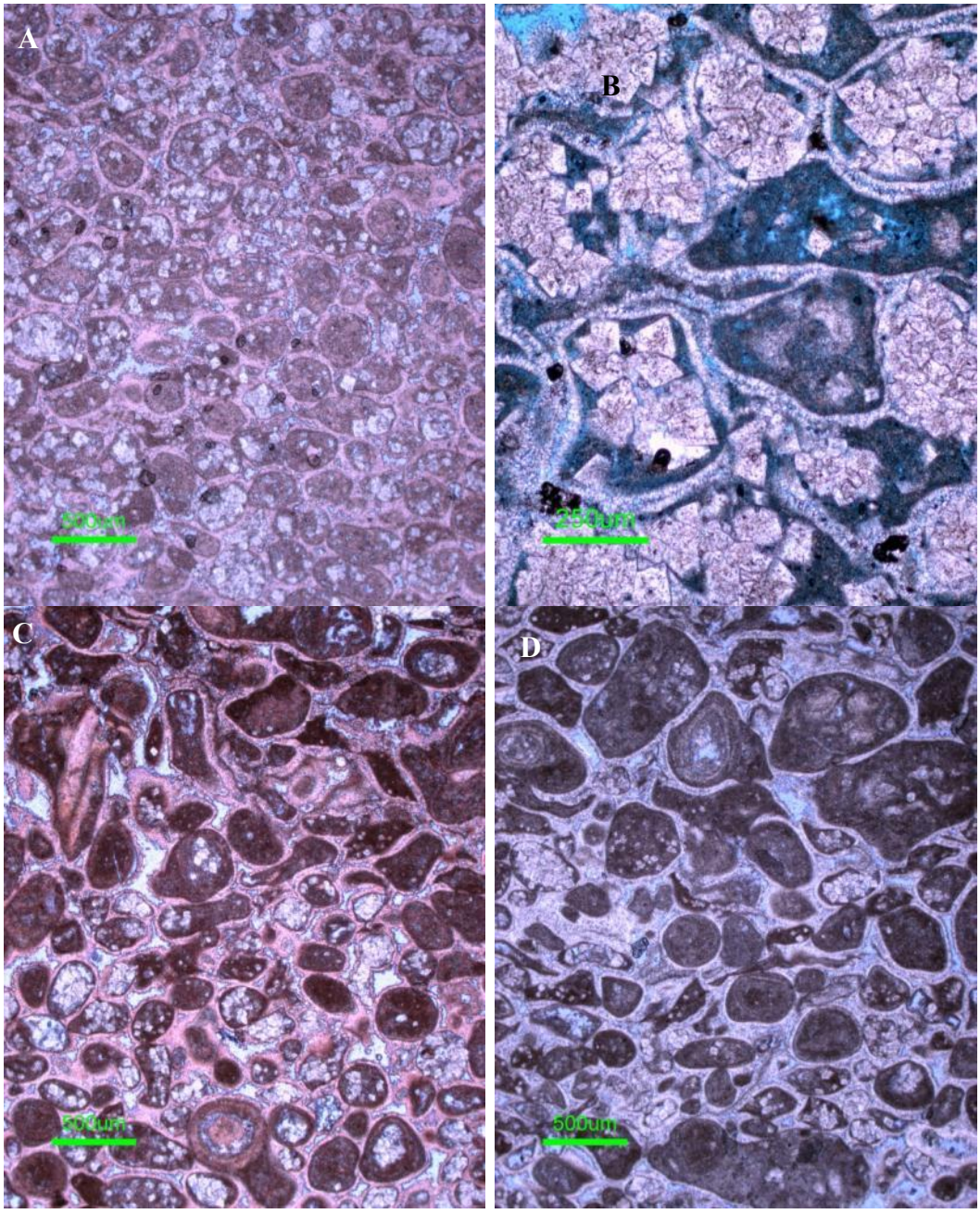

Plate 4. 3: Several photomicrographs displaying fitted fabric which characterized by concavo-convex contacts. The early dissolution of internal structures of grains resulted in the flow and fitting of the grains and was followed by the growth of the rim cements. Another dissolution event occurred prior to the final stage of diagenesis characterized by replacement dolomite.

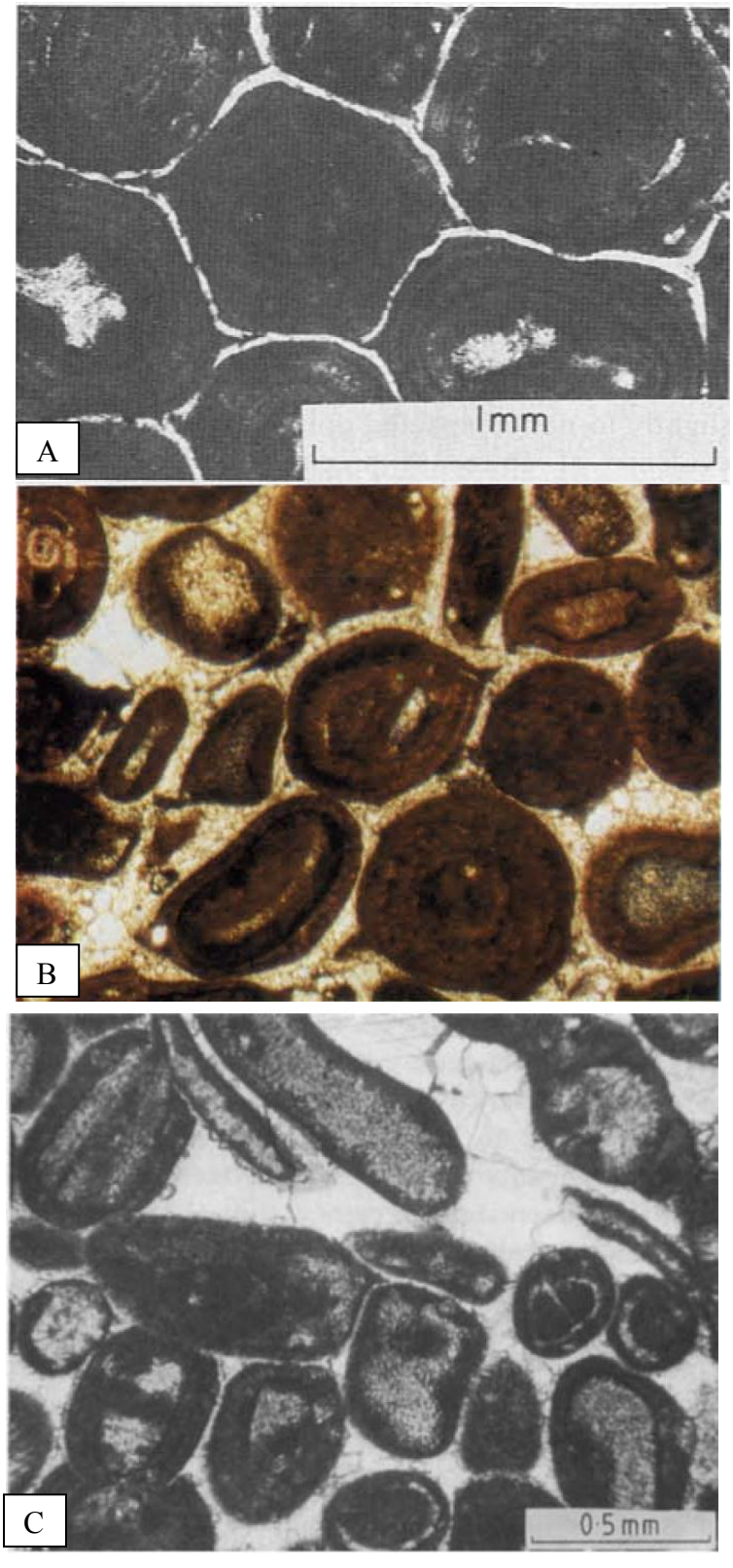

Plate 4. 4: Fitted fabric documented in earlier studies A) Cussy and Friedman (1977), B) Sellwood et al. (1985), C) Hird and Tucker (1988).

Plate 4. 5: Modern example from Turtle Cove beach, Turks and Caicos where fitting occur on beach with incipient development of isopachous cement.

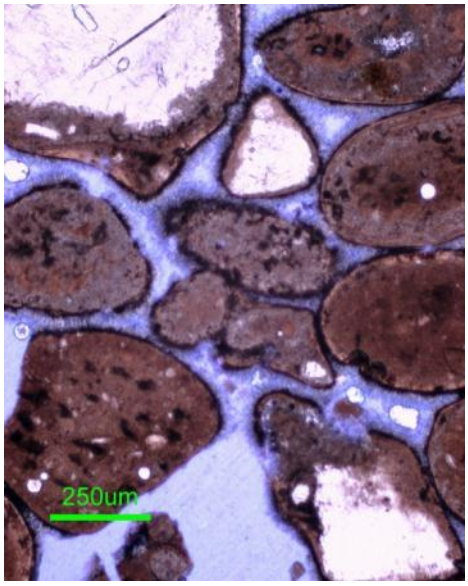

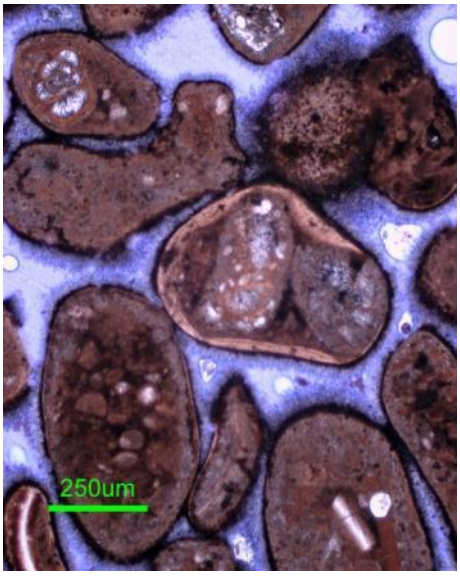

In order to illustrate this process in the Qatif Arab D, the distribution of fitted fabric was documented in detail by describing thin sections at one-foot intervals through multiple upward-shallowing cycles in four wells (F, L, O, P) and was visually assessed in rest of cores (plate 4.8). The overall trend shows that toward the Rimthan Arch, to the north, the topographically higher grainstones are more prone to develop the fitted fabric (figure 4.3). The trend is predictable as the active meteoric phreatic lens will be more mobile and sensitive as sea level fluctuates.

The fitted fabrics and their vertical distribution within the cycle-capping grainstones could be of stratigraphic importance as they may reflect sea-level fall, or at least cycle-scale exposure. In essence, as relative sea level falls, the active meteoric phreatic lens will move downward and basinward and results in the development of such fabrics within the grainstones. This fabric appears to have a great potential in aiding cycle stacking patterns, especially when grainstones amalgamate during progradation, as cycle tops could be assigned to the greatest abundance where the fitted fabric occurs.

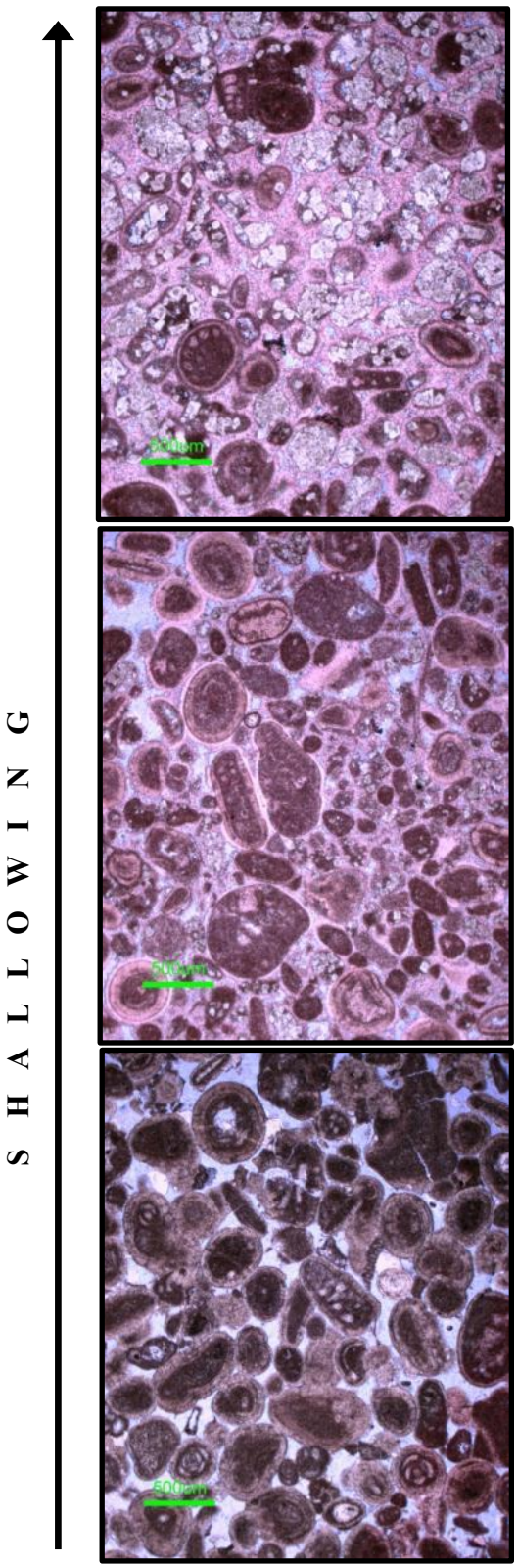

Plate 4. 6: Fitted fabric and cementation increases towards cycle tops.

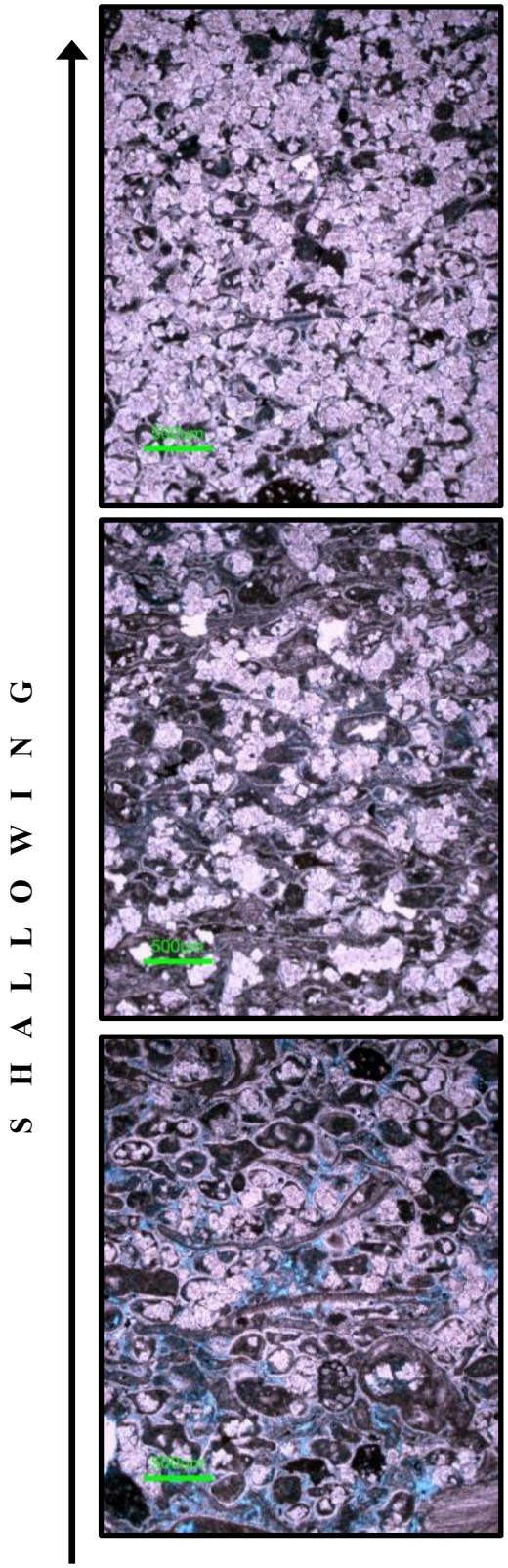

Plate 4. 7: Fitted fabric and cementation increases towards cycle tops with complete loss of interparticle porosity

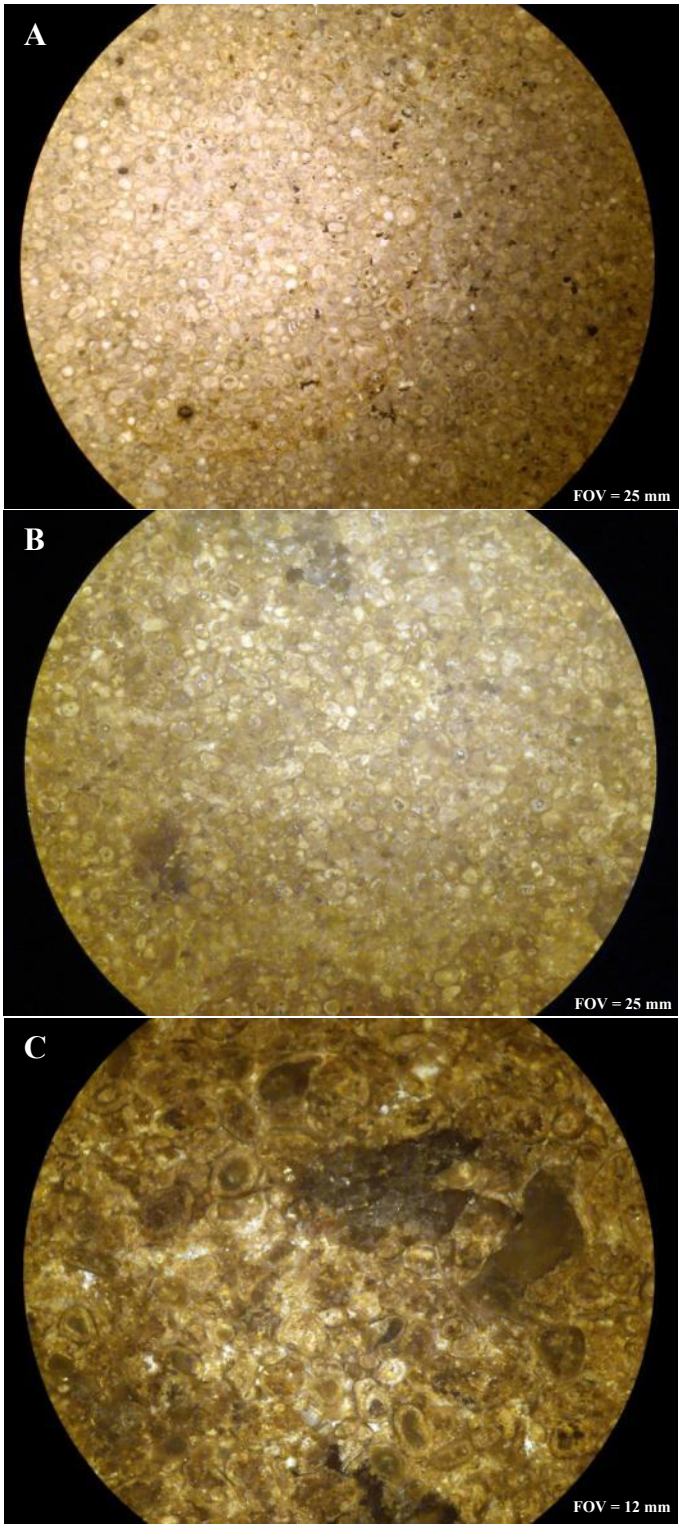

Plate 4. 8: Several photos taken down the ocular of a binocular microscope showing examples of fitted fabric in grainstones

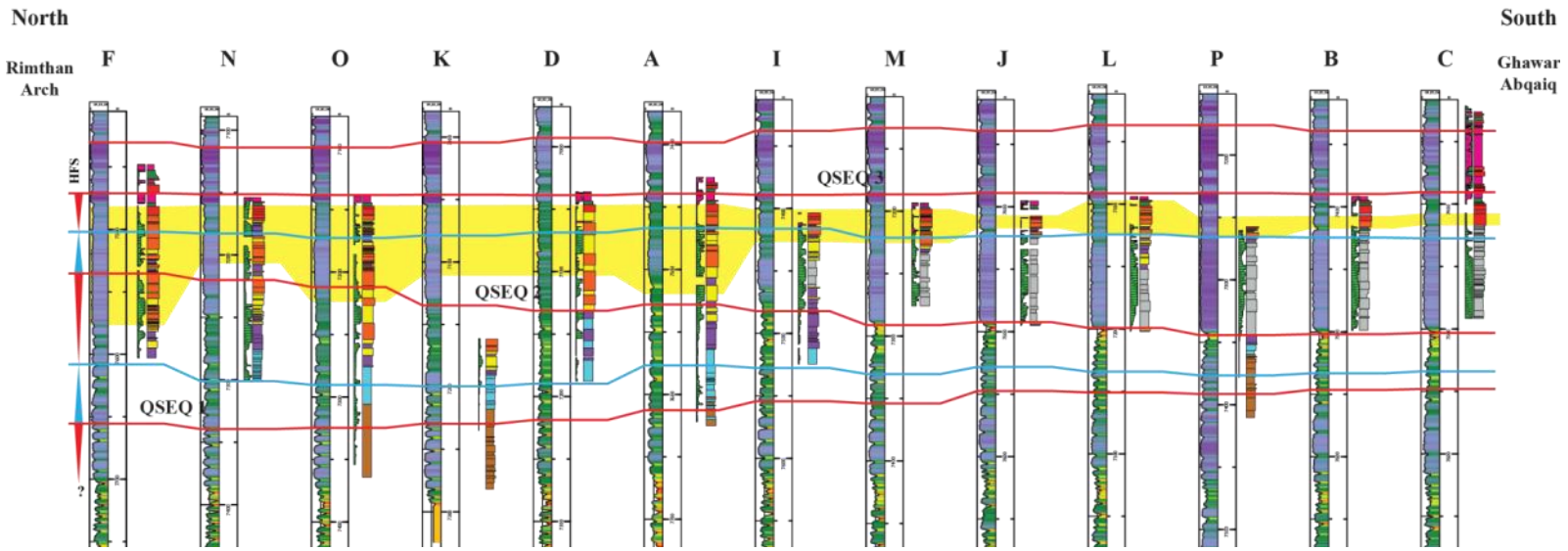

Figure 4. 3: Mapped fitted fabric using thin section and visual assessment from core. In general, fitted fabric diminishes towards the south.

DOLOMITIZATION

Dolomitization has a major impact on reservoir quality in the Arab D reservoir of the Qatif Field. Dolomite may or may not preserve the original depositional texture of the dolomitized host. In general, reservoir quality is enhanced where dolomitization exceeds 75%, while lower dolomitization percentages tend to reduce reservoir quality (plate 4.7). Further, in leached grainstones, dolomite tend reduce the porosity significantly as it occludes moldic porosity. Although dolomite can be recognized from the bulk density wireline log, it was not used as part of this study and dolomite was mapped using core and thin section data. In cores, it is easily identified as it has distinct rhombic crystal shape that often shows sucrosic texture. In addition, itching the cores with hydrochloric acid results in the dissolution of calcium carbonate surrounding the dolomite, and thus dolomite will be easily identified as it will have high relief with a rhombic crystal shapes. The dolomite will show very slow, almost absent, reaction to diluted to 10% hydrochloric acid, which will reveal a vigorous reaction with calcite. In thin section, dolomites appear as colorless rhombs with unit extinction that are not stained with Alizarin Red S, which will produce red-orange staining of calcium. The crystals are euhedral to subhedral and in general are less than 100 μm in size.

Dolomite is not evenly distributed across the field. In QSEQ 1, dolomitized strata are estimated to range between 0–15%, where core is available, with an average of 6% (figure 4.4) in which dolomite occurs as scattered crystals occur within the muddy matrix of the host sediment composed of subtidal spiculitic wackestone. The. Dolomite crystal size range between 20 to 45μm and lack any direct or indirect indication of precursor calcite.

In QSEQ 2, most of the dolomite occurs in ramp crest at the northern segment of the field. Dolomitization is more significant during highstand where an average of 35%

of the strata is dolomitized (figure 4.5). On the other hand, the dolomitized strata of the TST ranged between 10–40% with an average of 20%. In general, dolomitization front appears to diminish towards the southern area of the field which may suggest that most of the dolomitizing fluids where traveling downdip towards the intrashelf basin from the Rimthan Arch.

QSEQ 3 HFS displays the most extensive dolomitization; the average of dolomitized strata is about 45%. Despite lacking discernable pattern, dolomitization during the TST is significantly important at the southern segment of the field, average of 70%, occurring mostly in pelletal packstone deposited in the intrashelf basin (figure 4.6). On the ramp crest's TST facies, dolomites are generally less abundant; average is about 40% common in grainer shallow water facies. During the HST, dolomitization becomes less abundant in the southern segment of the field with only 12%, in average, of strata are dolomitized; whereas dolomite occurring in ramp's crest at the northern segment of the field averages about 38%.

In thin section, dolomite appears as colorless, rhombic crystals that replace early calcite matrix and/or grains in all lithofacies from spiculitic wackestone to anhydrite. Generally, dispersed dolomite crystals ranging in size between 25 to 60 microns are found in muddy facies, while in grainer facies dolomite crystals range in size between 50 and up 90 microns (plate 4.9). Dolomitization in grainy facies tend to increase towards cycle tops and decrease away from it. In general, the dolomite cannot be correlated across the field as it does not follow stratigraphic horizons but rather permeability pathways and hence it cross-cut stratigraphic boundaries (figure 4.6).

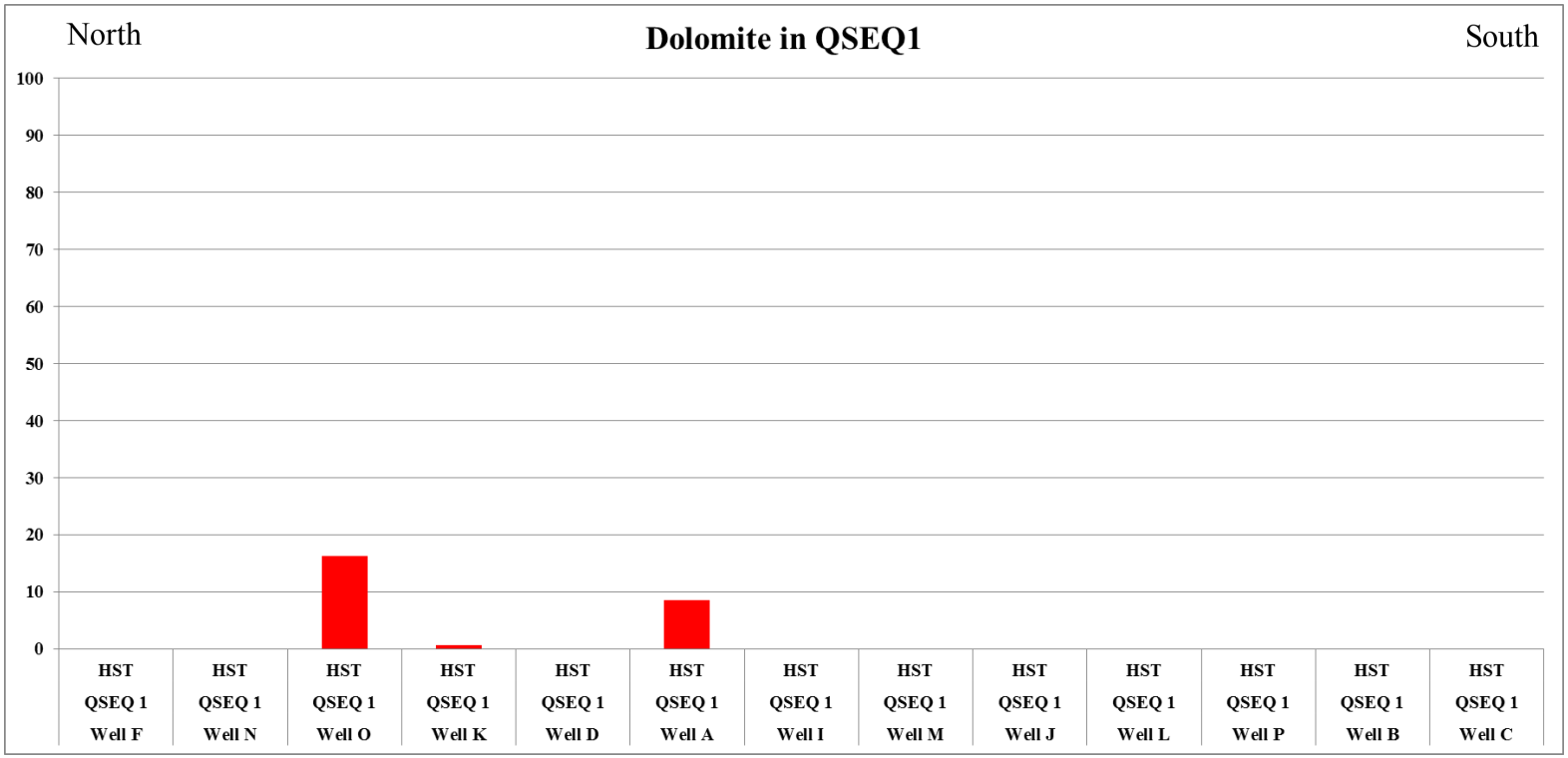

Figure 4. 4: Percentage of dolomitized strata in QSEQ 1. Data is limited due to poor core control. Dolomitization average is about 6%.

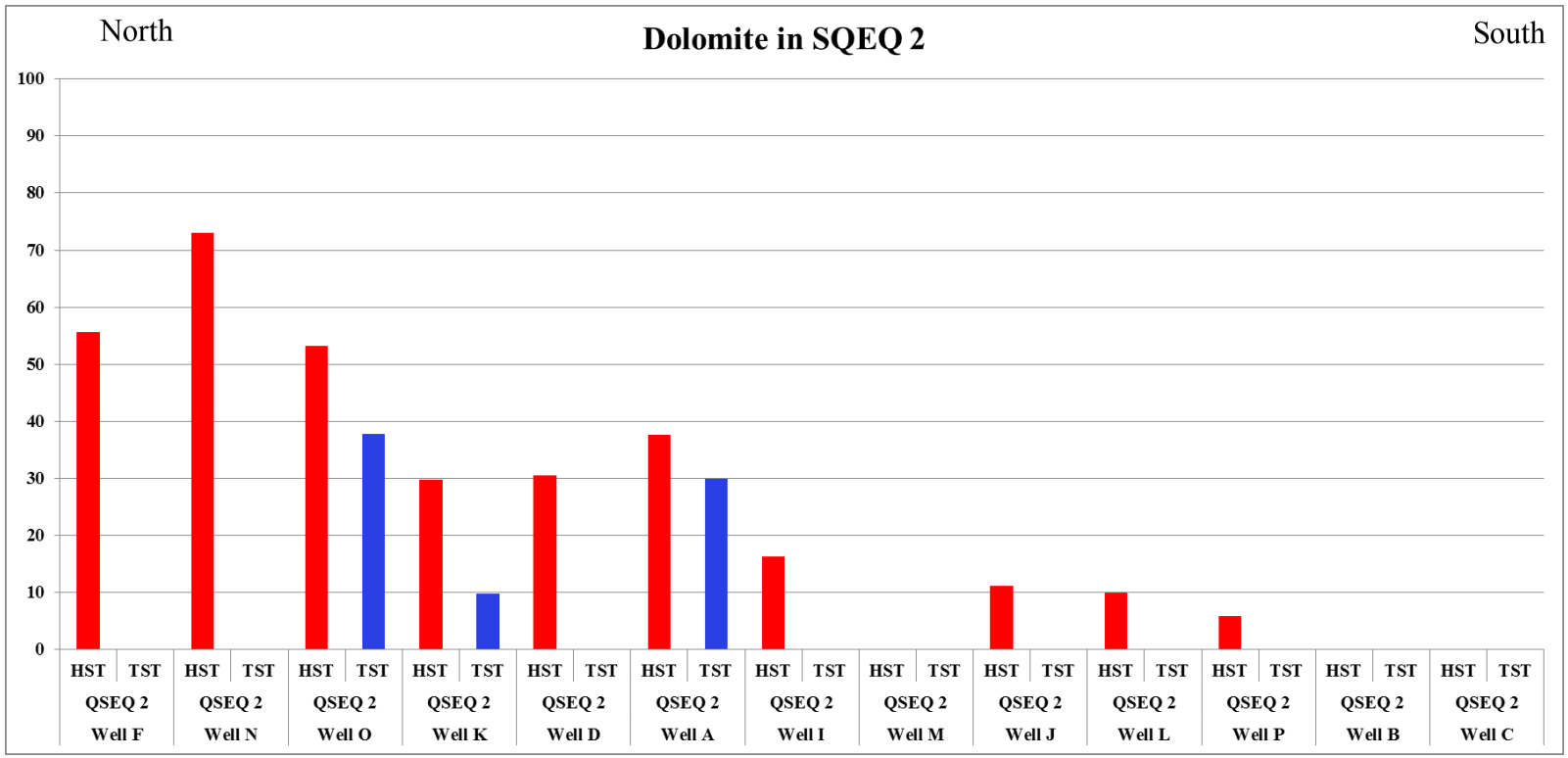

Figure 4. 5: Percentage of dolomitized strata in QSEQ 2. Dolomite is mostly common in the northern segment of the field during HST (6-75%) which diminishes towards the south with an overall average of 35%.

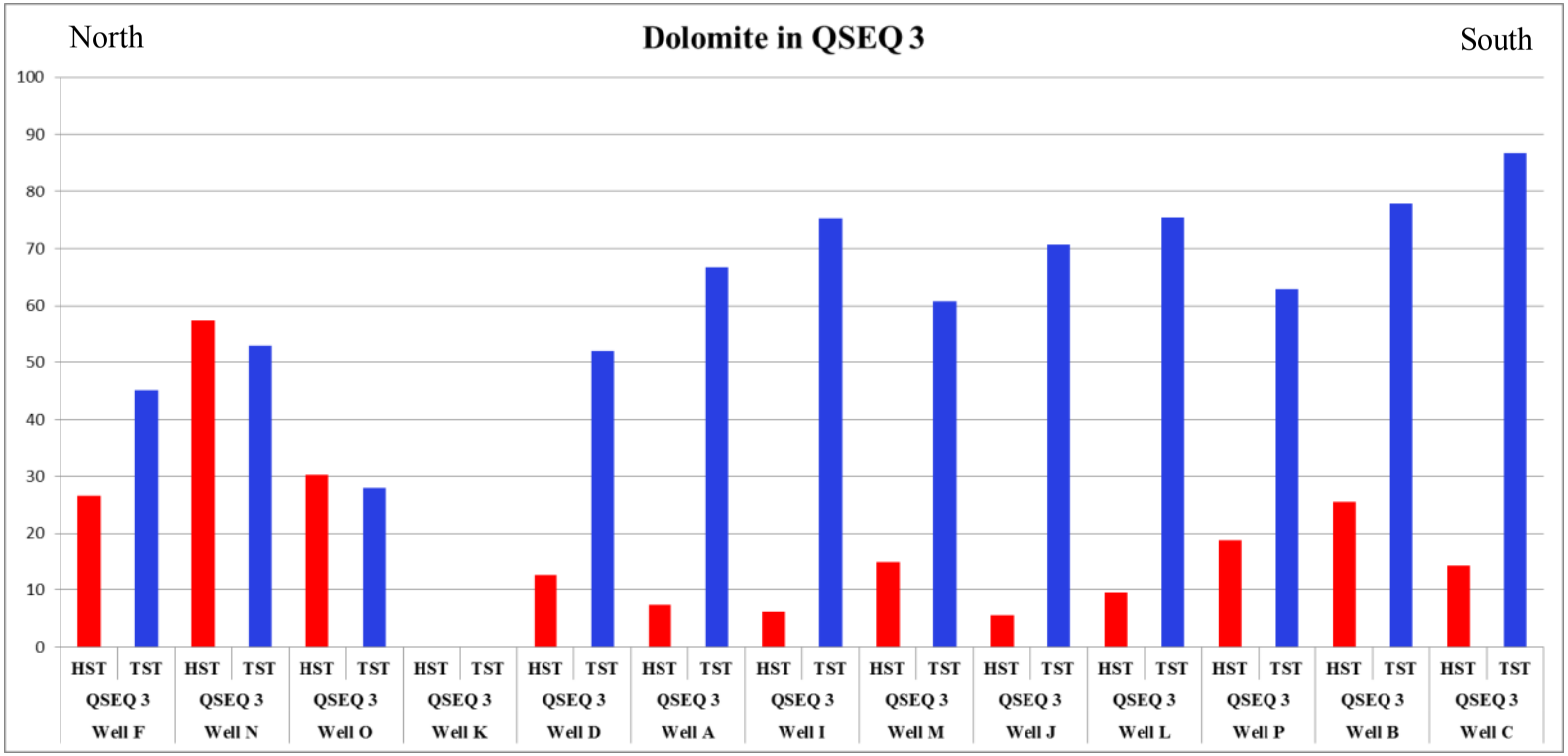

Figure 4. 6: Percentage of dolomitized strata in QSEQ 3. During TST, dolomite is mostly common in the southern segment of the field (~70% dolomitized) in pelletal packstone deposited in intrashelf basin settings, whereas dolomite in the northern segment averages about 40%. During the HST, dolomitization prevails in the northern segment of the field (about ~38%), mostlyin grainy, shallow water facies, which diminishes southward (average ~ 12%)

The dolomite that forms in grainstone and grain-dominated packstone beds increases in abundance when coinciding with the fitted fabric (plate 4.6, 4.7). This dolomite postdates the fitted-fabric-associated dissolution and bladed calcite cementation, making the dolomitization process the last in the diagenetic sequence. Following active meteoric lens migration and associated dissolution and precipitation of rim cement, further sea level fall may place these grainstones in the vadose zone. The vadose zone is characterized by under saturated waters which will result in the dissolution of allochems that are compositionally unstable.

The timing of dolomite replacement of the pelleted packstone in QSEQ 3, deposited in the intrashelf basin, is not clear, but it appears to have started the replacement during sea-level lowstands. Increased evaporation, during lowstands, results in increased salinity which may drive the replacement process (see next section). The other dolomite that forms in muddy lithofacies including spiculitic wackestone, *Planolites*-burrowed wackestone and peloidal MDP (plate 4.6 A-D) is dispersed in the matrix and may have formed during burial.

On the ramp crest, shallow water facies, the progressive dissolution of high-Mg calcite was followed by the precipitation of dolomite crystals found in void space or growing within the allochems (plate 4.3B, 4.6E). Dissolution of Mg-calcite allochems and associated expelling of Mg^{2+} into solution is not volumetrically significant raise Mg/Ca ratio to drive the dolomitization process in an open system setting (Kerans personal comm.). It is more likely that the seawater was the source of Mg to drive the dolomitization process (Warren 2000). This is supported by the diminishing of dolomite in the strata landward during the highstand of QSEQ 2 and QSEQ 3 (figure 4.5, 4.6) which was in closer proximity to seawater.

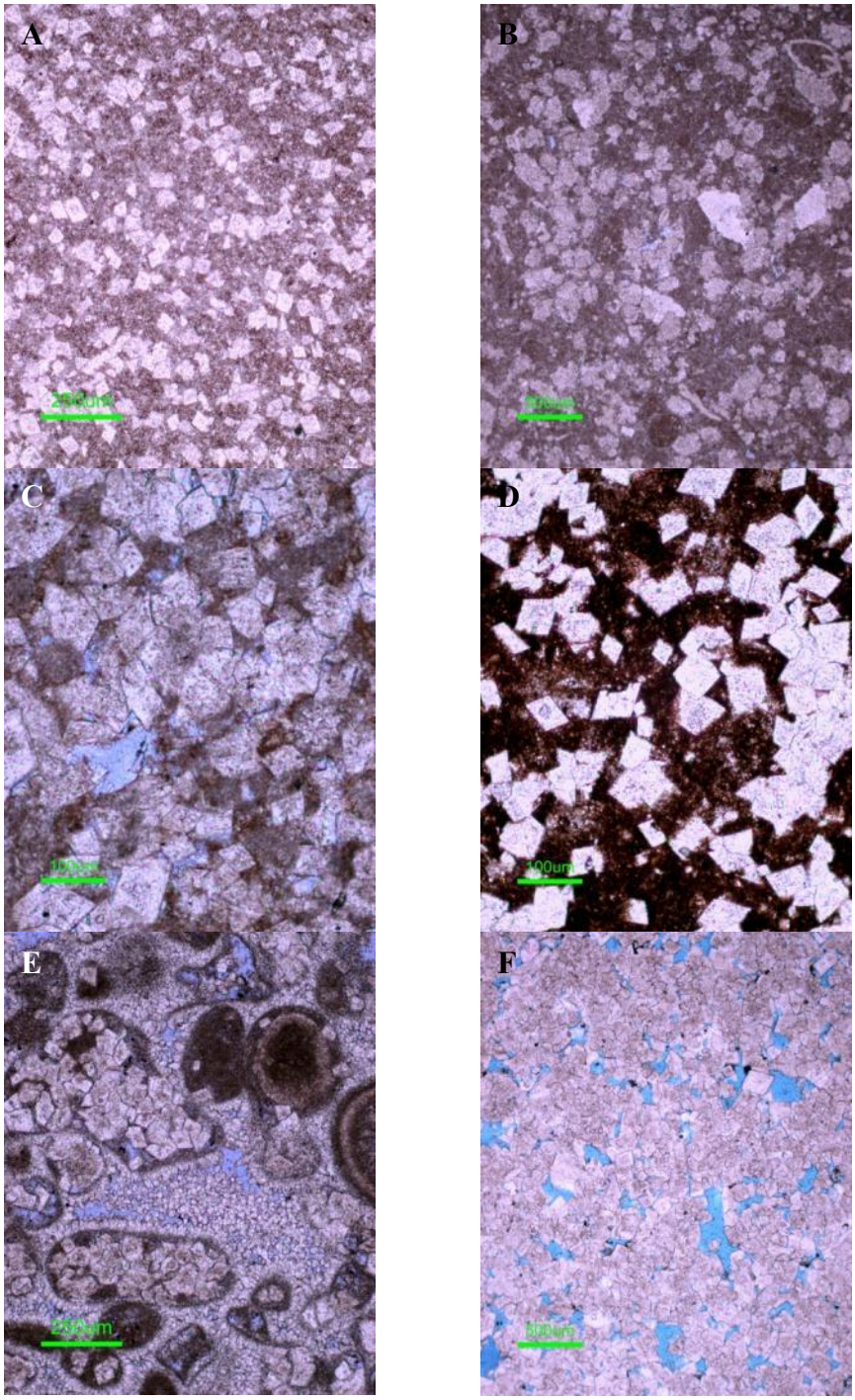

Plate 4. 9: Photomicrographs of dolomite development in muddy facies (A-D) and grainy facies (E-F).

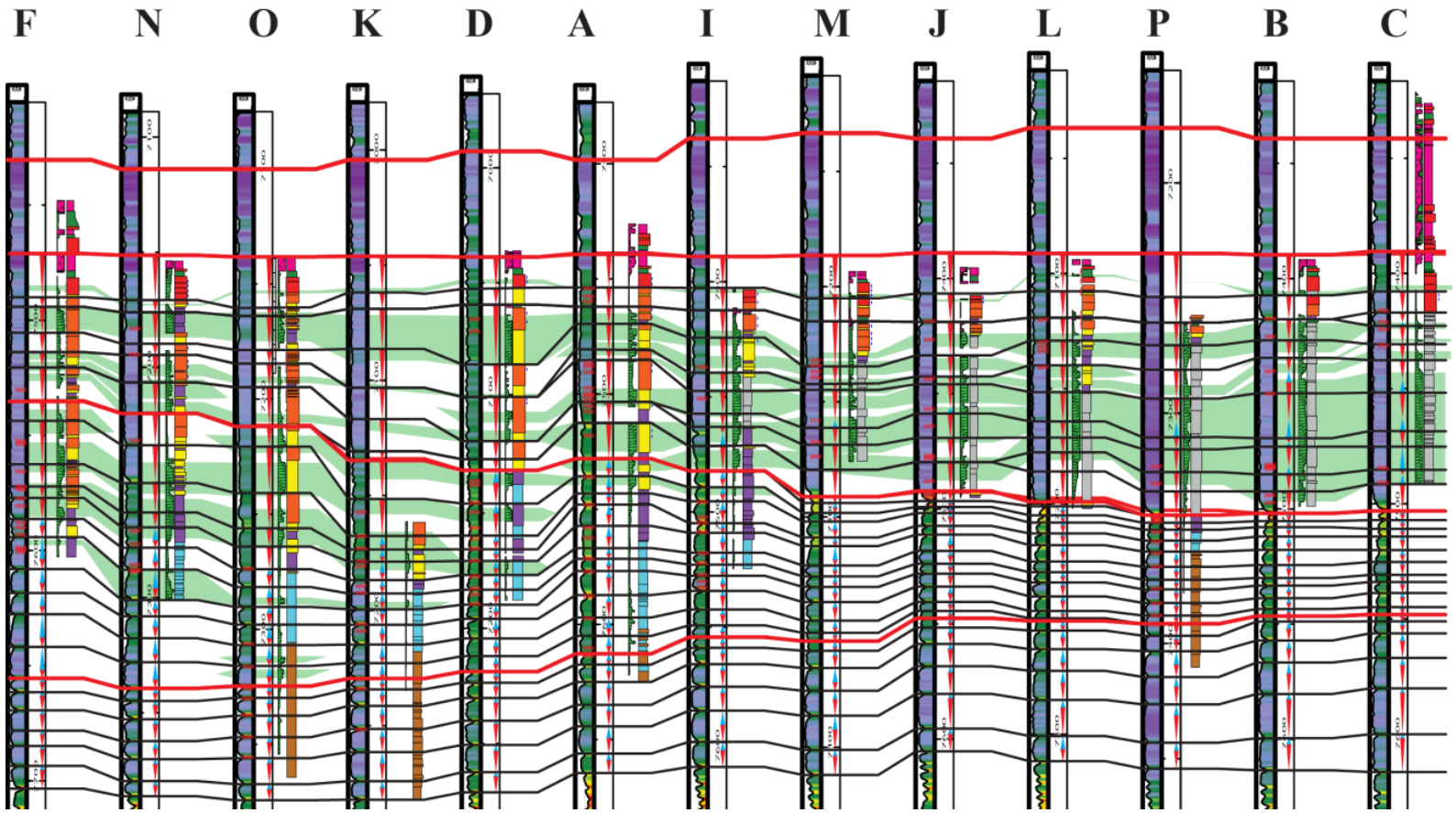

Figure 4. 7: Dolomite distribution across the field does not show any relation with stratigraphic framework.

Qatif Intrashelf Basin Dolomite

The dolomite fabric observed in the Qatif cores and thin sections (plate 4.7) has rhombic crystals. The dolomite percentage of the pelleted packstone in the restricted intrashelf basin increases towards cycle tops while decrease towards the base of cycles (figure 4.8). The trend is not evident but certainly is noticeable. The increase of dolomite percentage closer to cycle tops suggests increased Mg/Ca ratios to drive the dolomitization process. The optimum period would be during the cycle-scale lowstand where longer residence times associated with continuous evaporation will result in increased Mg/Ca to drive dolomitization (Gunatilaka et al., 1984). In addition, the reduction is attributed to the cycle-scale transgression events where sea waters reduce the salinities creating schizohaline conditions (Folk 1974) reducing the Mg/Ca ratios (Gunatilaka et al. 1984) inhibiting dolomite precipitation. Well J is perfectly located to record pulses of transgression and several cycles show the coincidence of cycle top with the highest percentage of the dolomite in HFC 3.1 to HFC 3.6 (figure 4.8).

Within the intrashelf basin, the increase of dolomite towards cycle tops is interpreted to have formed during as early as the highstand or that cycle and/or during shallow burial by seawater evaporated to gypsum saturation, as the same unit is observed in Fazran Field to be overlain by evaporites (Kerans personal comm.). Early dolomites likely consisted of metastable protodolomites that were later recrystallized to more organized structure shortly after being precipitated in shallow burial environments when early replacement dolomites were still in contact with dolomitizing brines (Warren, 2000). Thus, dolomitization was probably controlled by water chemistry, permeability pathways and burial and cannot be related to stratigraphic architecture.

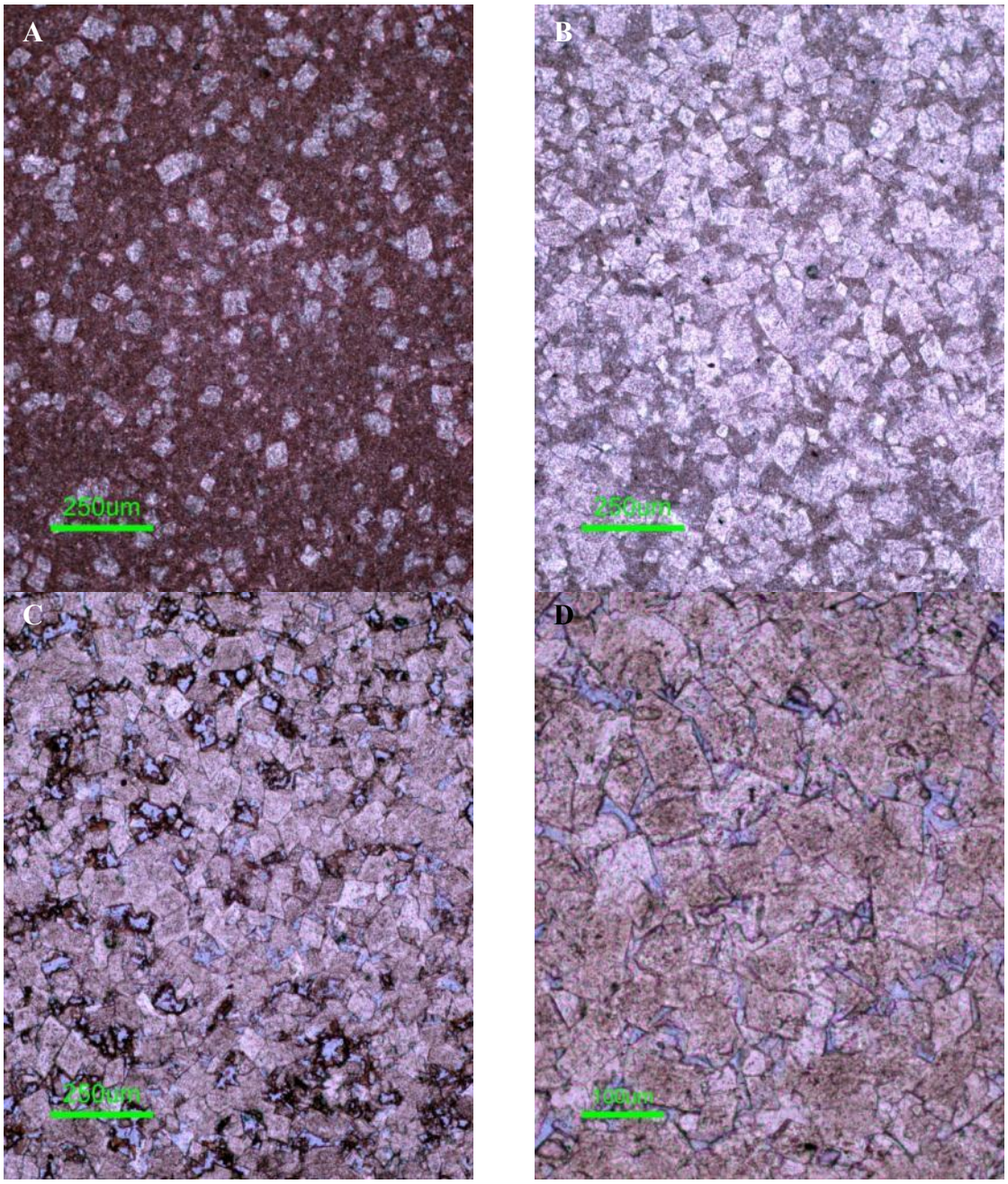

Plate 4. 10: Dolomite developed in intrashelf basin at different percentages of dolomitization.

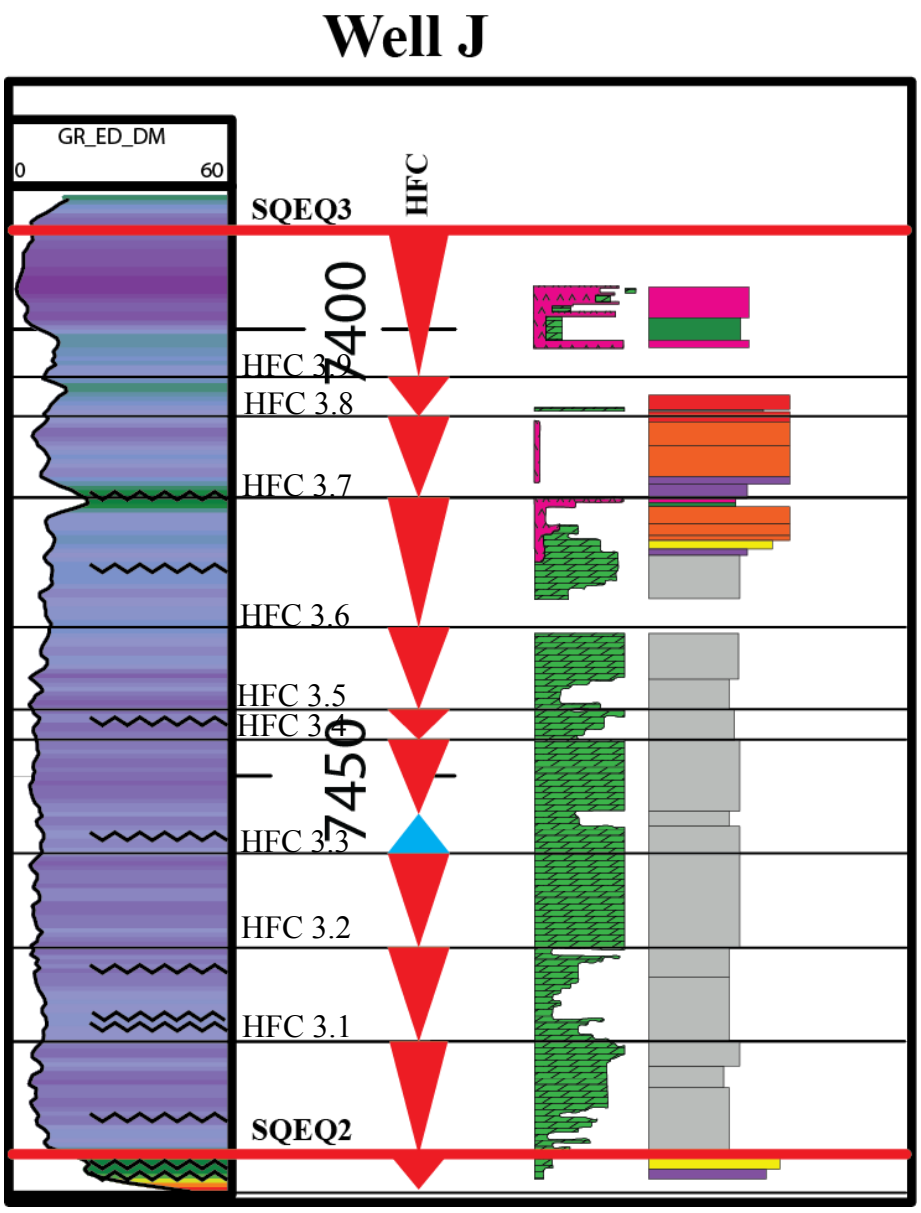

Figure 4. 8: Dolomite percentage increases towards cycle tops especially in the intrashelf basin and decreases at times of flood backs.

The Origin of Qatif Intrashelf Basin Dolomite

Primary dolomite, or dolomite forming syndepositionally as a precipitate at earth surface temperature, is very rare and is only found in certain lakes and lagoons. The Coorong, a long, shallow lagoon more than 100 km in length that is separated from the Southern Ocean by a narrow sand dune peninsula, in southern Australia, is one site were primary dolomite is found. On the other hand, dolomite of replacement origin is found in evaporative settings including tidal flats, sabkhas and hypersaline lagoons. Examples of dolomite found in tidal flats include Bonaire, Netherland Antilles (Daffeyes et. al 1965, Andros Island, Bahamas (Shinn et. al 1965) and Sugarloaf, Florida (Shinn, 1968). Dolomite found in sabkha setting include example from the Trucial Coast, Abu Dhabi, UAE where poorly ordered dolomite (proto dolomite) was documented (Illing et. al 1965, McKenzie, 1981, Patterson and Kinsman 1982). Most important setting of all is the dolomite documented in hypersaline lagoons of Baffin Bay, Texas (Behrens and Land 1972) and of Al-Khiran Lagoon in Kuwait (Gunatilaka et al., 1984). Al-Khiran Lagoon setting in Kuwait is the most plausible and available analogue model for the observations documented in the Qatif's intrashelf lagoon dolomite.

The salinities recorded in Al-Khiran Lagoon ranged between 42-44% and up to a maximum 50-52% during July and August when average temperatures are between 45-47 ˚C. Gunatilaka et al. (1984) reported that lagoon's sediments are composed of a mixture of pelleted muds, biodegraded material and some ooids. They documented moderate Mg/Ca ratios but significantly reduced sulfate compared with surface water. Sulfate reduction dominates in sulfate-rich environments including hypersaline lagoons (Fauque, 1995). The reduction in sulfate is due to high degree of microbial sulfate reduction (Vasconcelos & McKenzie, 1997, Wright 1999, Stal 2000, Lith 2001, Mauger and Compton 2011) which creates an excellent environment for carbonate, and especially

dolomite, precipitation by producing carbonate ions though the oxidation of organic matter and increasing carbonate alkalinity (Compton, 1988).). Thus reduction of sulfate could be a more important factor, or critical additional factor along with high Mg/Ca ratios as it may provide a mechanism to overcome the precipitation kinetics caused by high concentration of sulfate ions (SO_4^{-2}) (Baker and Kastner, 1981; Gunatilaka et al., 1984).

Discussion

The isopachous bladed relic HMC cement is the most extensive cement in the Arab D of Qatif field. Syntaxial and blocky calcites are rare throughout the field. The isopachous cement in grainstones aids the preservation of interparticle porosity which offsets the effect of mechanical compaction (plate 4.1 A). Porosity is further enhanced by the dissolution following cementation creating moldic pores resulting in better reservoir quality. Grain-grain dissolution-compaction that generates the "fitted fabric" may significantly decrease porosity and permeability where it is extensive. In some extreme cases where fitting is characterized by concavo-convex contacts, porosity and permeability could be reduced to near zero (plate 4.7). The fitting is a chemical compaction process that occurs in the vadose zone, where grains experience exposure and submergence, e.g. beach, and is termed vadose chemical compaction (Dunham, 1969).

Dolomitization is a very important process in the Arab D of Qatif Field. In the southern segment of the field in QSEQ 3, dolomitization enhances the porosity of pelletal packstone significantly. In general, when dolomitization is greater than 75%, porosity generally increases to an average of 12% (plate 4.9F, 4.10-C, -D). However, dolomitization of ramp crest tract strata and shallow-intertidal skeletal-ooid grainstones

has, in general, a negative impact on reservoir quality. It precipitates in intraparticle and moldic pores and hence results in reduction of porosity (plate 4.6, 4.7).

During burial, the presence of the isopachous cement resulted in the preservation of most of the interparticle. In addition, mechanical compaction postdates all diagenetic processes. Figure 4.1-A shows that grain breakage was not followed by any dissolution or precipitation.

Chapter 5: Conclusions

The Kimmeridgian Arab D member in Qatif Field, Saudi Arabia provides a wealth of key observations on the lithofacies and architecture of a Late Jurassic carbonate ramp. The Arab D member in Qatif Field is a composite sequence composed of three high-frequency sequences (QSEQ1-QSEQ2-QSEQ3). Each HFS is formed by several high-frequency cycles that can be traced across the field. The HFCs are likely to have formed by short-term precessional cycles associated with low-amplitude sea level oscillation typical of greenhouse settings of the Late Jurassic.

During the Late Jurassic, the Qatif Field was bounded by an intrashelf basin to the south and by the Rimthan Arch to north (figure 5.1). The model developed for this study shows for the first time that the northern segment of the Qatif Field developed on the south-facing limb of NNW trending Rimthan Arch (figure 5.2), whereas the southern segment development was within the intrashelf basin which was influenced by Abqaiq and Ghawar structures to the south (figure 5.1). As a result, a ramp configuration with a localized dip to the south developed, where the Rimthan Arch had a prominent influence of the stratigraphic evolution of the Qatif Field. During highstands, progradation was directed to the south as a result of the back building of the Rimthan Arch, while platform-wide progradation was directed to the north-northeast (figure 5.1). This observation led to the new correlation scheme proposed here, one that differs substantially from earlier published models (Wilson, 1985).

On the ramp crest, HFCs are dominantly comprise asymmetrical, upward-shallowing stacks of facies, whereas the more deeper, middle to outer ramp setting, HFCs display symmetrical upward deepening, or upward shallowing stacks.

QSEQ1 HFS at the base of the reservoir section displays only northward prograding distal clinoform toes composed dominantly of subtidal, spiculitic wackestone (figure 5.3). QSEQ2 and QSEQ3 HFSs show a distinct change in paleogeography, recording north-to-south paleoslope, and the gradual filling of the resultant intrashelf basin that was developed between the Rimthan Arch to the north and the Ghawar complex to the south. The QSEQ2 and 3 are symmetrical and display transgressive system tracts and highstand system tracts. The TST of QSEQ2 is composed of middle and outer ramp, low-energy lithofacies developed in a restricted intrashelf basin, followed by higher-energy shallow water lithofacies dominating the ramp crest along the northern half of Qatif, outlining for the first time the southern limit of the Rimthan in the area of the reservoir. The TST of QSEQ3 was dominated by low energy, pelleted wackestone filling most of the intrashelf basin, followed by higher energy grainer lithofacies that are capped by peritidal lithofacies during the HST. HFS boundaries are best defined in dip-oriented 2-D sections especially in close proximity of the intrashelf basin margins, which could be difficult from 1-D sections. At the close of QSEQ3, the intrashelf basin relief was filled across, leaving expansive sabkha/salina topography from the Rimthan through to Ghawar.

Diagenetic features observed in the Arab D reservoir include fitted fabric (chemical compaction), dolomitization, and cementation. These features play a major role altering reservoir quality properties. On the ramp crest, the fitted fabrics are best developed in high-frequency-cycle (HFC) capping grainstones where early stage exposure-related meteoric leaching of grains resulted in their characteristic concavo-convex contacts where optimum conditions were met (figure 5.4). The fitted fabric was followed by the precipitation of isopachous bladed cements. The isopachous cement was followed by a phase of dissolution where dolomite crystals precipitated in moldic pores

created. These dolomites are best developed in grainstones closer to HFCs tops and their association with the fitted fabric completely nullifies porosity in these cycle caps.

In the intrashelf basin, dolomitization is extensive and it appears to have a positive impact on the reservoir enhancing the porosity significantly. In the portion of the reservoir where dolomitization was less than 75% reservoir quality was not improved with no visual porosity observed.

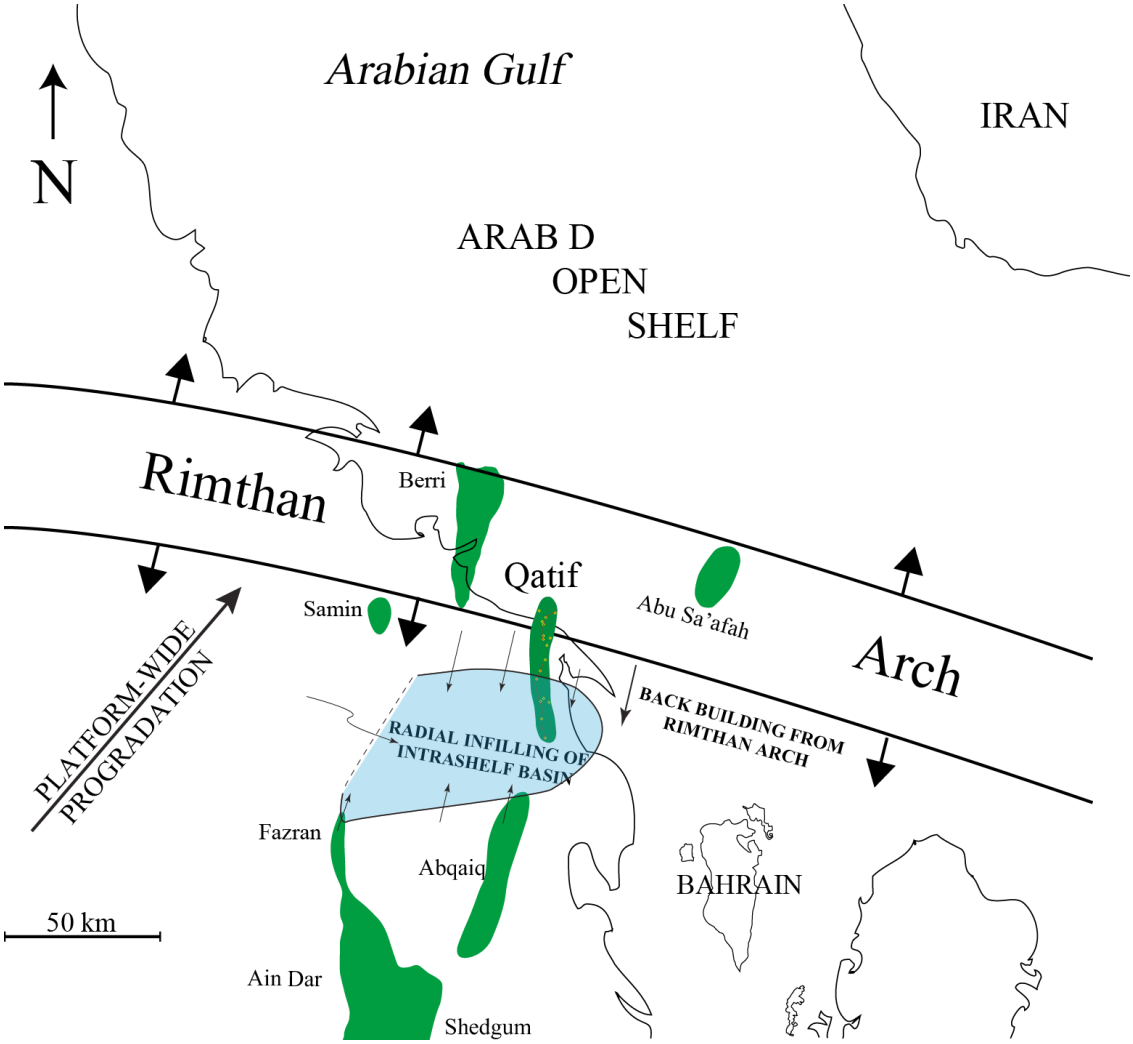

Figure 5. 1: Regional overview of the ramp configurations during Arab D time and Rimthan Arch structural-control the sedimentation styles recorded in Qatif field.

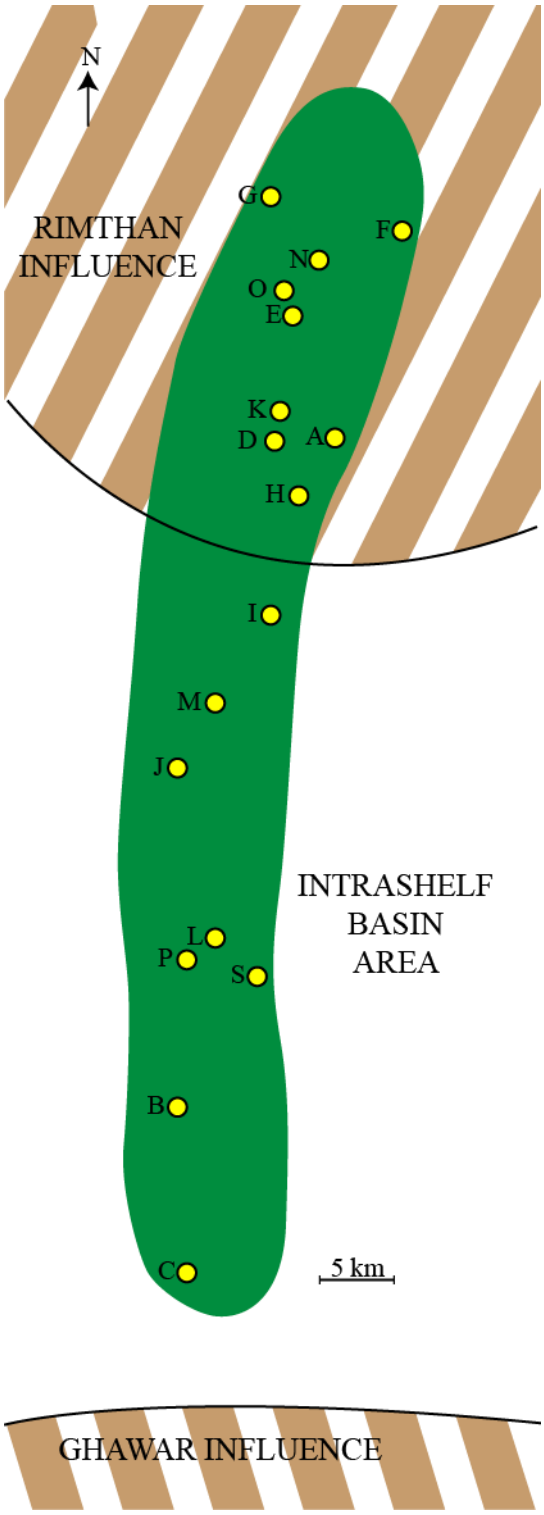

Figure 5. 2: Qatif field map showing well locations and areas of influence of Rimthan Arch and Ghawar anticline.

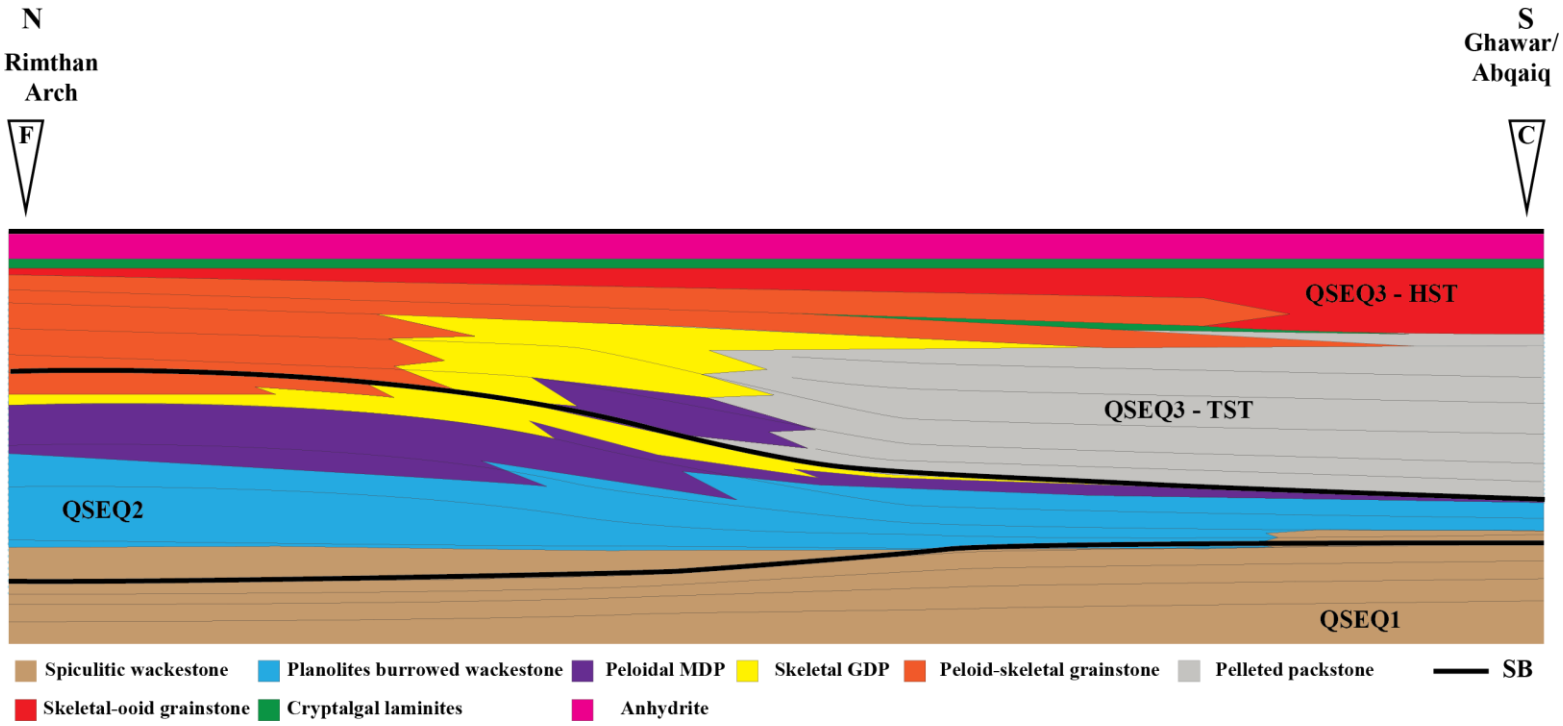

Figure 5. 3: Schematic model showing an overall stratigraphic architecture of the Arab D of Qatif Field

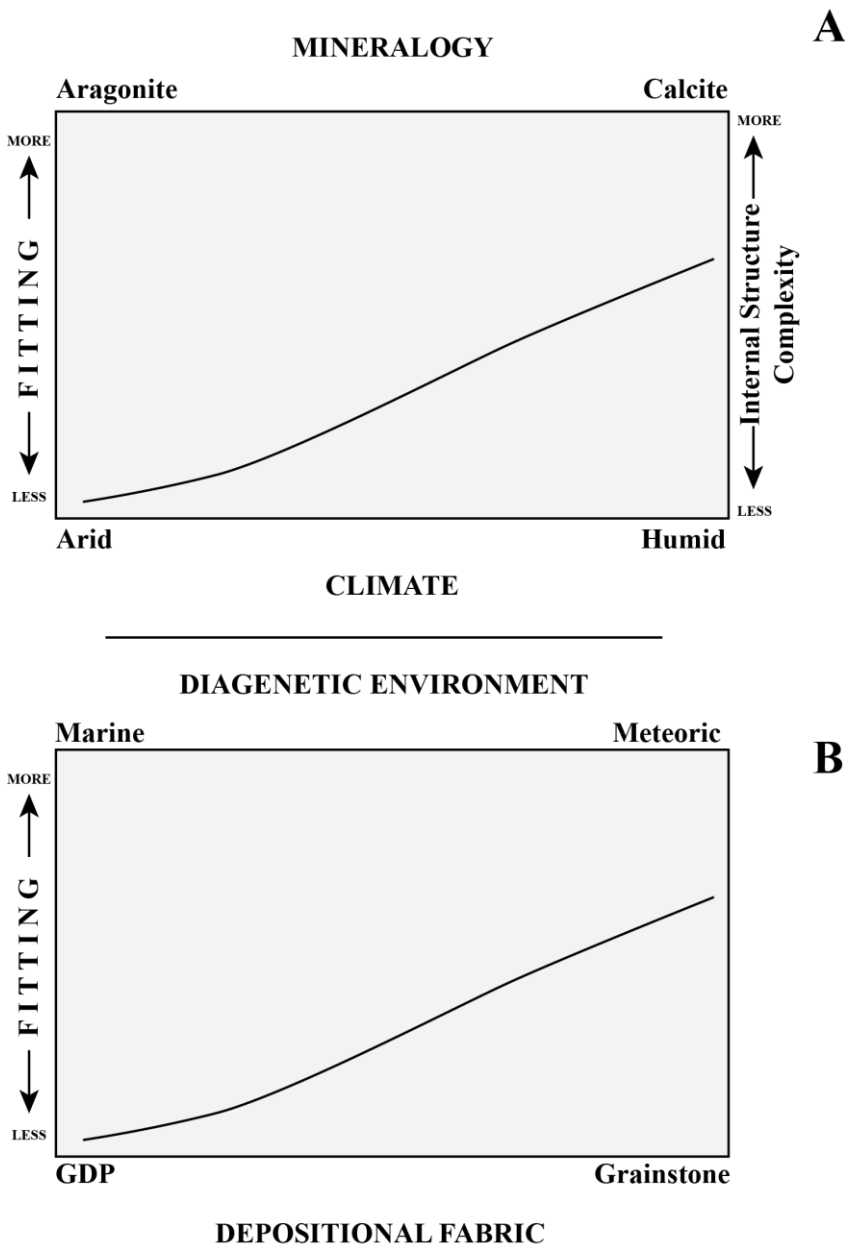

Figure 5. 4: Two figures showing different variables controlling the development of fitted fabric. A) A small degree of leaching of internal structure is needed to aid the fitting of grains which then is followed by precipitation of isopachous cement favored in semi-humid environment (Hird and Tucker, 1988). B) Calcitic grains are more likely to experience the leaching in the undersaturated meteoric setting, favored in grainstones.

References

Ainsworth, R. B., Sanlung, M., Duivenvoorden, S. and C Theo 1999.Correlation technique, perforation strategies, and recovery factors; an integrated 3-D reservoir modeling study, Sirikit Field, Thailand. *American Association of Petroleum Geologists* **88** (10): 1535-1551

Al-Dossary, F. M., Al-Ghamdi, A. A. and A. S. Al-Ahmari 2008. Experiences and Benefits Gained through Implementation of the First Intelligent Field in Saudi Aramco (QATIF Field). *Abu Dhabi International Petroleum Exhibition and Conference*.

Al-Fares, A. A., Bouman, M. and Jeans, P. 1998. A New Look at the Middle to Lower Cretaceous Stratigraphy, Offshore Kuwait. *GeoArabia*. **3**(4): 543-560

Al-Husseini, M. I. 1997. Jurassic Sequence Stratigraphy of the Western and Southern Arabian Gulf. *GeoArabia* **2**(4): 24.

Al-Husseini, M.I. 2000. Origin of the Arabian Plate Structures: Amar Collision and Najd Rift. *GeoArabia*. **5**(4): 527-542

Alnaji, N. S. 2002. The Geology of the Upper Permian - Permian Basin. Department of Geological Sciences. Columbia, University of South Carolina. **MSc.**

Alpert, S. P. 1975. Planolites and Skolithos from the upper Precambrian-lower Cambrian, White-Inyo Mountains, California. *Society of Economic Paleontologists and Mineralogists*. **49**(3):508-521

Alsharhan, A. S. and Kendall, C. 1986. Precambrian to Jurassic Rocks of Arabian Gulf and Adjacent Areas: Their Facies, Depositional Setting, and Hydrocarbon Habitat, *American Association Petroleum Geologists Bulletin* **70** (8): 977–1002

Alsharhan, A. S. and A. E. M. Nairn, 1997. Sedimentary basins and petroleum geology of the Middle East.

Andres, M. S. and Reid, R. P. 2006. Growth morphologies of modern marine stromatolites: A case study from Highborne Cay, Bahamas. *Sedimentary Geology* **185:** 319-328.

Assereto, R. and Kendall, C. 1977. Nature, origin and classification of peritidal tepee structures and related breccias. *Sedimentology*, **24**(2): 153-210

Ayres, M. G., M. Bilal, R. W. Jones, L. W. Slentz, M. Tartir and A. O. Wilson 1982. Hydrocarbon Habitat in Main Producing Areas, Saudi Arabia. *American Association of Petroleum Geologists* **66** (January): 9.

Bagotzky, V. S., 1993, Fundamentals of Electrochemistry: New York, Plenum Press.

Bottjer, D. J., Arthur, M. A., Dean, W. E., Hattin, D. E. and Savrda, C. E. 1986. Rhythmic bedding produced in Cretaceous pelagic carbonate environments; sensitive recorders of climatic cycles. *Paleoceanography*, **1**(4):467-481

Breton, J. P., Brosse, J. M., Cavelier, C., Fourniguet, J., Le Nindre, M., Manivit, J., Vaslet, D., and Vincent, P. L. 1983. Evolution structurale des grabens du centre de l'Arabie du Cretace au Quaternaire. *Societe Geologique du Nord*: *Lille, France*. **11**: 297-307.

Bromley, R. G. 1996. Trace fossils: biology, taphonomy and applications. Second edition. London, Chapman & Hall

Bromley, R. G. and Ekdale, A. A. 1984. Trace fossil preservation in flint in the European chalk. *Journal of Paleontology*, **58**: 298–311.

Buatois, L. A., Mangano, M. and Carr, T. 1999. Sedimentology and ichnology of Paleozoic estuarine and shoreface reservoirs, Morrow Sandstone, Lower Pennsylvanian of Southwest Kansas,USA: Current Research in Earth Sciences, *Kansas Geological Survey Bulletin*, **243**

Buczynski, C., and Chafetz, H.S., 1991, Habit of bacterially induced precipitates of calcium carbonate and the influence of medium viscosity on mineralogy. *Journal of Sedimentary Petrology*. **61**: 226-233.

Burchette, T. P. and V. P. Wright 1992. Carbonate Ramp Depositional System. *Sedimentary Geology* **79**: 3-57.

Butler, G. P. 1970. Holocene Gypsum and Anhydrite of the Abu Dhabi Sabkha, Trucial Coast: An alternative explanation of origin. Third Symposiom on Salt. *N. Ohio Geological Society* **1**: 120-152

Cantrell, D. L., P. K. Swart, and R. M. Hagerty, 2004, Genesis and characterization of dolomite, Arab-D reservoir, Ghawar field, Saudi Arabia: *GeoArabia*, **9**: 11–36.

Carrigan, W. J., G. A. Cole, E. L. Colling, and P. J. Jones, 1995, Geochemistry of the Upper Jurassic Tuwaiq Mountain and Hanifa Formation Petroleum Source Rocks of Eastern Saudi Arabia, *in* B. J. Katz, ed., Petroleum Source Rocks: Berlin, Springer-Verlag.

Chafetz, H.S., 1986, Marine peloids: A product of bacterially induced precipitation of calcite: *Journal Sedimentary Petrology*, **56**:812-817

Chafetz, H.S., 1994, Bacterially induced precipitates of calcium carbonate: habit and mineralogy: in, Sasowsky, I.D., and Palmer, M.V., eds.,Breakthroughs in karst geomicrobiology and redox geochemistry, Special Publication 1, Karst Waters Institute, Colorado Springs, Colorado, p. 9-10.

Chafetz, H.S., and Folk, R.L., 1984, Travertines: Depositional morphology and the bacterially-constructed constituents: *Journal Sedimentary Petrology*, **54**:289-316

Clarkson, E. N. K. 1998. Invertebrate palaeontology and evolution. 4th Edition. Blackwell Science, Oxford.

Clifton, H., Hunter, R. and Phillips, R. 1971, Depositional structures and processes in the non-barred high-energy nearshore, Journal of Sedimentary Petrology. **41**: 651–670.

Crevello, P. 1991. High frequency carbonate cycles and stacking patterns: Interplay of orbital forcing and subsidence on Lower Jurassic rift platforms, High Atlas, Morocco. In: Franseen, K.E, Watney, L.W, Kendall, C.C.st, Ross, & W. (eds) . Sedimentary Modelling: Computer Simulations and Methods for Improved Parameter Definition. *Kansas Geological Survey*, **223**: 207-230.

Dabbagh, M. E. 2006. Diagenesis of Jurassic Tuwaiq Mountain Limestone, Central Saudi Arabia. *Journal of King Saud University of Science* **19**: 28.

Dunham, R., J., 1962, Classification of carbonate rocks according to depositional texture, *in* Ham, ed., Classification of Carbonate Rocks, *American Association of Petroleum Geologists*, **1:** 108-121.

Dupraz, C. and Visscher, P.T., 2005, Microbial lithification in marine stromatolites and hypersaline mats. *Trends in Microbiology*, **13**(9): 429-438.

Einsele, G. 2000.Sedimentary Basins: Evolution, Facies, and Sediment Budget. Springer

Ekdale, A. A. 1992. Muckraking and mudslinging: the joys of deposit-feeding. *Palentological Society: short Cours*e, **15**: 1-317

Ellis, D. and J. Singer, 2008. Well Logging for Earth Scientists. Dordrecht: Springer Science & Business Media.

Elrick, M., 1996, Sequence stratigraphy and platform evolution of Middle Devonian carbonates, eastern Great Basin: *Geological Society of America Bulletin*, **108**, 392-416

Embry, A.F., 2009, Practical Sequence Stratigraphy. *Canadian Society of Petroleum Geologists*

Embry, A.F. & Klovan, J.E. 1971: A Late Devonian reef tract on northeastern Banks Island, Northwest Territories.-*Bulletin of Canadian Petroleum Geologists*, **19**: 730-781

Enay, R., Le Nindre, Y. M., Mangold, C., Manivit, J., and D. Vaslet. 1987. Le Jurassique d'Arabie Saoudite centrale; nouvelles donnees sur la lithostratigraphie, les paleoenvironnements, les faunes d'ammonites, les ages et les correlations. *Geobios, Memoire Special* **9**: 13-65

Fluegel, Erik. 2004. Microfacies of carbonate rocks; analysis, interpretation and application. Springer.

Friedman, G.M. 1994. Great Bahama Bank aragonitic muds: mostly inorganically precipitated, mostly exported - Discussion. *Journal of Sedimentary Research*. **64**:921.

Frisch, W., Meschede, M. and R. Blakey 2011. Plate Tectonics: Continental Drift and Mountain Building.

Frey, R. W. (ed.). 1975. The study of trace fossils: a synthesis of principles, problems, and procedures in ichnology. New York, Springer-Verlag

Galloway, W.E., 1989, Genetic stratigraphic sequences in basin analysis. I. Architecture and genesis of flooding-surface bounded depositional units. *American Association of Petroleum Geologists Bulletin* **73**: 125–142.

Ginsburg, R.N., 1991. Controversies about stromatolites: vices and virtues. In: Müller, D.W., McKenzie, J.A., Weissert, H. (Eds.), Controversies in Modern Geology. Academic Press, London, pp. 25–36.

Goldhammer, R. K., P. A. Dunn and L. A. Hardie 1990. Depositional Cycles, Composite Sea-Level Changes, Cycle Stacking Patterns, and the Hierarchy of Stratigraphic Forcing: Examples from Alpine Triassic Platform Carbonates. *Geological Society of America* **102**: 28.

Goldhammer, R.K., Oswald, E.J., AND Dunn, P.A., 1994, High-frequency, glacio-eustatic cyclicity in the Middle Pennsylvanian of the Paradox Basin: an evaluation of Milankovitch forcing, in de Boer, P.L., and Smith, D.G., eds., Orbital Forcing and Cyclic Sequences: *International Association of Sedimentologists, Special* Publications. **19**: 243–283.

Gardner, M. H., 1992. Sequence stratigraphy of eolian-derived turbidites: deep water sedimentation patterns along an arid carbonate platform and their impact on hydrocarbon recovery in Delaware Mountain Group reservoirs, West Texas, in D. H. Mruk and B. C. Curran, eds., Permian Basin Exploration and Production Strategies: Applications of Sequence Stratigraphic and Reservoir Characterization Concepts, West Texas Geological Society, Inc. Symposium, Publication Number **92-91**: 7-11.

Grotzinger, J. P. 1986. Cyclicity and paleoenvironmental dynamics, Rocknest platform, northwest Canada. *Geological Society of America Bulletin*, **97**: 1208-1231

Grotzinger, J.and Knoll, A. 1999. "Stromatolites in Precambrian Carbonates: Evolutionary Mileposts or Environmental Dipsticks?" *Annual Review of Earth and Planetary Sciences* **27**: 313–58

Gunatilaka, A., Saleh, A, Al-Temeemai, A. and Nassar, N. 1984 Occurrence of subtidal dolomite in a hypersaline lagoon, Kuwait. *Nature*, **311**,450-452.

Hallock, Pamela and Schlager, Wolfgang. 1986. Nutrient excess and the demise of coral reefs and carbonate platforms. *Society of Economic Paleontologists and Mineralogists* **1**(4): 389-398

Hanford, R. C., D. L. Cantrell and T. H. Keith 2002. Regional Facies Relationships and Sequence Stratigraphy of a Supergiant Reservoir (Arab-D Member), Saudi Arabia. Sequence Stratigraphic Models for Exploration and Production: 22nd Bob F. Perkins Research Conference. J. M. Armentrout and J. A. Pacht.

Haq, B. U., Hardenbol, J., and Vail, P. R., 1987, Chronology of fluctuating sea levels since the Triassic: *Science*, **235**

Harris, P. M., C. Kerans and D. G. Bebout 1993. Ancient Outcrop and Modern Examples of Platform Carbonate Cycles—Implications for Subsurface Correlation and Understanding Reservoir Heterogeneity. *American Association of Petroleum Geologists* **53**: 18.

Hoffman, P.F. 1989. Pethei Reef Complex (1.9 Ga), Great Slave Lake, N.W.T. *Canadian Society of Petroleum Geologists*, **13:** 38-48

Hughes, G.W. 1995. The Great Pearl Bank Barrier of the southern Arabian Gulf - a possible analogue for the Aptian rudist banks of the Arabian Peninsula. *International Conference on Quaternary deserts and climatic change, IGCP-349, A1 Ain, United Arab Emirates*.

Hughes, G. W. 1996. A New Bioevent Stratigraphy of Late Jurassic Arab-D Carbonates of Saudi Arabia. *GeoArabia* **1**(3): 18.

Hughes, G. W. 2004. Middle to Upper Jurassic Saudi Arabian carbonate petroleum reservoirs: biostratigraphy, micropalaeontology and palaeoenvironments. *GeoArabia* **9** (3): 79-114

Hughes, G. W. 2010. The palaeoenvironmental significance of Aeolisaccus, Favreina and Prethocoprolithus in Permian to Jurassic Saudi Arabian carbonates. *In Press*.

Hydrocarbon Technology Website. http://www.hydrocarbons-technology.com/projects/qatif/

Inden, R.F. and Moore, C.H., 1983. Beach environment. In: P.A. Scholle, D.G. Bebout, and C.H. Moore (eds.), Carbonate Depositional Environments. Tulsa, Oklahoma. American Association Petroleum Geologists, 211-265.

Johannessen, E.P., and Steel, R.J., 2005, Clinoforms and their exploration significance for deepwater sands: *Basin Research*, **17**: 521-550

Kasprzyk, A. 2003. Sedimentological and diagenetic patterns of anhydrite deposits in the Badenian evaporite basin of the Carpathian Foredeep, southern Poland. *Sedimentary Geology*, **158**(3-4): 167-194

Kendall, C.G.G.S.C., Alsharhan, A., and WHITTLE, G., 1994, Field Guidebook to Examine the Holocene Carbonates/Evaporites of Abu Dhabi, United Arab Emirates: for the International Geological Correlation Program (IGPCP-349): Abu Dhabi, U.A.E. *University Publication Department,* 46 p

Kendall, C. and Skipwith, P. 1968. Recent algal mats of a Persian Gulf lagoon. Journal of Sedimentary Research, **38**(4): 1040-1058

Kerans, Charles, 1995, Stratigraphic framework of the San Andres Formation, Algerita Escarpment, Guadalupe Mountains, New Mexico, in The San Andres in outcrop and subsurface: guidebook to the Permian Basin–SEPM 1995 Annual Field Conference: Permian Basin Section, SEPM, Publication **95-37**: 7–30.

Kerans, C. 1982. Sedimentology and stratigraphy of the Dismal Lakes Group. Ph.D. thesis, Carlton University, Ottawa, 404 pp.

Kerans, C and Loucks, R. G. 2002. Stratigraphic Setting and Controls on Occurrence of High-Energy Carbonate Beach Deposits: Lower Cretaceous of the Gulf of Mexico. *Gulf Coast Association of Geological Sciences Transactions*. **52:** 517-526.

Kerans, Charles; Fitchen, W. M. 1995. Sequence hierarchy and facies architecture of a carbonate-ramp system; San Andres Formation of Algerita Escarpment and western Guadalupe Mountains, West Texas and New Mexico. Report of Investigations-Texas, University, Bureau of Economic Geology.

Kerans, Charles and Tinker, Scott W. 1997. Sequence stratigraphy and characterization of carbonate reservoirs. *Society of Sedimentary Geology: SEPM Short Course Notes*, **40**

Kershaw, S 1994. Classification and Geological Significance of Biostromes. *Facies* **31**: 81-92

Kinsman, D. L. 1964. The Recent carbonate sediments near Halat El Bahrani, Trucial coast, Persian Gulf. In: L.M.J.U. Van Straaten, Editor, *Deltaic and Shallow Marine Deposits, Developments in Sedimentology*, Elsevier, Amsterdam: 129–135.

Kirkham, A. 1997. Shoreline evolution, aeolian deflation and anhydrite distribution of the Holocene, Abu Dhabi. *GeoArabia.* **2**(4): 403-416.

Koerschner, W.F. III and Read, J.F., 1989, Field and modelling studies of Cambrian carbonate cycles, Virginia Appalachians: Journal of Sedimentary Petrology, **59**: 654-687

Le Nindre, Y. M., Vaslet, D., Le Metour, J.,Bertrand, J.and M. Halawani 2003. Subsidence modelling of the Arabian Platform from Permian to Paleogene outcrops. Sedimentary Geology. **165** (1-4): 263-285

Lindsay, R. F., D. L. Cantrell, G. W. Hughes, T. H. Keith, H. W. Mueller and S. D. Russell 2006. Ghawar Arab-D Reservoir: Widespread Porosity in Shoaling-upward Carbonate Cycles, Saudi Arabia. *American Association of Petroleum Geologists* **88**: 41.

Lock, B. E. 2002. Sabkhas Ancient and Modern. The Gulf of Mexico. *Gulf Coast Association of Geological Sciences Transactions*. **52:** 645-657.

Lock, B.E., B.K. Darling, I.D. Roy, 1983, Marginal Marine Evaporites, Lower Cretaceous of Arkansas: *Gulf Coast Association of Geological Societies Transactions*. **33**: 145-152

Logan, B. W., Rezak, R. and Ginsburg, R.N. 1964. Classification and Environmental Significance of Algal Stromatolite. *The Journal of Geology*, **72** (1): 68-83

Longman, M. W. 1980. Carbonate Diagenetic Textures from Nearsurface Diagenetic Environments. *American Association of Petroleum Geologists*, **64** (4): 461-487

Loucks, R.G., Sarg, J.F. (Eds.), 1993. Carbonate Sequence Stratigraphy. American Association of Petroleum Geologist, Memoir **57**: 545

Loutit, T.S., Hardenbol, J., Vail, P.R., Baum, G.R., 1988, Condensed sections: the key to age-dating and correlation of continental margin sequences. In: Wilgus, C.K., Hastings, B.S., Kendall, C.G.St.C., Posamentier, H.W., Ross, C.A., Van Wagoner, J.C. (Eds.), Sea Level Changes—An Integrated Approach, *SEPM Special Publication,* **42**: 183–213.

Lowenstein, T. K., 1987, Evaporite depositional fabrics in the deeply buried Jurassic Buckner Formation, Alabama: *Journal of Sedimentary Petrology,* **57**:108-116.

Lowestam, H., AND Epstein, S., 1957. On the origin of sedimentary aragonite needles of Great Bahama Bank: Journal Geology, **65**: 364-37

MacEachern, J. A. and Pemberton, G. 1997.Ichnology; biogenic utility in genetic stratigraphy. Canadian Society of Petroleum Geologists, Canada, pp. 387-412

Markello, J.R., R.B. Koepnick, L.E. Waite, and J.F. Collins, 2008, The carbonate analogs through time (CATT) hypothesis and the global atlas of carbonate fields – a systematic and predictive look at Phanerozoic carbonate systems: *SEPM Special Publication* **89**: 15-45.

Matthews, R.K., 1966. Genesis of recent lime mud in Southern British Honduras. *Journal of Sedimentary Petrology.* **36**: 428-454.

Matthews, R.K. and C. Frohlich 2002. Maximum flooding surface and sequence boundaries: Comparisons between observation and orbital forcing in the Cretaceous and Jurassic (65-190 Ma). *GeoArabia,* **7**(3): 503-538.

Mattner J. and Al-Husseini M. I. 2002. Essay: applied cyclo-stratigraphy for the Middle East E&P industry. *GeoArabia,* **7**:734-744.

McCubbin, D.G., 1982, Barrier-island and strand-plain facies, in Scholle, P.A., and Spearing, D., eds., Sandstone Depositional Environments: *American Association of Petroleum Geologists*, Memoir **31**: 247–279

McGuire, M. D., R. B. Koepnick, J. R. Markello, M. L. Stockton, L. E. Waite, G. S. Kompanik, M. J. Al-Shammery and M. O. Al-Amoudi 1993. Importance of Sequence Stratigraphic Concepts in Development of Reservoir Architecture in Upper Jurassic Grainstones, Hadriya and Hanifa Reservoirs, Saudi Arabia. *Society of Petroleum Engineers*, 489-499.

McIlroy, D. (ed.) 2004. The Application of Ichnology to Palaeoenvironmental and Stratigraphic Analysis. Geological Society Special Publication no. 228

Meyer, F.O. and R.C. Price 1993. A new Arab-D depositional model, Ghawar field, Saudi Arabia. Proceedings of the 8th Society of Petroleum Engineers, Middle East Oil Conference, p. 465-474.

Meyer, F., Price, C., Al-Ghamdi, I. A., Al-Goba, I. M., Al-Raimi, S. M., Cole, J. C. 1996. Sequential stratigraphy of outcropping strata equivalent to Arab-D Reservoir, Wadi Nisah, Saudi Arabia. *GeoArabia*. **1**(3): 435-456

Middleton, G. 1973. Johannes Walther's Law of Correlation of Facies. *Geological Society of America Bulletin*. 38: 979-988

Miller, W. C., 2007. Trace fossils: concepts, problems, prospects. Elsvier

Milliman, J. D., Freile, D., Steinen, R. P., and Wilber, R. J., 1993. Great Bahamas Bank aragonitic muds: Mostly inorganically precipitated, mostly exported. *Journal of Sedimentary Petrology*. **63**: 589–595.

Milliman, J., Ross, D. and Ku, T. 1969. Precipitation and lithification of deep-sea carbonates in the Red Sea. *Journal of sedimentary Petrology*. **39**: 724-736.

Milliman, J. D. and Muller, J. 1977. Characteristics and genesis of shallow water and deep- sea limestones. In: The fate of fossil fuel CO2 in the Oceans (ed. N.R. Anderson and A. Malahoff), Plenuim Publishing Corporation, N.Y. pp. 655-672

Milsom, C. and Rigby, S., 2004. Chapter 15. Precambrian Life, pp. 131-136, in Fossils at a Glance. Blackwell.

Mitchell, J. C., Lehmann, P. J., Cantrell, D. L., Al-Jallal, I. A.and Al-Thagafy, M. A. R. 1988. Lithofacies, diagenesis and depositional sequence; Arab-D Member, Ghawar Field, Saudi Arabia. *Society of Economic Paleontologists and Mineralogists*. **12**: 459-514.

Mitchum, R.M., Jr. and Van Wagoner, J.C., 1991. High frequency sequences and their stacking patterns: Sequence stratigraphic evidence of high-frequency eustatic cycles. In: W. Schlager and K.T. Biddle (Editors). The Record of Sea level Fluctuation. *Sedimentary Geology*.**70**: 131-160.

Montaggioni, L., and Camoin, G. 1993. Stromatolites associated with coralgal communities in Holocene high-energy reefs: *Geology*, **21**: 149–152.

Morgan, W. A. 2008. Holocene sediments of northern and western Caicos Platform, British West Indies. *SEPM Core Workshop*. **22**

Murris, R. J. 1980. Middle East: Stratigraphic Evolution and Oil Habitat. *American Association of Petroleum Geologists* **64**(5): 597-618.

Neumann, A. C., and Land, L. S., 1975, Lime mud deposition and calcareous algae in the Bight of Abaco, Bahamas: A budget: *Journal of Sedimentary Petrology*. **45**: 763–786.

Oliveri, E., Neri, R., Bellanca, A., and Riding, R. 2009. Carbonate stromatolites from a Messinian hypersaline setting in the Caltanissetta Basin, Sicily: petrographic evidence of microbial activity and related stable isotope and rare earth element signatures. *Sedimentology*. **57**: 142–161

Pemberton, S. G. 1992. Applications of Ichnology to Petroleum Exploration. *SEPM Core Workshop*, **17**

Pemberton, S. G. and Frey, R. W. 1982. Trace fossil nomenclature and the Planolites-Palaeophycus dilemma. *Society of Economic Paleontologists and Mineralogists*. **56**(4): 843-881

Pemberton, S. G., Spila, M., Pulham, A. J., Saunders, T., MacEachern, J. A., Robbins, D., and Sinclair, I. K., 2001, Ichnology and Sedimentology of Shallow to Marginal Marine Systems: Ben Nevis and Avalon Reservoirs, Jeanne d'Arc Basin: Geological Association of Canada, Short Course Notes, St. John's, Newfoundland, **15**: 1-343.

Pomar, L. (2001). Types of Carbonate Platforms: A Genetic Approach. *Basin Research* **13**: 22.

Pomar, L. and Hallock, P. 2008. Carbonate factories; a conundrum in sedimentary geology. *Earth-Science Reviews* **87**(3-4): 134-169.

Posamentier, H., Jervey, M., Vail, P.R., 1988, Eustatic controls on clastic deposition. I. Conceptual framework. In: Wilgus, C.K., Hastings, B.S., Kendall, C., Posamentier, H., Ross, C.and Van Wagoner, J.C. (Eds.), Sea Level Changes: An Integrated Approach. *SEPM Special Publication*. **42**: 110– 124.

Postma G. and Ten Veen, J. H., 1999. Astronomically and tectonically controlled variations in gamma-ray intensity in late Miocene hemi-pelagic successions of the eastern Mediterranean basin. *Sedimentary Geology*, **128**: 1-12

Pope, M. and J. F. Read 1998. Ordovician Metre-Scale Cycles: Implications for Climate and Eustatic Fluctuations in the Central Appalachians during a Global Greenhouse, Non-Glacial to Glacial Transition. *Palaeogeography, Palaeoclimatology, Palaeoecology* **138**: 27-42.

Powers, R. W. 1962. Arabian Upper Jurassic Carbonate Reservoir Rocks. *American Association of Petroleum Geologists*, **1**: 122-192.

Powers, R. W., L. R. Ramirez, C. D. Redmond, and E. L. Elberg, 1966, Sedimentary geology of Saudi Arabia: Geology of the Arabian Peninsula: U.S. Geological Survey Professional Paper 560-D, 150 p.

Prothero, D. R. and Schwab, F. 1996. Sedimentary Geology: An Introduction to Sedimentary Rocks and Stratigraphy. W. H. Freeman, New York

Raspini, 2001. Stacking pattern of cyclic carbonate platform strata; Lower Cretaceous of Southern Apennines, Italy. *Journal of the Geological Society of London*, **158**(2): 353-366

Read, J. F. 1985. Carbonate Platform Facies Models. *American Association of Petroleum Geologists* **69**(1): 1-21.

Read, J.F. 1995. Overview of carbonate platform sequences, cycle stratigraphy and reservoirs in greenhouse and icehouse worlds: in Read, J.F., Kerans, C., Weber, L.J., Sarg, J.F., and Wright F.W., Milankovitch sea level changes, cycles and reservoirs on carbonate platforms in greenhouse and icehouse worlds, SEPM Short Course Notes No. **35**, p. 1-102.

Read, J. F. 1998. Phanerozoic carbonate ramps from greenhouse, transitional and icehouse worlds: clues from field and modelling studies. *Geological Society, London* **149**: 107-135

Read, J.F., M.E. Elrick, and D.A. Osleger, 1990, Computer models for defining eustatic sea level fluctuations in carbonate rocks: *American Association of Petroleum Geologists*, **74**(5): 746.

Read, J. F., and Goldhammer, R. K., 1988, Use of Fischer plots to define third-order sea-level curves in Ordovician peritidal cyclic carbonates, Appalachians: *Geology*, **16**: 895-899

Read, J. F., Grotzinger, J. P., Bova, J. A. & Koerschner, W. F. 1986. Models for generation of carbonate cycles. *Geology*, **14**:107–110

Reid, R., Visscher, P., Decho, A., Stolz, J., Bebout, B., Dupraz, C., Macintyre, I., Pearl, H., Pinckey, J., Prufert-Bebout, L., Steppe, T. and DesMarais, D. 2000. The role of microbes in accretion, lamination and early lithification of modern marine stromatolites. *Nature*. **406**: 989-992

Riding, R. 1999. The term stromatolite: towards an essential definition. *Lethaia* **32**: 321–330

Riding, R. 2000. Microbial carbonates: the geological record of calcified bacterial–algal mats and biofilms. *Sedimentology* **47** (Supplement 1): 179–214

Riding, R. and Tomás, S. 2006. Stromatolite reef crusts, Early Cretaceous, Spain: bacterial origin of in situ precipitated peloid microspar? *Sedimentology* **53**: 23–34

Robbins, L. L.,Yates, K. K., Shinn, E., and Blackwelder, P. 1997. Whitings on the Great Bahama Bank: A microscopic solution to a macroscopic mystery. *Bahamas Journal of Science*. **4**: 1–7.

Savrda, C.E. and D.J. Bottjer. 1987. The exaerobic zone: a new oxygen-deficient marine biofacies. Nature, **327**: 54-56

Savrda, C.E. and D.J. Bottjer. 1989. Trace fossil model for reconstructing oxygenation histories of ancient marine bottom-watess: application to Upper Cretaceous Niobrara Formation, Colorado. *Palaeogeography, Palaeoclimatology, Palaeoecology*, **74**: 49-74

Savrda, C. E., Bottjer, David J. 1991. Oxygen-related biofacies in marine strata; an overview and update. *Geological Society Special Publications*, **58**: 201-219

Schlager, W., 1981, The paradox of drowned reefs and carbonate platforms: *Geological Society of America, Bulletin*. **92**(4): 197-211

Schlager, Wolfgang 2000. Sedimentation rates and growth potential of tropical, cool-water and mud-mound carbonate systems. Geological Society Special Publications, 178: 217-227

Schlager, Wolfgang. 2003. Benthic carbonate factories of the Phanerozoic. *International Journal of Earth Sciences*. **92**(4): 445-464

Sharland, P.R.; Archer R.; Casey, D.M.; Davies, R.B.; Hall, S.H.; Heward, A.P.; Horbury, A.D. and Simmons M.D. 2001. Arabian Plate Sequence Stratigraphy.

Shinn, E. A., 1968 Selective dolomitization of Recent sedimentary structures: *Journal of Sedimentary Petrology*, **38**(2): 612-666.

Shinn, E., 1983. Tidal flat environment. In: Scholle, P.A., Babout D.G, Moore, C.H. (Eds.), Carbonate depositional environments, *American Association of Petroleum Geologist*. Memoir **33**: 171–210.

Shinn, E. A., R. P. Steinen, B. H. Lidz, and P K. Swart. 1989. Perspectives: Whitings, a sedimentologic dilemma. *Journal of Sedimentary Petrology*. **59**: 147-161

Souza, M., Kjerfve, B., Knoppers, B., Landim de Souza, W. and Damasceno, R. 2003. Nutrient budgets and trophic state in a hypersaline coastal lagoon: Lagoa de Araruama, Brazil. *Estuarine, Coastal and Shelf Science*. **57**: 843–858

Stal, L. 2000. Cyanobacterial mats and stromatolites. In: B.A. Whitton and M. Potts, Editors, The Ecology of Cyanobacteria, Kluwer Academic Publishers, Dordrecht. 61–120.

Strasser, A. 1986. Ooids in Purbeckian limestones (lowermost Cretaceous) of the Swiss and French Jura. Sedimentology, **33**: 711-727

Steineke, M., R. A. Bramkamp and N. J. Sander 1958. Stratigraphic Relations of Arabian Jurassic Oil. *American Association of Petroleum Geologists*: 1294–1329.

Stockman, K.W., Ginsburg, R.N., and Shinn, E.A. 1967. The production of lime mud by algae in South Florida. *Journal of Sedimentary Petrology.* **37**(2):633-648.

Stricklin, F.L., Jr., and C.I. Smith, 1973, Environmental reconstruction of a carbonate beach complex, Cow Creek (Lower Cretaceous) Formation of Central Texas: *Geological Society of America Bulletin*, **84**: 1349-1367.

Sun, Q. and Wright, V. 1989. Peloidal fabrics in Upper Jurassic reefal limestones, Weald Basin, southern England, *Sedimentary Geology*. **65**: 165–181

Swart, P. K., D. L. Cantrell, H. Westphal, R. C. Hanford and C. G. Kendall 2005. Origin of Dolomite in the Arab-D Reservoir from the Ghawar Field, Saudi Arabia: Evidence from Petrographic and Geochemical Constraints. *Journal of Sedimentary Research* **75**(3): 476-491

Taylor, A. M.and Gawthorpe, R. L. 1993. Application of sequence stratigraphy and trace fossils analysis to reservoir description; examples from the Jurassic of the North Sea. Geological Society of London, **4:** 317-335

Tebbutt, G. E., Conley, C. D.; Boyd, D. W. 1965. Lithogenesis of a distinctive carbonate rock fabric.Contributions to Geology, **4**(1): 1-13

Tucker, M. E. and Wrigh, V. P. 1990. Carbonate Sedimentology. Blackwell Science.

Vail, P.R., Hardenbol, J., Todd, R.G., 1984, Jurassic unconformities, chronostratigraphy and sea-level changes from seismic stratigraphy and biostratigraphy. In: Schlee, J.S. (Ed.), Interregional Unconformities and Hydrocarbon Accumulation, *American Association of Petroleum Geologists Memoir* **36**: 129–144.

Vail, P., Todd, R. and Sangree, J. 1977. Seismic Stratigraphy and Global Changes of Sea Level: Part 5. *Chronostratigraphic Significance of Seismic Reflections*: Section 2. Application of Seismic Reflection Configuration to Stratigraphic Interpretation Memoir **26**: 99–116

Van Wagoner, J.C., Mitchum, R.M., Jr., Posamentier, H.W. and Vail, P.R., 1987. Seismic stratigraphy interpretation using sequence stratigraphy. Part II: Key definitions of sequence stratigraphy. In: A.W. Bally (Editor), Atlas of Seismic Stratigraphy. *American Association of Petroleum Geology*. **27**(1): 11-14.

Van Wagoner, J.C., R.M. Mitchum, K.M. Campion, and V.D. Rahmanian, 1990, Siliciclastic sequence stratigraphy in well logs, cores, and outcrops: Tulsa, Oklahoma, *American Association of Petroleum Geologists Methods in Exploration Series,* No. **7:** 55p

Vasconcelos, C. and McKenzie, J. 1997. Microbial Mediation of Modern Dolomite Precipitation and Diagenesis Under Anoxic Conditions (Lagoa Vermelha, Rio de Janeiro, Brazil). *Journal of Sedimentary Research*. **67**: 378-390

Walter, M.R., Grotzinger, J.P., Schopf, J.W., 1992. Proterozoic stromatolites. In: Schopf, J.W., Klein, C. (Eds.). The Proterozoic Biosphere: A Multidisciplinary Study, pp. 253–260. Cambridge University Press, Cambridge.

Warren, J. K. 2006. Evaporites: Sediments, Resources and Hydrocarbons. Springer

Wehr, F. L., and L. D. Brasher, 1996, Impact of sequence-based correlation style on reservoir model behaviour, lower Brent Group, North Cormorant field, UK North Sea, in J. A. Howell and J. F. Aitken, eds., High resolution sequence stratigraphy: innovations and applications. *Geological Society Special Publication* **104**: 115–128.

Wignall, P.B. and Myers, K.J., 1988. Interpreting benthic oxygen levels in mudrocks: a new approach. *Geology* **16**: 452–455

Wilson, A. O. 1981.z Jurassic Arab-C and -D carbonate petroleum reservoirs, Qatif Field, Saudi Arabia. *Society of Petroleum Engineers*. **7**: 171-177

Wilson, A. O. 1985. Depositional and diagenetic facies in the Jurassic Arab-C and -D, Qatif field, Saudi Arabia. Carbonate Petroleum Reservoirs. P. O. Rohl and P. W. Choquette, Springer Verlan**:** 320-340

Wilson, J. L. 1975. Carbonate facies in geologic history.

Ziegler, M. A., 2001, Late Permian to Holocene Paleofacies evolution of the Arabian plate and its hydrocarbon occurrences: GeoArabia, **6**: 445–504.